

https://dspace.org/

The study of the expression of hepatitis B surface antigen (HBsAg) and hepatitis B e antigen (HBeAg) by pres deletion mutants and an occult strain of subgenotype A1 hepatitis B virus (HBV) using subcellular fractionation

Vos, Hillary Justine

2019
https://hdl.handle.net/10539/29719

Downloaded from a DSpace repository. https://dspace.org/



The Study of the Expression of Hepatitis B Surface Antigen (HBsAg) and Hepatitis B e Antigen (HBeAg) by PreS Deletion Mutants and an Occult Strain of Subgenotype A1 Hepatitis B virus (HBV) using Subcellular Fractionation

Hillary Justine Vos

A dissertation submitted to the Faculty of Health Sciences, University of the Witwatersrand, for the fulfilment of the degree of Master of Science in Medicine

Johannesburg, August 2019

DECLARATION

I, Hillary Justine Vos declare that this dissertation "**The study of the expression of hepatitis B surface antigen (HBsAg) and hepatitis B e antigen (HBeAg) by deletion mutants and an occult strain of subgenotype A1 hepatitis B virus (HBV) using subcellular fractionation**" is my own original work, and that all sources that I have used have been indicated by complete references. This dissertation is being submitted for the degree of Master of Science in Medicine at the University of the Witwatersrand, Johannesburg, South Africa.



Hillary Justine Vos

26-08-2019

Date

PRESENTATIONS

Ms Hillary Vos has been awarded a travel grant to present the research at the 2019 International HBV Meeting in Melbourne, Australia in October 2019.

DEDICATION

To my dearest family, you are my source of strength and empowerment. I love you profoundly, with all my soul has to offer.

ACKNOWLEDGEMENTS

This dissertation was compiled with blood, sweat and tears, but most importantly, with the support and contribution of several individuals.

First and foremost, let glory and praise be to my Lord and Saviour Jesus Christ of Nazareth for the strength to pull through all the challenges I faced in the years leading up to this submission.

To my supervisor Professor Anna Kramvis, the kind-hearted mother of the HVDRU, I give you my sincerest gratitude for your endless encouragement, pep talks, supervision and tremendous patience throughout the course of this study. My intact sanity and the completion of this dissertation would not have been possible without your contribution. If anything can be considered commendable, it can be undoubtedly accredited to you.

Thank you Prof. Kramvis, you are a remarkable woman.

To my colleagues, the members of the HVDRU, I am privileged and thankful for your guidance, mentorship and friendship. I would like to give a special thanks to Dr Nimisha Bhoola for her time and effort.

I would like to extend my deepest gratitude to all the benevolent benefactors for the financial support required to conduct this study, this includes; The University of the Witwatersrand (Postgraduate Merit Award and FRC grant), CANSA Research Division, Poliomyelitis Research Fund (PRF) and the National Research Foundation (NRF). I would also like to thank Professor Patrick Arbuthnot, Dr Peter Revill, Dr Clement Penny, and Dr Therese Dix-Peek for allowing me to utilize their laboratory equipment and facilities.

Lastly, I would also like to take a moment to thank my previous supervisor, Professor Caroline Knox, another phenomenal woman I have had the pleasure to know. Thank you for providing me with the training wheels I required to become the scientist I am today. You have always believed in me and that has facilitated my academic growth in ways that words cannot fully express.

ABSTRACT

Hepatitis B surface antigen (HBsAg) expression is a vital diagnostic marker in the course of HBV infection. Its presence in the serum for longer than six months heralds chronic infection. The large, middle and small hepatitis B surface protein (LHBs, MHBs and SHBs, respectively), are three types of HBsAg that are expressed from the preS/S opening reading frame (ORF), with varying lengths since they are translated from separate in-frame initiation codons. LHBs comprises the preS1, the preS2, and the S domains; MHBs comprises the preS2 and the S domains whereas the SHBs contains the S domain. Strains of HBV, with deletions in the preS1 and/or preS2 regions, have been identified in HIV-infected individuals and are also frequent in HBV strains from hepatocellular carcinoma (HCC) patients. These deletions have been shown to be a risk factor for the development HCC. The objective of the study was to functionally characterize deletion mutants and an occult strain isolated from South African HIV-infected adults. In this study, previously constructed plasmids shown to express HBV DNA and proteins for wild-type (A1 WT SW), occult strain (SHH193A), and with different HBsAg mutations: preS1 & preS2 deletion mutant (SHH011A), preS2 deletion mutants (SHH045A and SHH167A) of subgenotype A1 were transfected in Huh7 cells. Intracellular protein expression was determined following subcellular fractionation and subsequent immunoblotting. Extracellular protein expression was determined by ELISA. The subcellular localization, extracellular expression and the ratios of the different types of HBsAg was determined for the occult and preS deletion mutant strains relative to the wild-type strain. This study demonstrated that the ratio and subcellular localization of the occult and preS deletion mutant strains were affected relative to the A1 wild-type. Furthermore, we found that HBsAg from the occult strain aggregated primarily in the membrane-bound fraction, suggesting that these proteins were retained in this cellular compartment. The retention of HBsAgs in the ER, can result in ER stress and lead to reactive

oxygen species accumulation, which can trigger oxidative DNA damage and lead to hepatocarcinogenesis. These findings may provide a further explanation as to why the occult and preS deletion mutants may contribute to an increased hepatocarcinogenic potential and/or the HBsAg-negative phenotype.

TABLE OF CONTENTS

DECLARATION I

PRESENTATIONS II

ACKNOWLEDGEMENTS IV

ABSTRACT V

TABLE OF FIGURES XI

LIST OF TABLES XV

LIST OF ABBREVIATIONS AND ACRONYMS XVI

UNITS XIX

CHAPTER 1: INTRODUCTION 1

1.1 BRIEF HISTORY OF HEPATITIS B VIRUS 1

1.2 CLASSIFICATION OF THE HEPATITIS B VIRUS 2

1.3 EPIDEMIOLOGY AND CLINICAL MANIFESTATION OF HBV 3

1.3.1 GLOBAL HBV GENOTYPE DISTRIBUTION 4

1.3.2 GLOBAL IMPACT OF THE DIFFERENT HBV GENOTYPES 6

1.3.3 SUBGENOTYPES OF HBV IN AFRICA 8

1.4 HEPATITIS B VIRUS STRUCTURE 9

1.4.1 HEPATITIS B CORE ANTIGEN (HBCAG) 10

1.4.2 HEPATITIS B E ANTIGEN (HBEAG) 11

1.4.3 SURFACE ANTIGEN (HBSAG) 12

1.4.4 POLYMERASE/REVERSE TRANSCRIPTASE 14

1.4.5 HBX PROTEIN 15

1.5 HEPATITIS B VIRUS REPLICATION CYCLE 16

1.6 HBSAG DELETION MUTATIONS: PRES1 AND PRES2 DELETION MUTATIONS 19
1.7 HBV INFECTION 20
1.8 OCCULT HBV INFECTION 22
CHAPTER 2: MATERIALS AND METHODS 26
2.1 ETHICS 26
2.2 MATERIALS 26
2.3 OVERVIEW OF METHODS 29
2.4 PREPARATION OF REPLICATION COMPETENT PLASMIDS 30
2.4.1 PLASMID DNA EXTRACTION 30
2.4.2 RESTRICTION DIGESTION 32
2.4.3 SEQUENCING 33
2.5 CELL CULTURE AND TRANSFECTION 34
2.5.1 CELL CULTURE 34
2.5.2 TRANSIENT TRANSFECTION 35
2.5.3 TRANSFECTION EFFICIENCY 36
2.6 PREPARATION OF WHOLE CELL LYSATES 37
2.7 SUBCELLULAR FRACTIONATION 37
2.7.1 COMMERCIAL KIT 37
2.7.2 MANUAL PROTOCOL 39
2.8 PROTEIN CONCENTRATION DETERMINATION ASSAY 42
2.8.1 PREPARATION OF PROTEIN STANDARDS 42
2.8.2 ASSAY 43
2.9 IMMUNOBLOTTING 43
2.9.1 SDS-PAGE & PROTEIN TRANSFER 43
2.9.2 BLOCKING OF THE NITROCELLULOSE MEMBRANE 44

2.9.3 BINDING OF ANTIBODIES 44
2.9.4 DEVELOPMENT OF PROTEIN SIGNAL OF INTEREST 45
2.9.5 STRIPPING OF NITROCELLULOSE MEMBRANE 46
2.10 ENZYME-LINKED IMMUNOSORBENT ASSAY (ELISA) 47
2.10.1 HBEAG ELISA PROTOCOL 47
2.10.2 HBSAG ELISA PROTOCOL 48
2.11 STATISTICS 51
2.11.1 ANOVA ANALYSIS 51
2.11.2 F-TEST ANALYSIS 51
CHAPTER 3: RESULTS 52
3.1 PLASMID PREPARATION: SEQUENCING & RESTRICTION DIGESTION 52
3.2 CELL CULTURE & TRANSFECTION 57
3.2.1 MYCOPLASMA DETECTION ASSAY 58
3.2.2 TRANSFECTION EFFICIENCY 58
3.3 SUBCELLULAR FRACTIONATION 59
3.3.1 COMMERCIAL KIT OPTIMIZATION 59
3.3.2 MANUAL SUBCELLULAR FRACTIONATION 65
3.4 IMMUNOBLOTTING RESULTS 67
3.5 ELISA RESULTS 72
3.5.1 HBEAG ELISA RESULTS 72
3.5.2 HBSAG ELISA RESULTS 74
CHAPTER 4: DISCUSSION 77
4.1 INTEGRITY OF PLASMID CONSTRUCTS 78
4.2 SUBCELLULAR FRACTIONATION 79
4.3 INTRACELLULAR EXPRESSION OF HBSAG 80

4.4 EXTRACELLULAR EXPRESSION OF HBEAG AND HBSAG 85
4.5 LIMITATIONS 86
4.6 CONCLUSION 86
APPENDIX A: ETHICS CLEARANCE & PERMISSIONS 88
APPENDIX B: COMPOSITION OF REAGENTS & SOLUTIONS 90
APPENDIX C: PRIMER SEQUENCES 103
APPENDIX D: THE GENERATION OF A COMPUTATIONAL PLASMID MAP FOR THE RECOMBINANT 1.28 MER HBV A1 WT PLASMID 104
APPENDIX E: COMPLETE SEQUENCE OF HBV SUBGENOTYPE A1 WT 109
APPENDIX F: PCDNA™ 4/TO EXPRESSION VECTOR 112
APPENDIX G: SUPPLEMENTARY PROTOCOLS 113
APPENDIX H: CALCULATIONS 117
APPENDIX I: PROTEIN & DNA LADDERS 119
REFERENCES 121

TABLE OF FIGURES

Figure 1: The global rate of diagnosis and treatment of hepatitis B infection 3

Figure 2: A schematic of the various HBV genotype distribution in each country..... 5

Figure 3: The impact of the various HBV genotypes to global chronic HBV infections..... 7

Figure 4: Overview of the geographical distribution of the HBV genotypes and subgenotypes. The prevalent HBV subgenotypes in South Africa are A1 and D3, with subgenotype A1 being the most prevalent subgenotype 9

Figure 5: A schematic representation of the mature HBV virion..... 10

Figure 6: An illustration of the non-infectious subviral particles (SVP), in the form of either 25 nm spheres or 22 nm filaments. 13

Figure 7: Graphical representation of HBV Polymerase showing the terminal protein (TP), spacer, polymerase/reverse transcriptase (Pol/RT) and RNase H regions. 14

Figure 8: A Schematic Representation of the Hepatitis B Virus Life Cycle. 18

Figure 9: A diagram of the HBV wild-type, occult and deletion constructs employed in this study 28

Figure 10: Overview and strategy of the techniques included in the study..... 29

Figure 11: Schematic diagram of the protocol for the manual subcellular fractionation of cultured cells 41

Figure 12: Schematic representation of the Immunoblotting procedure 46

Figure 13: A summary of the ELISA procedure 50

Figure 14: The previously constructed subgenotype A1 1.28 mer replication competent plasmids utilized in this study..... 52

Figure 15: An illustration of the A1 WT SW plasmid construct highlighting the 784 bp region that was replaced with either SHH011A, SHH045A or SHH167A subgenomic deletion fragments or the SHH193A occult full-length fragment. 54

Figure 16: Agarose gel (0.8%) electrophoresis of the plasmid restriction digestions of the wild-type, occult and deletion mutant strains 57

Figure 17: Agarose gel (1.2%) electrophoresis of the PCR amplicons generated from the mycoplasma detection assay 58

Figure 18: A measurement of the transfection efficiency using GFP expression. 59

Figure 19: A Ponceau stained blot comprising of whole cell lysate and the five fraction extracts of interest 60

Figure 20: Panel A represents the original Ponceau stained blot comprising of the five fraction extracts of interest 61

Figure 21: An example of the possible rearrangement of the sample loading to demonstrate how blots can be easily distinguished based on the distinctive banding pattern of the protein migration for the various fractions 62

Figure 22: An illustration of two trials both conducted with 2µg and 4µg protein for each fraction as indicated by panels A to D 64

Figure 23: Summary of the optimization for the manual subcellular fractionation 66

Figure 24: The control antibodies Anti-Cytokeratin 18, Anti-Calreticulin and Anti-Histone H3 selected to identify each fraction of interest as well as the Anti-eGFP 68

Figure 25: Mouse monoclonal antibody against the S region of HBsAg stained in the unfractionated samples of the wild-type, deletion mutant and occult strains 69

Figure 26: Mouse monoclonal antibody against the S region of HBsAg stained in each fraction of interest, namely; the cytosolic, membrane-bound and nuclear fractions..... 71

Figure 27: The extracellular HBeAg expression in cultured Huh7 cellular supernatants. The two-way ANOVA statistical analysis of the negative controls..... 73

Figure 28: The extracellular HBeAg expression in cultured Huh7 cellular supernatants of the test sample constructs and positive controls at day 1, 3 & 5 time points analyzed by the two-way ANOVA statistical analysis 74

Figure 29: The extracellular HBsAg expression in cultured Huh7 cellular supernatants of the test sample constructs (011A, 045A, 167A, 193A) and positive controls (A1 WT and SW) at day 1, 3 & 5 time points analyzed by the two-way ANOVA statistical analysis..... 75

Figure 30: The F-test statistical analysis employed to measure the statistical relationship / association of HBsAg expression between each respective sample in relation to the SW wild-type backbone..... 76

APPENDICES: TABLE OF FIGURES

Figure A.1: Ethics clearance certificate..... 88

Figure A.2: Creative Commons Attributions Non-Commercial License agreement. 89

Figure D.1: The HBV Subgenotype A1 Over-length Wild-type constructed according to Bhoola et al (2014) 104

Figure D.2: Step-by-step protocol of the computational construction of the plasmid map... 105

Figure D.3: An illustration of the SnapGene software employed to simulate the restriction digestions of *Bam*HI, *Eco*NI, *Ssp*I and *Xba*I 106

Figure D.4: A comparison of the predicted restriction digestion contrasted with the actual restriction digestions 107

Figure E.1: The Complete Sequence of the 1.28 mer Over-Length HBV Subgenotype A1 Wild-type Clone employed to generate the computational plasmid construct..... 111

Figure F.1: The Invitrogen Life Technologies pcDNA^{TM} 4/TO expression vector was employed as a negative control in this study 112

Figure G2.1: The HBeAg ELISA plate set up for the wild-type, deletion mutant and occult strains 115

Figure G2.2: The HBsAg ELISA plate set up for the wild-type, deletion mutant and occult strains 116

Figure H.1: An illustration of a haemocytometer 117

Figure I. 1: The Thermo Scientific GeneRuler 1 kb DNA Ladder..... 119

Figure I. 2: The Bio-Rad Laboratories Precision Plus Protein™ WesternC Standards™ 120

LIST OF TABLES

Table 1: *BamHI, EcoNI* & *XbaI* Restriction Digestion Setup (10µl reactions)..... 32

Table 2: Volume of Buffer required per 10µl of Packed Cell Volume 39

Table 3: The Preparation of Protein BSA Standards..... 42

Table 4: The predicted restriction digestions of the various plasmids used in the study 55

APPENDICES: LIST OF TABLES

Table B1: Reagents composition for plasmid preparation 90

Table B2: Reagents composition for Cell culture & Mycoplasma detection Assay 93

Table B3: Reagents composition for the Subcellular Fractionation Protocol 94

Table B4: Reagents composition for the Protein Concentration Determination Assay 96

Table B5: Reagents composition for the Immunoblotting Assay..... 96

Table C1: List of sequencing primers utilized to determine the sequences of HBV clones ... 103

Table D.1: Restriction Digestions Comparison Summary 108

Table G1.1: PCR Reaction Set Up for the Mycoplasma Detection Assay..... 113

Table G1.2: PCR Cycling Parameters for the Mycoplasma Detection Assay..... 114

LIST OF ABBREVIATIONS AND ACRONYMS

ADV	Adefovir
ALT	Alanine Aminotransferase
Anti-HBs	Hepatitis B Surface Antibody
Anti-HBe	Hepatitis B E Antibody
Au	Australia antigen
APS	Ammonium Persulfate
BCA	Bicinchoninic Acid
BCP	Basal Core Promoter
BLAST	Basic Local Alignment Search Tool
$CaCl_2$	Calcium Chloride
CAF	Central Analytical Facility
CBNE	Chromatin-Bound Nuclear Extract
cccDNA	Covalently Closed Circular DNA
CEB	Cytoplasmic Extraction Buffer
CF	Cytosolic Fraction
CHB	Chronic Hepatitis B
CPE	Cytoplasmic Extract
CSE	Cytoskeletal Extract
CTD	C-terminal Domain
Cu^{+1}	Cuprous Cation
Cu^{+2}	Cupric Cation
DHBV	Duck Hepatitis B Virus
DMEM	Dulbecco's Modified Eagle's Medium
DMSO	Dimethyl Sulfoxide
DNA	Deoxyribonucleic Acid

EDTA	Ethylenediamine Tetraacetic Acid
ELISA	Enzyme-linked Immunosorbent Assay
ER	Endoplasmic Reticulum
ETV	Entecavir
GFP	Green Fluorescent Protein
GGHs	Ground Glass Hepatocytes
HBeAg	Hepatitis B E Antigen
HBcAg	Hepatitis B Core Antigen
HBsAg	Hepatitis B Surface Antigen
HBV	Hepatitis B Virus
HBx	Hepatitis B X Protein
HCC	Hepatocellular Carcinoma
HIV	Human Immunodeficiency Virus
LB	Luria Broth
LdT	Telbivudine
LHBs	Large Hepatitis B Surface Protein
LMV	Lamivudine
MBF	Membrane-Bound Fraction
MDPI	Multidisciplinary Digital Publishing Institute
ME	Membrane Extract
MEB	Membrane Extraction Buffer
MHBs	Middle Hepatitis B Surface Protein
mTOR	Mammalian Target Of Rapamycin
NaCl	Sodium Chloride
NaOH	Sodium Hydroxide
NEB	Nuclear Extraction Buffer
NTCP	Sodium Taurocholate Cotransporting Polypeptide
NF	Nuclear Fraction

OBI	Occult HBV infection
ORF/s	Open Reading Frame/s
PBS	Phosphate Buffered Saline
PC	Precore
PCR	Polymerase Chain Reaction
PEB	Pellet Extraction Buffer
pgRNA	Pregenomic Ribonucleic Acid
Pol/P	Polymerase
RNA	Ribonucleic Acid
RT	Reverse Transcriptase
SDS	Sodium Dodecyl Sulfate
SDS-PAGE	Sodium Dodecyl Sulfate Polyacrylamide Gel Electrophoresis
SHBs	Small Hepatitis B Surface Protein
SH	Serum Hepatitis
SNE	Soluble Nuclear Extract
SVP	Subviral particles
TBE	Tris-Borate-EDTA
TBS	Tris Buffered Saline
TBS-T	TBS + Tween 20
TEMED	Tetramethylethylenediamine
TLR2	Toll-like receptor 2
TP	Terminal Protein
Tris-HCl	Trisaminomethane Hydrochloride
WHO	World Health Organization
WHV	Woodchuck Hepatitis Virus
WT	Wild-type

UNITS

aa	Amino Acid
bp	Base Pairs
g	Grams
kb	Kilobases
kDa	KiloDalton
L	Litre
mg	Milligram
ml	Millilitre
mM	Millimolar
nt	Nucleotide
µl	Microlitres
µM	Micromolar
V	Volts

CHAPTER 1: INTRODUCTION

1.1 Brief History of Hepatitis B Virus

Epidemics of hepatitis have been recognized since Hippocrates (ca 450 BC). However, in 1885, Lurman documented the first account of an epidemic of 'serum hepatitis' among 191 German ship workers in Bremen, who had received the small pox vaccine enriched with human lymph (Lurman, 1885). Later, in 1963, Baruch Blumberg, identified the Australia antigen (Au), which later led to the discovery of the association of the Au antigen to viral hepatitis, when the recognition of a laboratory technician, diagnosed with jaundice, propelled further studies by Blumberg (Blumberg et al., 1984). Subsequently, in 1968, Alfred Prince identified a serum antigen that was distinctively associated with post-transfusion hepatitis, which he termed the serum hepatitis (SH) antigen (Prince, 1968). Later it was found that the Au antigen and the SH antigen were in fact indistinguishable and the antigen was renamed as the hepatitis B surface antigen (HBsAg). A few years later, David Dane led an electron microscopy study that successfully visualized the full 42 nm particle hepatitis B virion (Dane et al., 1970).

These discoveries were a significant breakthrough in progressing global health and the first step in the advancement of hepatitis screening assays, which furthered the generation of a blood-screening practice that has led to a decline in the incidence of post-transfusion hepatitis (Alter et al., 1972, Blumberg, 1977). This further pioneered the development of an effective vaccine that greatly reduced the global burden of HBV infection (Buynak et al., 1976). Additional studies also associated the presence of HBsAg with chronic liver diseases, including cirrhosis and hepatocellular carcinoma (HCC) (Blumberg et al., 2000, Prince et al., 1975).

However, even with the implementation of an effective vaccination strategy since the 1980s and decades of work between the discovery of hepatitis B virus (HBV) and our present knowledge of the virus, HBV is still a prominent cause of end stage liver diseases. It is estimated that approximately a third of the world's population has been infected with HBV at some point in their lifetime. This highlights the significance of a more complete understanding of HBV biology and pathogenesis (Kwon, 2011, Scaglione and Lok, 2012).

1.2 Classification of the Hepatitis B Virus

Distinctive structural features of the HBV separate it from other families of animal DNA viruses and have resulted in its categorization under the family *Hepadnaviridae*. The family *Hepadnaviridae* is divided into two distinct genera on the basis of their limited host range of infection and divergent genomic sequences. The members of the genus *Orthohepadnaviridae*, which includes HBV, the prototype and woodchuck hepatitis virus (WHV), infects mammals whereas the genus *Avihepativiridae,* which includes the duck hepatitis B virus (DHBV) and heron HBV, infect birds (Seeger and Mason, 2000).

Every division of the *Hepadnaviridae* family is predominantly species specific. Although there is substantial genomic diversity, which occurs among viral species, all hepadnaviruses share numerous mutual traits. For instance, all have preferential tissue tropism for hepatocytes (hepatotropic), they have compact DNA genomes of 3.0–3.3 kb, with overlapping open reading frames (ORFs). Furthermore, by means of utilizing the reverse-transcriptase activity of the polymerase, all hepadnaviruses replicate their DNA genome by reverse transcription of an RNA intermediate (Seeger and Mason, 1996).

Though several other viruses similarly employ reverse transcription for viral replication, hepadnaviruses can be distinguished from these groups by key distinctive characteristics including:

1) The virus has a DNA instead of an RNA genome.

2) The initiation of reverse transcription in HBV replication is protein-primed, which is fundamentally distinctive from retroviral replication though related (Beck and Nassal, 2007a).

These major variations led to the classification of *Hepadnaviridae* as an individual family of viruses (Marion and Robinson, 1983, Seeger and Mason, 2015).

1.3 Epidemiology and Clinical Manifestation of HBV

Although an efficient vaccine for the prevention of HBV has been implemented, resulting in the drastic reduction of HBV incidence, HBV infection still poses a serious public health concern. Globally, over 292 million individuals are chronically infected with HBV (Razavi-Shearer et al., 2018), of which an estimated 10% are diagnosed and only 1% treated (*Figure 1*) (Debarry et al., 2017).



Figure 1: The global rate of diagnosis and treatment of hepatitis B infection. At present it is estimated that only 10% of HBV-infected patients are diagnosed with a 1% treatment rate (Debarry et al., 2017). [Permissions license number: 4537251307696 under John Wiley & Sons, Inc].

HBV infection is associated with a broad range of clinical conditions ranging from acute infection, fulminant hepatitis and chronic infection. Chronic infection with the virus may be asymptomatic but can cause chronic hepatitis B (CHB), cirrhosis, and HCC (Chen, 1993, Ganem and Prince, 2004). Moreover, HCC is the third major cause of cancer-associated mortality worldwide (El–Serag and Rudolph, 2007). Despite the fact that the mode of action of HBV in hepatocarcinogenesis is not fully understood, numerous viral factors have been linked with a greater risk for HCC development, including HBV genotype/subgenotype, viral load, basal core promoter and precore mutations and preS deletions, (Hsu et al., 2011, Liu et al., 2009).

1.3.1 Global HBV genotype distribution

HBV can be divided into nine genotypes, named A to I, with a putative tenth genotype named J. These genotypes have been assigned on the foundation of a sequence variation larger than 4% in the S region or 7.5% to 8% in the complete HBV genome. With a suitable bootstrap support, genotypes A-D, F, H and I have been further grouped into at 35 subgenotypes (Kramvis, 2014, Kramvis et al., 2005). Hyperendemic areas with a high prevalence of hepatocellular carcinoma have been identified in sub-Saharan Africa (genotype A) and East Asia (genotypes B and C) (Cao, 2009).

The genotype distribution found in sub-Saharan Africa is quite distinct with genotype E prevailing in the western/central region and genotype A more predominantly found in the in eastern-southern region (aside from Madagascar) (*Figure 2*). Globally, the HBV genotype distribution displays comparable distribution amongst countries within the same world region. However, across diverse parts of the world it can vary considerably (Velkov et al., 2018).

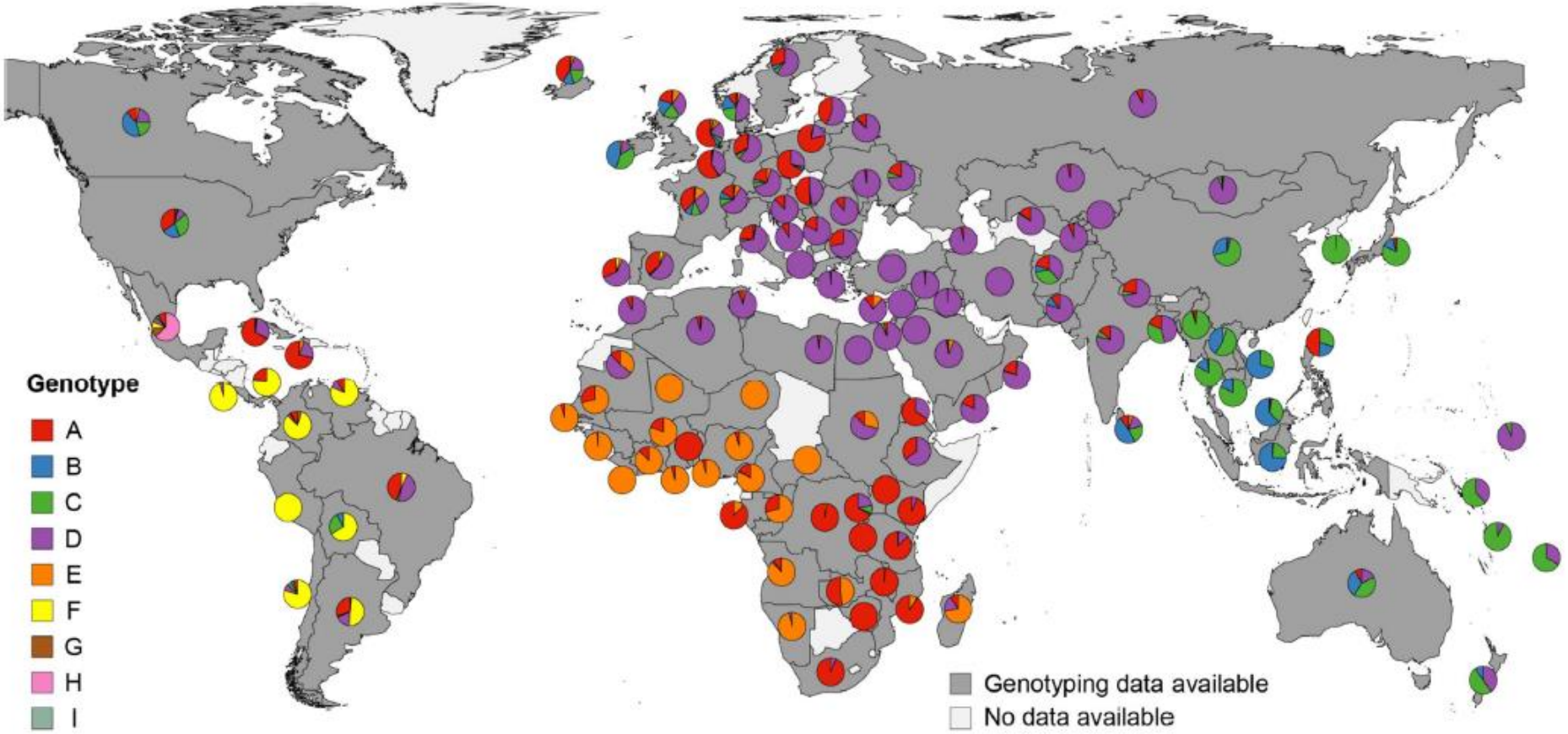


Figure 2: A schematic of the various HBV genotype distribution in each country. The pie charts specify the relative HBV genotype distributions in the respective countries (Velkov et al., 2018). [No special permission/license required for the use of this figure]

1.3.2 Global impact of the different HBV genotypes

The total number of HBV infections within each genotype in each respective country was established by taking into consideration the variations of HBV-infected individuals in diverse regions of the world, in conjunction with the deviations in genotype occurrences (*Figure 3*). The most evident impact can be seen for genotypes with high frequencies in regions harbouring high HBV prevalence, such as sub-Saharan Africa (32.3% of global HBV infections, predominantly genotypes A or E) or Eastern and Southeast Asia (~30% mainly infected with genotypes B or C) (Velkov et al., 2018).

Globally, genotypes A to E were estimated to contribute to 96.2% of global chronic HBV infections with the other 4 genotypes (F to I) only accounting for 1.3% of all infections with incidences predominantly found in Eastern Asia (genotype I) or Latin America (genotypes F to H) (Velkov et al., 2018). Genotypes C, D and E infected 26.1%, 22.1% and 17.6% of all HBV chronic carriers worldwide, respectively. Overall, sub-Saharan Africa, with 12% of the global area, contributes to a third of global HBV infections. The subgenotypes primarily present in Africa are discussed in the next section (*Figure 4*).

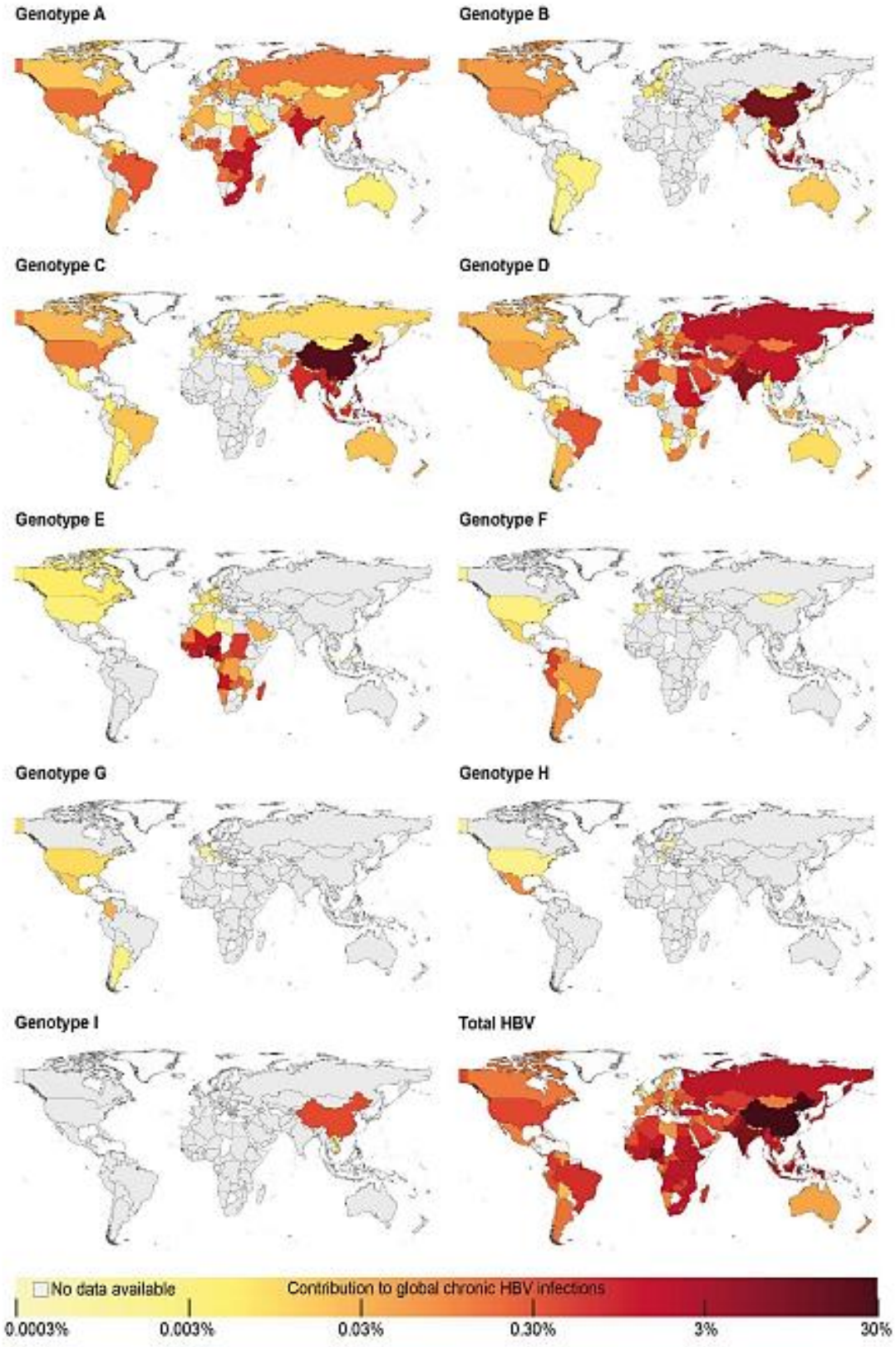


Figure 3: The impact of the various HBV genotypes to global chronic HBV infections. The number of infections is demonstrated as percentage of global chronic HBV infections relative to each country (Velkov et al., 2018). [No special permission/license required for the use of this figure]

1.3.3 Subgenotypes of HBV in Africa

Within genotype A, subgenotype A1, which is the most predominant in Africa (*Figure 4*) (Kimbi et al., 2004, Kramvis et al., 2002), has been associated with increased hepatocarcinogenic ability (Gopalakrishnan et al., 2013, Kramvis et al., 2005, Kew et al., 2005). Moreover, distinctive sequence alterations within subgenotype A1 result in lower HBV DNA levels in individuals infected with this subgenotype in comparison to subgenotype A2 and genotype D carriers (Kimbi et al., 2004, Kramvis et al., 1997, Kramvis et al., 1998, Sugauchi et al., 2004, Sugiyama et al., 2006). Furthermore, subgenotype A1 is connected to early seroconversion of hepatitis B e antigen (HBeAg) to antibodies against HBeAg (Kew, 1994, Kramvis et al., 1997, Kramvis et al., 1998, Song et al., 1984, Tanaka et al., 2004). The seroconversion stage from HBeAg-positive to HBeAg-negative/anti-HBeAg-positive typically heralds resolution of the infection. Moreover, when compared to subgenotype A2, infection with subgenotype A1 presents early HBeAg seroconversion, low viral loads, high transmissibility and higher hepatocarcinogenic potential (Kimbi et al., 2004, Kramvis and Kew, 2007). The predominant HBV subgenotypes in South Africa are A1 and D3, with subgenotype A1 being the most prevalent and most researched in South Africa owing to its predominance and association with serious clinical consequences of infection (Kramvis et al., 2008).

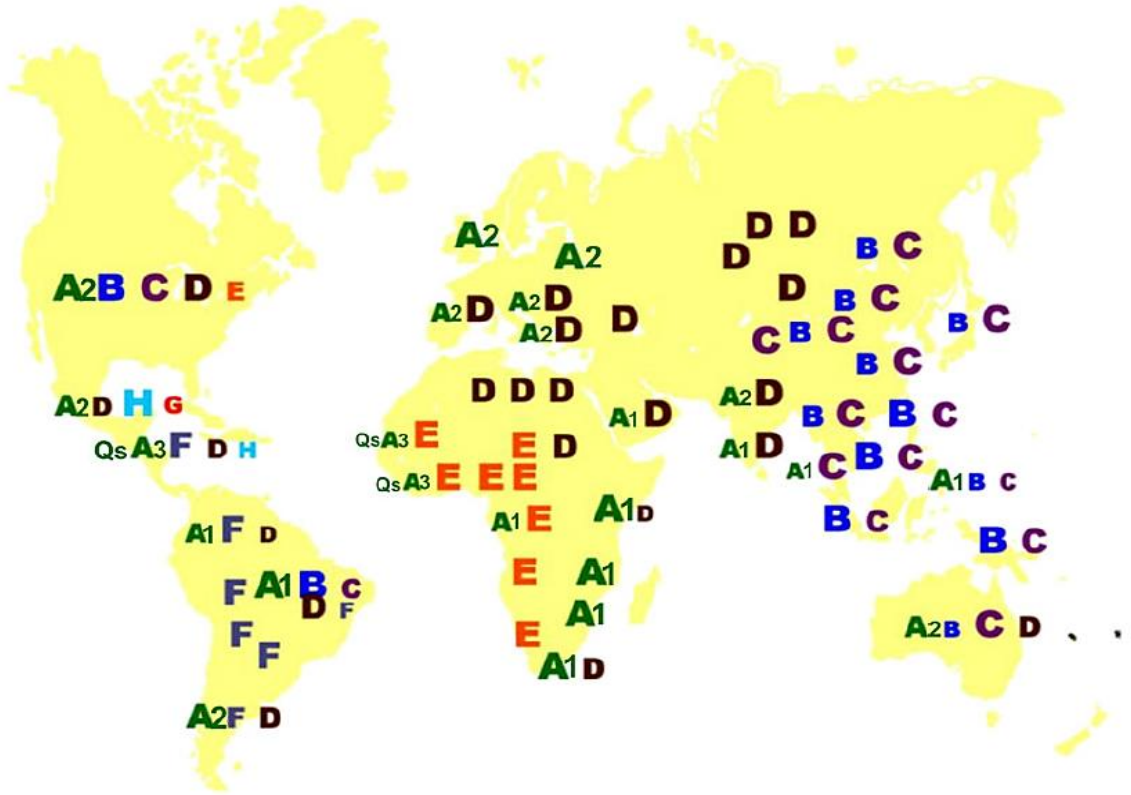


Figure 4: Overview of the geographical distribution of the HBV genotypes and subgenotypes. The prevalent HBV subgenotypes in South Africa are A1 and D3, with subgenotype A1 being the most prevalent subgenotype. The proportional size of the letter/number denotes the relative predominance of the genotype or subgenotype (Kramvis, 2016) [No permission/license required for the use of this figure].

1.4 Hepatitis B Virus Structure

The HBV genome is comprised of a circular, partially double stranded DNA, approximately 3.2 kb in size with all the coding material on the minus DNA strand. In addition, the genome is composed of four overlapping open reading frames (ORFs), namely: X protein (a transcriptional trans-activator), precore/core (e antigen, HBeAg), the core protein (HBcAg), polymerase regions (reverse transcriptase) and finally, the preS1/preS2/S surface proteins of HBsAg: large (LHBs), middle (MHBs) and small (SHBs) proteins (*Figure 5*) (Lee, 1997, Tiollais, 1985).

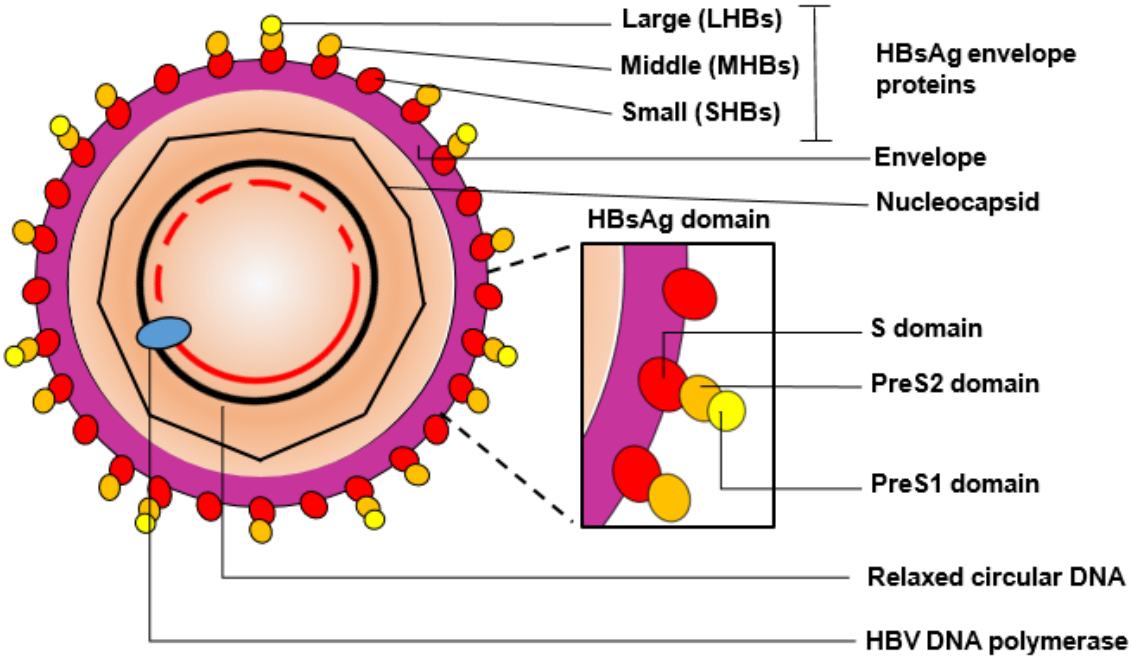


Figure 5: A schematic representation of the mature HBV virion. The virion comprises of two key elements: a nucleocapsid enclosing a partially double-stranded DNA genome bound to HBV DNA polymerase and a viral envelope comprising of the three HBV envelope proteins; large (LHBs), middle (MHBs) and small (SHBs) surface proteins, collectively known as the HBV surface antigen (HBsAg).

1.4.1 Hepatitis B Core Antigen (HBcAg)

The HBcAg is a 21 kDa protein that acts as the primary structural unit for HBV icosahedral capsid (Stannard and Hodgkiss, 1979). HBcAg is translated from the pgRNA (pregenomic RNA) with the first 149 amino acids responsible for the nucleocapsid assembly (Birnbaum and Nassal, 1990). The residual 34–36 amino acids constitute the arginine-rich C-terminal domain (CTD). Studies suggest that several phases of the viral life cycle and maturation is controlled by the phosphorylation of numerous amino acids in the CTD (Ludgate et al., 2012, Melegari et al., 2005). In addition, the CTD is required for pgRNA packaging (Nassal, 1992), and HBcAg also acts as an essential factor in the activation of reverse transcription as well as the maturation of nucleocapsid envelopment (Le Pogam et al., 2005, Lewellyn and Loeb, 2011, Perlman et al., 2005).

1.4.2 Hepatitis B e Antigen (HBeAg)

The HBV precore/secretory antigen more commonly known as the e antigen (HBeAg) is encoded by a region that overlaps a major part of the ORF that encodes the core protein (HBcAg) (Seeger and Mason, 2000). Thus, HBeAg is a secretory version of HBcAg that is not mandatory for replication and appears to promote viral persistence by suppressing both the adaptive and innate host immune response; thus supporting HBV immune evasion (Chen et al., 2004, Chen et al., 2005). It has been demonstrated that the presence of HBeAg leads to the disruption of signaling pathways, which in turn leads to the constraining of the intracellular innate immunity (Lang et al., 2011). In addition, research has shown that the precore directly down regulates Toll-like receptor 2 (TLR2) which is considered to be a crucial innate immune receptor (Lang et al., 2011, Visvanathan et al., 2007). This protein does not form part of the infectious virion and acts as a decoy agent (tolerogen), which may assist in reducing the neutralizing immune response by deterring the response away from the infectious HBV viral particles (Seeger and Mason, 2015, Kramvis et al., 2018).

Over the years, HBeAg has become a fundamental marker of replication and infectivity. Additionally, the levels of serum HBeAg are typically expected to be consistent with viral load and HBeAg seroconversion is recognized as an essential characteristic of the transition to the inactive carrier state of infection (Liaw, 2009). In HBV chronic infection, the loss of HBeAg expression and the emergence of antibodies directed against it (anti-HBe) typically signals the termination of viral replication. HBeAg-negative chronic hepatitis B can result from mutations in the precore and core regions in the presence of anti-HBe, where replicative infection persists and HBV DNA remains at relatively high levels (Schödel et al., 1993).

1.4.3 Surface antigen (HBsAg)

HBV expresses three envelope proteins that are collectively known as the HBV surface antigen (HBsAg). The primary role of the HBsAg proteins is to form the framework for the viral envelope, namely: the large (LHBs), middle (MHBs), and small (SHBs) surface antigen proteins (Blumberg et al., 1967). Furthermore, the envelope proteins are products of the preS/S ORF and share an identical C-terminal, though they have varying lengths as a result of the dissimilarities in their N-terminal. The LHBs protein (39 kDa) is composed of the 108/119 amino acid preS1 domain, which is genotype-specific, the 55 amino acid preS2 domain and the 226 amino acid S domain. The LHBs protein is translated by a separate specific mRNA transcript that is regulated by the preS1 promoter. The MHBs protein (31 kDa) is composed of the PreS2 and S domains and its expression is initiated by the S promoter. Additionally, the SHBs protein (24 kDa) is solely composed of the S region and its expression is also driven by the S promoter (Liang, 2009, Tong and Revill, 2016, Wei et al., 2010).

Of the three S gene products, the LHBs and MHBs proteins are less predominant in comparison to the SHBs protein. These three varying forms of viral proteins are secreted from a HBV-infected cell as a result of the differing expression of each of the three surface antigens. These HBsAg proteins are distributed in different ratios in the mature virion and subviral particles (Bruss, 2004, Ganem and Prince, 2004). The SHBs proteins are the most expressed of the S gene product. The complete infectious HBV virion also known as the Dane particle is comprised of the partially double stranded DNA genome, enclosed in the capsid composed of HBcAg and surrounded by the envelope composed of lipid bilayer in which the three envelope proteins are embedded (Beck and Nassal, 2007b, Seeger and Mason, 1996).

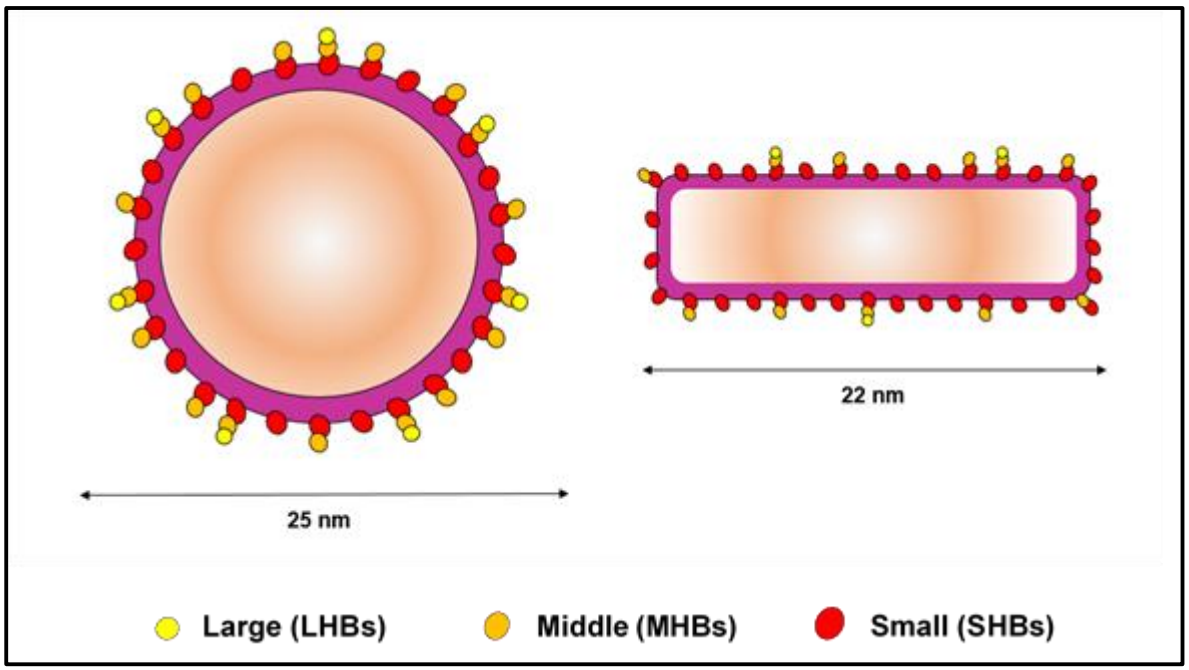


Figure 6: An illustration of the non-infectious subviral particles (SVP), in the form of either 25 nm spheres or 22 nm filaments.

Furthermore, non-infectious subviral particles (SVP) generated from a HBV-infected cell are predominantly composed of SHBs proteins with very little LHBs and MHBs proteins in the SVPs and moderately more LHBs protein in the Dane particles (Liang, 2009, Tong and Revill, 2016). There are two forms of SVPs, either 25 nm spheres or 22 nm filaments (*Figure 6*). The spheres are virtually completely composed of SHBs proteins while the filaments contain low quantities of MHBs proteins and LHBs proteins in addition to the SHBs proteins. Both of these SVPs are present in the serum of infected individuals in a much higher proportion than the mature HBV virions. In fact, the ratio of SVPs can be as high as 10,000-fold greater than that of the infectious virion particles (Bruss, 2004, Ganem and Prince, 2004, Hu and Liu, 2017). Studies suggest that the production of excessive amounts of SVPs plays a role in deterring neutralizing antibodies away from infectious particles, thus leading to immune evasion necessary for an ongoing chronic infection (Bruns et al., 1998).

1.4.4 Polymerase/reverse transcriptase

HBV polymerase (90 kDa protein), encoded by the polymerase (Pol) ORF, consists of four regions, namely: the terminal protein (TP), spacer, polymerase/reverse transcriptase (Pol/RT) and RNase H domains (*Figure 7*) (Bartenschlager and Schaller, 1988, Ganem and Prince, 2004).

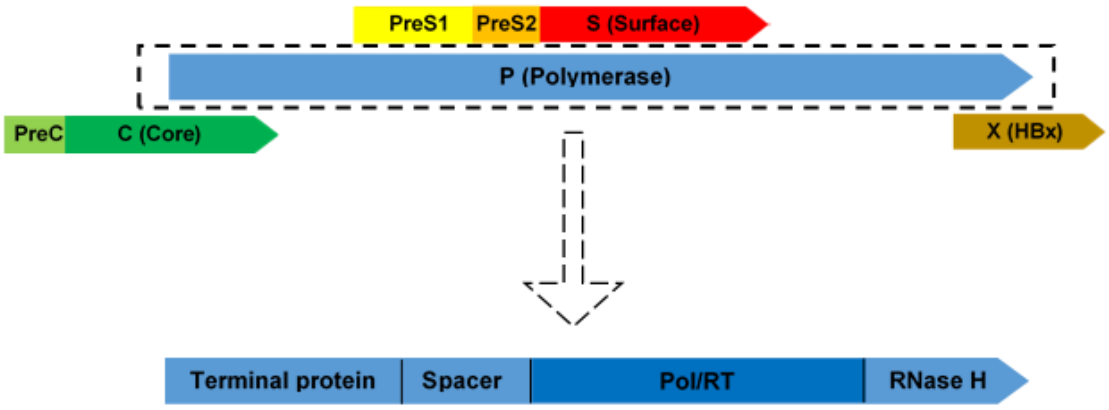


Figure 7: Graphical representation of HBV Polymerase showing the *terminal protein (TP), spacer, polymerase/reverse transcriptase (Pol/RT) and RNase H* regions.

Though several viruses utilize reverse transcription as a method of genome replication, hepadnaviruses employ this mode of viral replication with several distinct mechanisms. Interestingly, the members of the family *Hepadnaviridae*, encode their own polymerase. This is not typical in smaller viruses, which generally utilize the host polymerases to replicate their genome (Flint et al., 2008, Seeger and Mason, 2015). In the *Hepadnaviridae*, a terminal protein domain is responsible for the encapsidation and priming of pgRNA in order to initiate DNA synthesis, while the spacer domain acts as a linker between the TP and the reverse transcriptase (RT) domain (Clark and Hu, 2015). The Pol/RT domain lacks proofreading capacity, resulting in an error prone reverse transcription of the minus DNA strand from a RNA intermediate (Ganem and Prince, 2004, Thio and Locarnini, 2007). The RNase H domain is mandatory for

the removal of the template RNA and is situated at the end of the C-terminal (Clark and Hu, 2015).

Within the polymerase/reverse transcriptase domain of the Pol protein, a YMDD motif (Tyr–Met–Asp–Asp) encodes amino acid positions rt203–206. Studies have shown that mutations within the YMDD motif may result in drug resistance. For example, mutations at position rtM204 are characteristic of Telbivudine (LdT) and Lamivudine (LMV) resistance (Thio and Locarnini, 2007), while rtN236T and/or rtA181T/V mutations can lead to Adefovir (ADV) resistance (Hadziyannis S et al., 2006) and the occurrence of at least three mutations: rtL180M, rtM204V and either rt184G/S, rtS202I or rtM250V can prompt Entecavir (ETV) resistance (Tenney et al., 2004).

1.4.5 HBx protein

HBx is a 17 kDa regulatory protein (154 aa in length) expressed from the X ORF with slight to no sequence homology to any known genes, hence the name "X" protein. It can modulate several hepatocyte signaling cascades and factors associated with to mechanisms that induce cellular transformation. HBx has been shown to regulate calcium, apoptosis and proliferation signals, among other pathways (Clippinger et al., 2009, Gearhart and Bouchard, 2010b, Gearhart and Bouchard, 2010a, Rawat and Bouchard, 2015).

Unlike mammalian hepadnaviruses, the avian hepadnaviruses do not express the HBx protein (Wei et al., 2010). This knowledge has lead researchers to postulate that HBx protein may have oncogenic potential since hepadnavirus-associated HCC seems to be specific to mammalian hepadnaviruses, which all express a form of the HBx protein while, avian hepadnaviruses (which do not express an HBx protein or express a vastly deviating form) can cause chronic infection without triggering the progression of HCC (Arbuthnot et al., 2000, Bouchard and Schneider, 2004). Various studies have provided considerable evidence that support the role of

HBx as an essential factor during HBV replication. More specifically, studies have shown that HBx binds to cccDNA (Belloni et al., 2009) and is mandatory for transcription from cccDNA and thus, downstream HBx-mediated effects are a prerequisite for HBV replication (Lucifora et al., 2011, Seeger and Sohn, 2014). The non-existence of an established model for the study of HBV and HBx has created some difficulty in the understanding of the overall effects of HBx expression in viral replication (Slagle et al., 2015).

1.5 Hepatitis B Virus Replication Cycle

HBV is distinctive amongst other human viral pathogens, as it is a DNA virus that replicates by reverse transcription of a RNA intermediate, the pregenomic RNA (*Figure 8*). HBV initiates replication by binding to a HBV-preS-specific cellular entry receptor expressed on hepatocytes, the bile acid transporter designated sodium taurocholate cotransporting polypeptide (NTCP) (Yan et al., 2012). Once bound the virus is internalized by endocytosis into the cytoplasm where the DNA is uncoated. The DNA is transported to the nucleus where it is then converted to the covalently closed form (cccDNA), which serves as a template for transcription of viral RNA, including the pregenomic RNA. Thereafter, the RNAs are transported to the cytoplasm, where the proteins are translated followed by viral assembly. Then, the pregenomic RNA, which is packaged into subviral core particles in conjunction with a virus-encoded reverse transcriptase (RT), is reverse transcribed into the viral DNA. Finally, the core particles with mature DNA are then able to assemble with viral envelope proteins and form mature virions by budding into the endoplasmic reticulum, after which the virus is transported to the cell surface and released (Beck and Nassal, 2007b, Seeger and Mason, 1996) or recycled to the nucleus to maintain a reservoir of cccDNA.

Although HBV is a DNA virus, it has a high mutation rate owing to its replicative approach, which employs a reverse transcriptase lacking proofreading activity, causing several variants at

each cycle of replication. Since HBV lacks proofreading activity, errors in HBV replication occur at a much greater rate than in other DNA viruses. As a result of this low reliability of the polymerase, the high replication rate and the overlapping reading frames, mutations emerge throughout the genome and they have been observed in both the non-structural and structural genes (Kim et al., 2014), although the overlapping reading frames, place a constraint on the development of mutations in all regions of the genome (Mizokami et al., 1997).

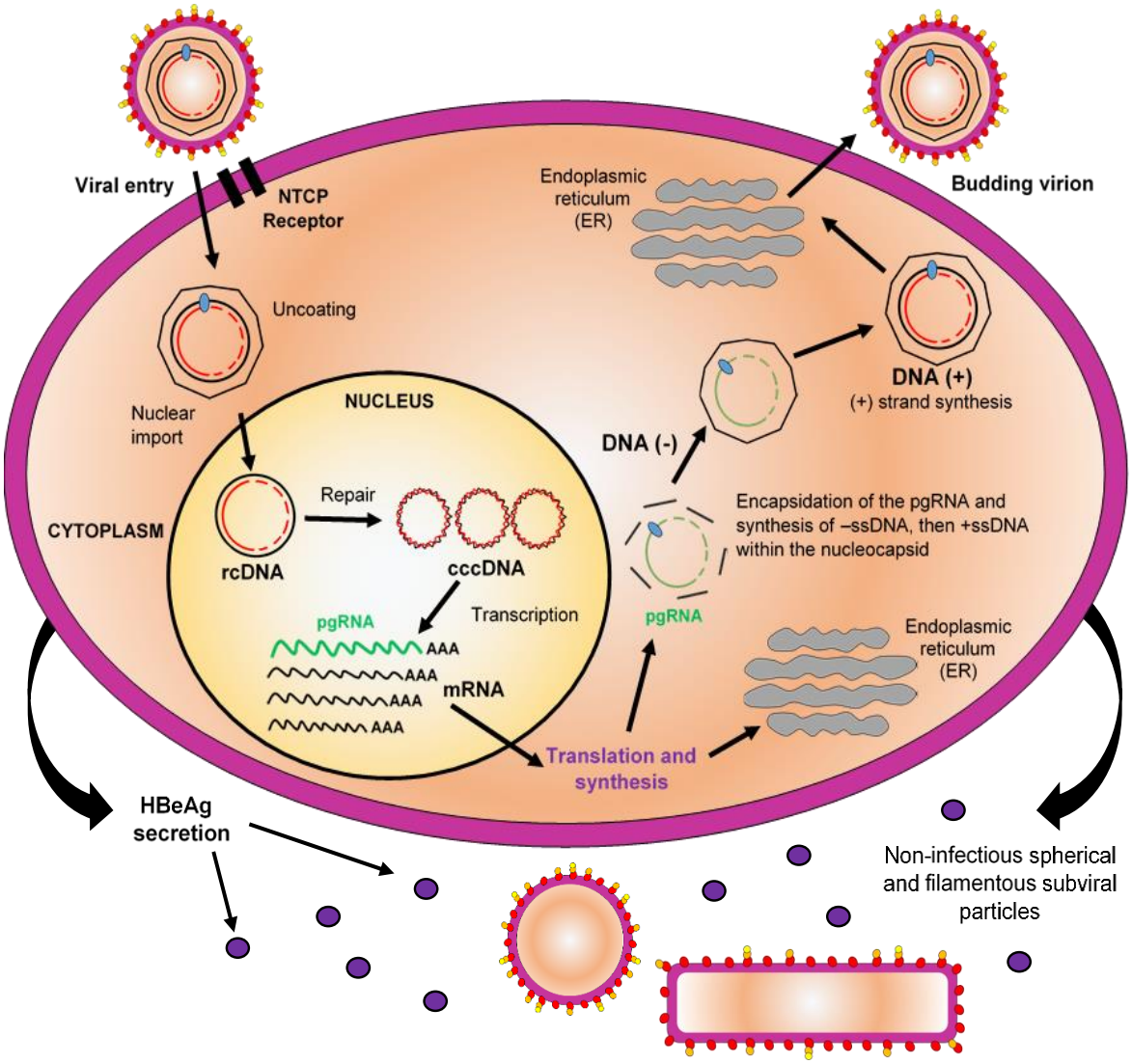


Figure 8: A Schematic Representation of the Hepatitis B Virus Life Cycle.

1.6 HBsAg Deletion Mutations: PreS1 and PreS2 Deletion Mutations

As previously mentioned, the preS1, preS2 and S ORFs encode three envelope proteins; LHBs, MHBs and SHBs, respectively. All three types of proteins are detected as HBsAg protein and are major components for viral assembly and adhesion to hepatocytes. Furthermore, this surface antigen, HBsAg, contains the major B cell epitope, the "a" determinant, which is situated in the major hydrophilic region (MHR – amino acids: 99-169) – this is a primary target for neutralizing antibodies (Petit et al., 1986). Additionally, the preS region includes both the B-cell and T-cell epitopes that facilitate immune interactions, hepatocyte binding sites that assist in viral adhesion and other functional domains. Consequently, the preS region performs several critical functions in viral-host interactions, HBV replication and infection (Chen et al., 2006, Kuroki et al., 1990, Sobotta et al., 2000). It has been demonstrated that mutations, which result in a conformational change within the "a" determinant, may affect the antigenicity of HBsAg, which is fundamental for stimulating defense antibodies. Thus, these mutations may be responsible for the virus escaping vaccine initiated immunity, anti-HBV immunoglobulin treatment and generating false negative results in serological assays (Chisari, 1992, Echevarría and Avellón, 2008).

PreS deletions, identified in the preS1 and preS2 regions, result in a decline in the synthesis and secretion of small surface antigen, which has a tendency to amass in the hepatocytes, particularly in the endoplasmic reticulum (Fan et al., 2001). This has been thought to cause stress in the ER, which consequently results in oxidative DNA impairment that generates mutagenesis and HCC (Huang et al., 2005, Hung et al., 2004, Wang et al., 2003). Furthermore, some mutations in the preS1/S region appear to be responsible for the inactivation of the preS2/S region promoter leading to an impediment of HBsAg secretion. Previous studies revealed that several preS1/preS2 alterations, including deletions and start codon mutations, occurred at a higher frequency in HBV isolates from patients at the later stage of chronic HBV infection and in the course of fulminant hepatitis (Chen et al., 2006, Pollicino et al., 1997,

Sugauchi et al., 2003). HCC patients have a greater frequency of HBV with preS deletions (Chen et al., 2006) and preS deletions have been shown to be independent risk factors for HCC progression (Chen et al., 2008, Yin et al., 2010).

The current availability of information regarding the role of other HBV mutations in preS or S regions in HCC is inadequate. In addition, distinct clinical and virological features of the HBV infection have been described in varying geographical regions of the world where different genotypes/subgenotypes circulate and are progressively related with the genetic diversity of the virus (Kurbanov et al., 2010).

1.7 HBV infection

Chronic HBV infection occurs in an estimate of 5-10% of instances involving HBV-infected adults with a substantially higher rate in infants (Yim and Lok, 2006). HBV-infected patients symptomatically display liver inflammation (i.e. hepatitis) accompanied with abdominal pain, jaundice and nausea. In several instances of HBV infection, HBV-infected individuals are asymptomatic and acute infections commonly clear within six months with untraceable DNA viral loads and anti-HBs expression (Lamontagne et al., 2016). Thus, the onset of chronic HBV infection is signaled by the persistence of detectable HBsAg expression for a minimum of six months subsequent to early infection.

In the immune tolerance stage, HBV infections are distinguished by the presence of high HBeAg and serum HBV DNA levels with minimal liver inflammation and standard ALT (alanine aminotransferase) levels (Takashima et al., 1992). ALT is an enzyme principally located in the kidney and liver cells. Increased levels of ALT have been associated with liver damage and this knowledge has been utilized in screening assays for the testing of liver disease (McPherson and Pincus, 2017). The development of HCC or cirrhosis in immune tolerance phase individuals are considered to be low (Shi and Shi, 2009).

The immune clearance phase is associated with the advancement of fibrosis and enhanced liver inflammation, ultimately resulting in more progressive liver disease. This phase is accompanied with elevated ALT, liver necroinflammation as well as low levels of serum HBV DNA, especially in comparison to the immune tolerant phase. The upsurge in ALT levels is thought to be due to the cytotoxic T-cell facilitated immune response resulting in the damage of hepatocytes infected with HBV (Chang and Liaw, 2014). Thus, extensive periods of this phase has been linked with the progression of HCC and cirrhosis (Liaw et al., 1988). A crucial outcome of the immune clearance phase is the seroconversion of HBeAg, along with untraceable levels of serum HBV and the stabilization of ALT levels. The HBeAg seroconversion in particular is considered to support positive long-lasting results in reducing the risk of liver disease progression (Liaw, 2009).

In the inactive HBsAg carrier phase, there is a lack of HBeAg expression due to anti-HBe seroconversion, a decrease in serum HBV DNA and anti-HBs seroconversion from HBsAg. Additionally, ALT levels become regulated with little to no hepatitis and fibrosis detected (depending on the duration of the immune clearance phase). Though this phase could theoretically be sustained with desirable clinical results (Gish et al., 2015, Yim and Lok, 2006); some patients in this phase reach a reactivation phase with the unprompted recovery of HBV replication due to immune suppression. Though these patients are HBeAg negative, they exhibit higher ALT levels with enhanced necroinflammation (Ganem and Prince, 2004, Gish et al., 2015, Yim and Lok, 2006).

Additionally, more advanced detection applications, such as PCR-based approaches have discovered that numerous individuals considered to be HBV negative (i.e. HBV clearance presumed due to the lack of measureable HBsAg expression) when in reality these patients presented trace amounts of quantifiable serum and viral HBV DNA. These low levels of HBV DNA have been identified in roughly 30% of infected individuals with liver disease with formerly undetermined etiology (Bläckberg and Kidd-Ljunggren, 2000, Chazouilleres et al.,

1994, Yim and Lok, 2006). This finding led to the identification of occult HBV infections (*see later*). Although the occult HBV infections are somewhat incompletely understood, research has shown that occult infections may be a risk factor for the persistence of chronic HBV infections, reactivation and the development of HCC (Pollicino et al., 2004).

Ultimately, though anti-HBV therapies are typically successful at reducing viral loads, these therapies are still not curative and are essentially long term treatments, which in time result in the generation of resistant HBV mutants. Accordingly, explicit strategies have been put into motion to regulate the implementation of antiviral therapies (Gish et al., 2015). In the end, several HBV-infected individuals will progress HBV related liver disease. Though there are currently numerous sanctioned treatments for chronic HBV, there is still no definite cure with a lifetime danger of HCC progression (Gish et al., 2015).

1.8 Occult HBV Infection

Occult HBV infection (OBI) occurs when HBV DNA is detectable in the absence of HBsAg in patients with/without other serological markers of previous HBV infection (Raimondo et al., 2008). To explain this phenotype, several mechanisms have been proposed. However, the modification in the steric configuration in HBsAg molecule, governed by mutations located within the "a" determinant is commonly present. Commercial assays cannot effectively detect these modified HBsAg molecules due to the weak recognition of the immune system (Chen et al., 2012).

Furthermore, HIV infection has been associated as a risk factor for the development of occult HBV infection (Mphahlele et al., 2006). Since liver biopsies are not generally accessible, OBI is typically detected by the analysis of sera. Finally, false occult can be distinguished from true occult when HBV DNA levels are comparable to those detected in HBsAg positive infection

(overt) and are typically due to infection by HBV variants with *S* gene escape mutants, thus generating HBsAg that is not detected in various assays (Raimondo et al., 2008). To date, the clinical impact and repercussions of OBI are not fully understood.

Members of our team have constructed a replication competent subgenotype A1 plasmid from a viral strain derived from a HBsAg-negative patient. This construct did not express HBsAg in cell culture thus mimicking the HBsAg negativity seen *in vivo* (Wolhuter, 2016). The HBsAg expression of the proteins was then further analyzed using immunofluorescence and confocal microscopy and revealed that although the constructs for the wild-type and deletion mutants expressed the envelope proteins at each time point, the occult strain (SHH193A) aggregated HBsAg proteins in the perinuclear region, suggesting that it may be retained in the endoplasmic reticulum and for that reason may not be secreted (Simelane, 2018). This finding was significant as it could explain the HBsAg negative result found in patient serum. Thus, there is great significance in studying these various strains and their role in the progression of occult HBV infection and development of HCC (Kim et al., 2014), especially in the context of subgenotype A1, which prevails in southern-eastern Africa and has been shown to be hepatocarcinogenic than other subgenotypes A2 and D3.

2. Rationale

HBsAg is the first serological marker to emerge in the course of acute HBV infection and is a key indicator of HBV infection. As a result, HBsAg expression is an essential marker for diagnosis analyses (Kao, 2008). The LHBs, MHBs and the SHBs are three types of HBsAg that are expressed from the preS/S ORF, which comprises of three in-frame initiation codons and one termination codon (Summers et al. 1975). The HBsAg proteins have varying sizes since they are translated from separate start codons. LHBs comprises of the preS1 domain, the preS2 domain, and the S domain; MHBs comprises of the preS2 and the S domain whereas the SHBs encompasses the S domain (Gerlich et al, 1992; Schadler & Hildt, 2009). These three proteins occur in dissimilar proportions in the HBV-related particles:

i. The LHBs is located in the following proportions in the various particles:
   virion > filamentous subviral particle > spherical subviral particle
ii. The MHBs has the same relatively low distribution in all HBV-related particles.
iii. The SHBs is the primary constituent of the viral envelope and is released from the cells in highest quantity in comparison to LHBs and MHBs (Heerman, et al., 1984).

Our team has identified strains of HBV in HIV-infected individuals with deletions in the preS1 and/or preS2 regions (Makondo et al, 2012). These mutants are frequent in HBV strains from hepatocellular carcinoma patients (Chen et al, 2006). Thus, since it is evident that preS deletion mutants may play a role in the rapid progression of HCC, it is essential to screen and assess the prevalence of these deletion-mutants, which can act as predictive tools and allow for a more comprehensive model of HBV. This study, which follows the expression of these mutants *in vitro* and may provide some explanation as to whether these deletion mutants and the occult strain may contribute to an increased hepatocarcinogenic potential and the HBsAg-negative phenotype, respectively.

3. Aims and Objectives

The aim of the study will be to determine whether HBsAg deletion mutants and the occult strain of subgenotype A1 HBV affect the subcellular localization, expression and release of the different HBsAgs and HBeAg and their relative ratios *in vitro*.

Following transfection of Huh7 cells with subgenotype A1 replication competent plasmids for the wild-type, occult strain, preS1 and preS2 deletion mutants, the objectives of the study were to:

i. Optimize the methods necessary to follow the intracellular and extracellular expression of the viral proteins.
ii. Determine the intracellular expression of LHBs, MHBs, SHBs in the nucleus, cytoplasm and membrane of the cell.
iii. Determine the extracellular expression of HBV proteins (LHBs, MHBs, SHBs and HBeAg)

CHAPTER 2: MATERIALS AND METHODS

2.1 Ethics

An ethics waiver for this study was obtained the University of the Witwatersrand Human Research Ethics Committee (Medical), Johannesburg, South Africa (Clearance Certificate Number: W-CJ-170308-1) (APPENDIX A: ETHICS CLEARANCE , page 88).

2.2 Materials

The following materials were used in this study:

- Plasmids:
    - 1.28 mer replication competent plasmid for subgenotype A1 (A1-WT) containing an endogenous promoter previously constructed by Dr Nimisha H. Bhoola (Bhoola et al., 2014).
    - 1.28 mer replication competent plasmids for subgenotype A1 containing either deletion mutations in the PreS1/PreS2 region or occult strain of the virus. These plasmids were constructed by the insertion of a region overlapping the 784 bp fragment (nt 2687-250, when numbered from the *Eco*RI restriction enzyme recognition site) (Galibert et al, 1979) into A1-WT. These plasmids, also containing endogenous promoters, were generated by Ms. Suzanne Wolhuter (Wolhuter, 2016). The plasmid construct is illustrated in *Figure 9* (page 28)
- A1-WT SW: Wild-type subgenotype A1 (*Xba*I restriction enzyme recognition site removed from the vector backbone)
- SHH011A: Mutant subgenotype A1 with deletion mutations in the PreS1 (nt. 2900-2929) and PreS2 (nt. 3211-3255) regions and *Xba*I restriction enzyme recognition site removed from the vector backbone

- SHH045A: Mutant subgenotype A1 with a deletion mutation in the PreS2 (nt. 23-55) region and *Xba*I restriction enzyme recognition site removed from the vector backbone
- SHH167A: Mutant subgenotype A1 with a deletion mutation in the PreS2 (nt. 9-54) region and *Xba*I restriction enzyme recognition site removed from the vector backbone
- SHH193A: Occult subgenotype A1 (*Xba*I restriction enzyme recognition site removed from the vector backbone)
- eGFP, a positive control plasmid to measure transfection efficiency was kindly donated by Prof. Hans Will Heinrich-Pette Institute for Experimental Virology and Immunology, University of Hamburg, Hamburg, Germany.

Huh7 cells (Japan Health Science Research Resources Bank, catalogue number JCRB0403) kindly donated by Prof. Charles M. Rice, Rockefeller University

Subcellular Protein Fractionation Kit for Cultured Cells (Pierce Biotechnology by Thermo Fisher Scientific, Waltham, Massachusetts, United States of America)

- Primary Antibodies:
    - Rabbit polyclonal antibody to Calreticulin (Abcam Inc., Cambridge, MA, United States of America)
    - Mouse monoclonal antibody to Cytokeratin 18 [CK-18] (Abcam Inc., Cambridge, MA, United States of America)
    - Mouse monoclonal antibody to Histone H3 (Abcam Inc., Cambridge, MA, United States of America)
    - Mouse monoclonal antibody against the S region of HBsAg (mAb HB1) (kindly donated by Prof. Dieter Glebe, Institute of Medical Virology, Justus-Liebig University, Giessen, Germany)
    - Rabbit polyclonal to GFP (ab6556) antibody (Abcam Inc., Cambridge, MA, United States of America)

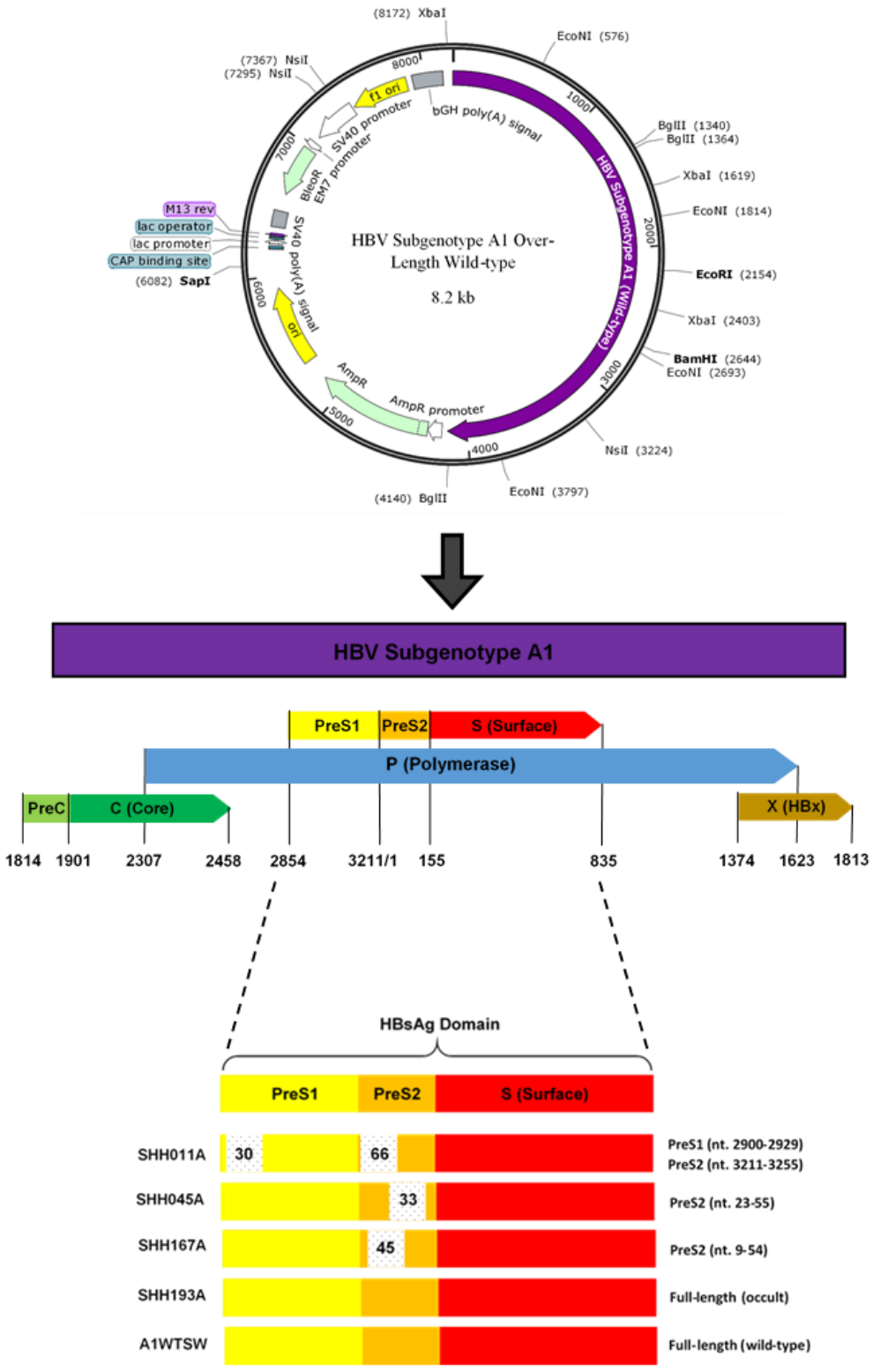


Figure 9: A diagram of the HBV wild-type, occult and deletion constructs employed in this study. The grey dotted boxes (with numbers) represent the size and positions of the deletions in each of the deletion mutant constructs (image adapted from Wolhuter, 2016).

2.3 Overview of Methods

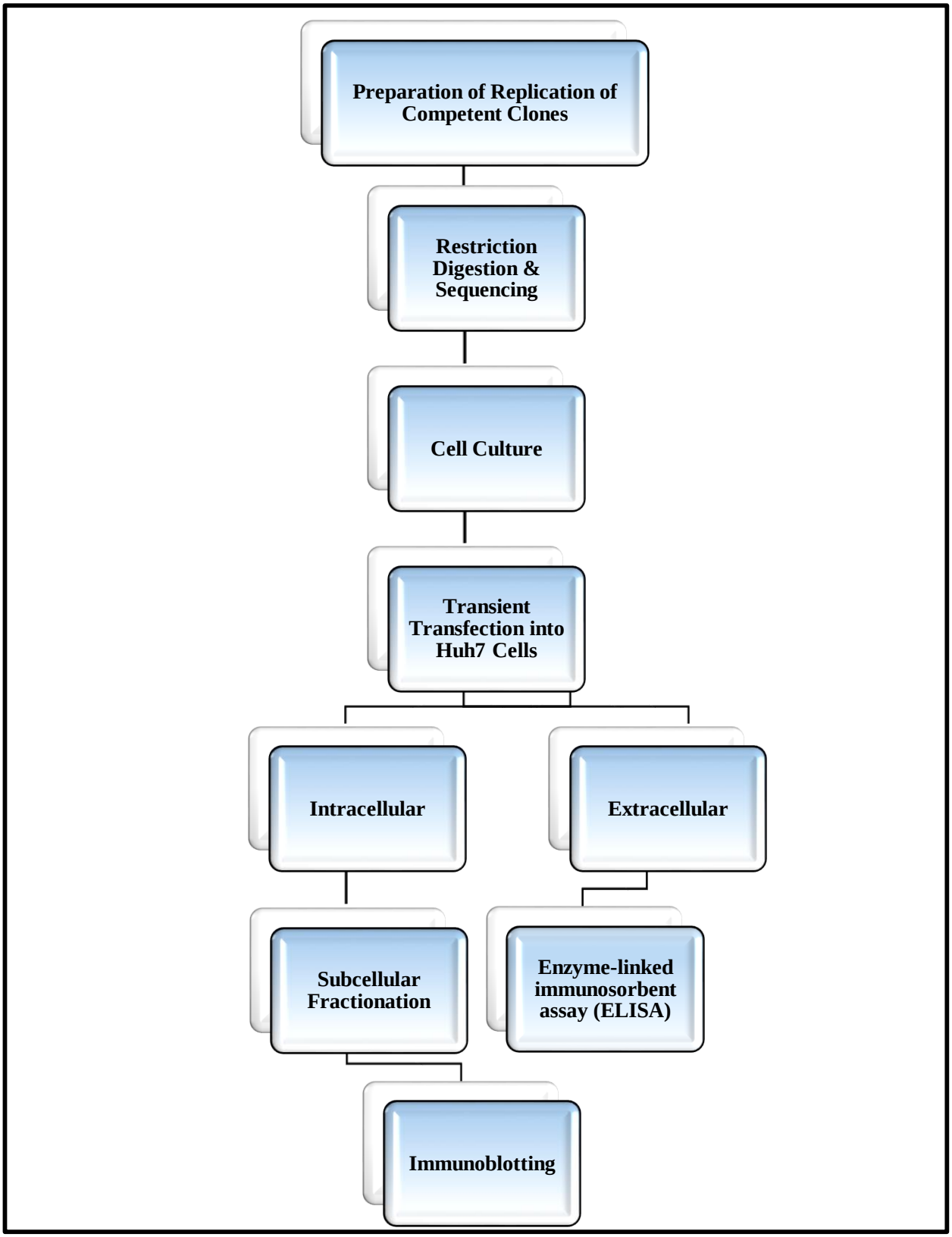


Figure 10: Overview and strategy of the techniques included in the study

2.4 Preparation of Replication Competent Plasmids

2.4.1 Plasmid DNA Extraction

Plasmid DNA was extracted on a large scale using the Plasmid DNA Purification NucleoBond Xtra Maxi EF PC 500 (Macherey-Nagel GmbH & Co. KG, Düren, Germany) following the manufacturer's protocol. A starter culture of Luria Broth (LB) medium with a single colony picked from a freshly streaked agar plate (i.e. from glycerol stocks) was prepared in order to perform the plasmid DNA extraction. Next, the bacterial cell pellet was harvested from this culture by centrifugation at 6000 x g for 15 minutes at 4°C. While the centrifugation was running, the NucleoBond® Xtra column together with the column filter was assembled and equilibrated with 35 ml Equilibration Buffer EQU-EF supplemented on the rim of the column filter and allowed to empty by gravity flow after which the flow-through was discarded. Subsequently, the supernatant was discarded and the cell pellet was resuspended in 12 ml Resuspension Buffer RES-EF supplemented with RNase A. The mixture was pipetted up and down until no clumps were visible.

Thereafter, 12 ml Lysis Buffer LYS-EF was added to the suspension and gently mixed by inverting the tube five times in order to prevent the release of contaminating chromosomal DNA from cellular debris into the suspension. Subsequently, the sample was incubated for 5 minutes at room temperature and immediately after incubation an aliquot of 12 ml Neutralization Buffer NEU-EF was added to the suspension and mixed by gently inverting the tube (until the blue sample lysate turned completely colourless). The crude lysate was then incubated on ice for 5 minutes resulting in the generation of a precipitate containing chromosomal DNA and other cellular components and the reversion of plasmid DNA to its native supercoiled structure that remains in solution, and neutralization of the lysate. Thereafter, the tube containing the bacterial lysate was inverted three times before the suspension was added to the equilibrated column filter in order to avoid the clogging of the filter. Next, the lysate was loaded onto the

NucleoBond® Xtra column filter placed on a 250 ml conical flask and the column was allowed to drain by gravity flow. This enabled the plasmid DNA to bind to the anion exchange resin, after which the flow-through was discarded. Thereafter, 10 ml Filtration Buffer FIL-EF was added to the funnel shaped rim of the NucleoBond® Xtra column filter. Subsequently, the NucleoBond® Xtra column filter was discarded from the NucleoBond® Xtra column. Next, the column was washed with 90 ml Wash Buffer ENDO-EF and allowed to drain by gravity flow. The column was then further washed with 45 ml Wash Buffer WASH-EF and also allowed to empty by gravity flow. Then, the NucleoBond® Xtra column was placed into a new 50 ml polypropylene tube and the plasmid DNA was eluted by the addition of 15 ml Elution Buffer ELU-EF to the column. The buffer was allowed to drain by gravity flow after which the column was discarded. An aliquot of 10.5 ml 100% (v/v) isopropanol (Saarchem (Pty) Ltd. by Merck Chemicals & Laboratory Supplies (Pty) Ltd., Wadeville, Gauteng, South Africa) was then added to the eluted plasmid DNA solution in order to precipitate the plasmid DNA and the mixture was vortexed thoroughly. The sample was then centrifuged at 15000 x g and 4°C for 30 minutes after which the supernatant was discarded. This was followed by the dehydration of the pellet by the addition of 70% (v/v) ethanol to the pellet, briefly vortexed and centrifuged at 15000 x g for 5 minutes after which the supernatant was discarded. Thereafter, the pellet was allowed to dry for 12 hours at room temperature.

The following day, the dried pellet was dissolved by the addition of 300 µl 10 mM Tris and incubated at 37°C, shaking continuously at 300 rpm for 30 minutes, after which the dissolved DNA was transferred to a sterile 1.5 ml microcentrifuge tube, incubated at 37°C with continuous shaking at 600 rpm for 30 minutes. The purity of the recovered plasmid DNA was determined by UV spectrophotometry using a Nanodrop 2000 UV/VIS spectrophotometer, and analysed using the Nanodrop 1000 UV/VIS version 3.7 software (Thermo Fisher Scientific, Waltham, Massachusetts, United States of America), by determining the optical density at 260

and 280 nm. Pure DNA has an ideal A260/A280 ratio of approximately 1.8. Once purity was confirmed, the plasmid DNA was stored at -20°C until further use.

2.4.2 Restriction Digestion

The presence of the correct size and orientation of the ~1.28 mer over-length HBV DNA in the wild-type, occult and deletion clones was confirmed by restriction digestion. Restriction digestion was performed using *Bam*HI, *Eco*NI and *Xba*l (Fermentas Molecular Biology Tools by Thermo Fisher Scientific, Waltham, United States of America) restriction enzymes.

*Table 1: BamHI, EcoN*I *& Xba*I *Restriction Digestion Setup (10µl reactions)*

	Volume (µl)					
	Nuclease-free water	**Buffer *Bam*HI (10X)**	**Buffer R (10X)**	**Buffer Tango (10X)**	**Restriction enzyme**	**Plasmid DNA (1 µg)**
A1 WT SW: 10-fold dilution						
***Bam*HI**	Up to 10 µl	1.0	-	-	1.0	1.0
***Eco*NI**	Up to 10 µl	-	1.0	-	1.0	1.0
***Xba*I**	Up to 10 µl	-	-	1.0	1.0	1.0
SHH011A: No dilution						
***Bam*HI**	Up to 10 µl	1.0	-	-	1.0	1.0
***Eco*NI**	Up to 10 µl	-	1.0	-	1.0	1.0
***Xba*I**	Up to 10 µl	-	-	1.0	1.0	1.0
SHH045A: 10-fold dilution						
***Bam*HI**	Up to 10 µl	1.0	-	-	1.0	1.0
***Eco*NI**	Up to 10 µl	-	1.0	-	1.0	1.0
***Xba*I**	Up to 10 µl	-	-	1.0	1.0	1.0
SHH167A: 10-fold dilution						
***Bam*HI**	Up to 10 µl	1.0	-	-	1.0	1.0

***Eco*NI**	Up to 10 µl	-	1.0	-	1.0	1.0
***Xba*I**	Up to 10 µl	-	-	1.0	1.0	1.0
SHH193A: 10-fold dilution						
***Bam*HI**	Up to 10 µl	1.0	-	-	1.0	1.0
***Eco*NI**	Up to 10 µl	-	1.0	-	1.0	1.0
***Xba*I**	Up to 10 µl	-	-	1.0	1.0	1.0

The reaction tubes were prepared as shown in Table 5, for each reaction 1 µg plasmid DNA was calculated per sample. Thereafter, the reaction tubes were briefly vortexed and centrifuged, then incubated at 37°C for 3 hours. Thereafter, 3 µl Blue/Orange 6X Loading Dye was added to each tube to stop the reaction. The size and orientation of the 1.28 mer greater-than-genome length HBV DNA was then determined by agarose gel electrophoresis, using 0.1 µg/µl O'GeneRuler™ 1 kb DNA Ladder as reference on a 0.8% (w/v) agarose gel (APPENDIX B, Reagent B1.1).

2.4.3 Sequencing

The presence and orientation of the 1.28 mer replication competent plasmids was confirmed by sequencing. Sequencing reactions were performed by the Central Analytical Facility (CAF) at the University of Stellenbosch (Stellenbosch, Western Cape, South Africa). The following sequencing primers were used: pCR-BGH3.1R, Post-BglII, 2058F, 2497R, 2497F, 3188F, 591F and 1040F (APPENDIX C: Primer sequences, page 103). The integrity of the sequence results were analysed with the FinchTV software (version 1.4.0, Geospiza Inc). Subsequently, the sequences were automatically aligned using Nucleotide Basic Local Alignment Search Tool (blastn) (https://blast.ncbi.nlm.nih.gov/Blast.cgi), and manually aligned and edited on the GeneDoc, Multiple Sequence Alignment Editor and Shading Utility software version 2.6.002. Next, the complete genome sequences were assembled on the MEGA software version 7.0

(Kumar et al, 2016). Once the genome was sequenced, a computational plasmid construct was generated and used as a prediction tool (APPENDIX D, page 104).

2.5 Cell Culture and Transfection

2.5.1 Cell Culture

Since HBV is a virus that targets the liver, Huh7, which is a hepatocellular carcinoma cell line, was utilized in this study to investigate the expression of HBV proteins from 1.28 mer replication competent plasmids containing either wild-type or mutant HBV genomes *in vitro*.

A frozen stock of Huh7 cells were thawed at 37°C and maintained in 5 ml complete growth Dulbecco's Modified Eagle's Medium (DMEM) medium (APPENDIX B: Reagent B2.1) in a 25 cm^2 Corning cell culture flask (Corning Inc., Corning, New York, United States of America), and incubated at 37°C in a humidified incubator containing 5% (v/v) carbon dioxide (CO_2). The medium was replaced with 5 ml complete growth DMEM medium every 2-3 days until the cells were at least 70-80% confluent. Once confluent, the medium was removed and the cells were briefly washed with 5 ml 1X phosphate buffered saline (PBS) in order to remove any residual serum, which could inactivate the trypsin. Thereafter, the PBS (APPENDIX B: Reagent B2.2) was discarded and 2 ml 0.25% trypsin-EDTA (Gibco® by Invitrogen, Life Technologies Corporation, Carlsbad, California, United States of America) was added to the cell culture flask, after which it was incubated at 37°C in a humidified incubator containing 5% (v/v) CO_2 for 5 minutes. Upon detachment of the cells, the trypsinization reaction was inactivated by the addition of 3 ml complete growth DMEM medium. To ensure detachment of all the cells from the flask surface, the medium was pipetted up and down against the flask surface six times. Thereafter, the medium containing the cells was transferred to a 75 cm^2 cell culture flask (Corning Inc., Corning, New York, United States of America) containing 5 ml complete DMEM medium and incubated at 37°C in a humidified incubator containing 5% (v/v) CO_2. These Huh7 cells were passaged every 2-3 days and split at a ratio of 1:1, 1:2, 1:4 or 1:5

depending on the confluency of the cells. As a precaution, after every tenth passage the cell culture supernatants were tested for *Mycoplasma* and *Acholeplasma* contamination using the LookOut™ Mycoplasma PCR Detection Kit (Company, City, Country) (for a detailed protocol, please refer to APPENDIX G.1, page 113).

2.5.2 Transient transfection

The transient transfection was carried out as previously described (Bhoola et al, 2014). Twenty four hours prior to transfection, 1.2 x 10^6 Huh7 cells were seeded into 10 cm^2 Corning® non-treated culture dishes (Corning Inc., Corning, New York, United States of America), each made up to a final volume of 10 ml with complete growth DMEM medium. The amount of cells required for each sample was determined using a haemocytometer (APPENDIX H, page 117). The Huh7 cells were then incubated overnight at 37°C in a humidified incubator containing 5% CO_2. The following day, the TransIT®-LT1 Transfection Reagent (Mirus Bio Corporation, Madison, Wisconsin, United States of America) was warmed to room temperature and vortexed gently prior to use. For each transfection sample, an aliquot of 1500 µl serum-free DMEM medium was added to a sterile 1.5 ml microcentrifuge tube and supplemented with 45 µl of TransIT®-LT1 Transfection Reagent.

The sample was then mixed by pipetting up and down after which 15 µg plasmid DNA was added to the mixture and further mixed in the same pipetting manner. Next, the TransIT®-LT1 Transfection Reagent-DNA complex was incubated at room temperature for 20 minutes and then added drop wise to the cells. Subsequently, the culture dishes were gently rocked back and forth to uniformly distribute the TransIT®-LT1 Transfection Reagent-DNA complex followed by incubation at 37°C in a humidified incubator containing 5% CO_2 for 5 days post-transfection. The media was replaced with complete DMEM medium on days 1 and 3 post-transfection. Supernatants were collected on days 1, 3 and 5 post-transfection, aliquoted into microcentrifuge

tubes and stored at -70 °C until further use. Transfected Huh7 cells were harvested on day 5 post-transfection by the addition of 2 ml trypsin-EDTA to each culture dish followed by incubation at 37°C in a humidified incubator containing 5% CO_2 for 5 minutes. An aliquot of 3 ml complete growth DMEM medium was added to inactivate the trypsinization reaction. The transfected Huh7 cells were scraped off the culture dish ensuring that all the transfected Huh7 cells were collected, after which the medium containing transfected Huh7 cells were transferred to a 15 ml polypropylene tube. An aliquot of 2 ml of these medium containing transfected Huh7 cells was transferred to a 2.0 ml microcentrifuge tube and centrifuged at 5000 x g at 4°C for 5 minutes after which the supernatant was discarded. The above-mentioned step was repeated until all the medium containing transfected Huh7 cells had being collected. Thereafter, the transfected Huh7 cells were washed with the addition of 1 ml 1X PBS, which was briefly vortexed, and centrifuged at 5000 x g at 4°C for 5 minutes after which the supernatant was discarded. This step was repeated after which the transfected Huh7 cells were stored at -70°C until further use. Culture dishes containing untreated Huh7 cells and Huh7 cells treated with TransIT®-LT1 Transfection Reagent only, served as the negative controls while Huh7 cells transfected with TransIT®-LT1 Transfection Reagent-eGFP complex served as the positive control.

2.5.3 Transfection Efficiency

The transfection efficiency was measured 1 day post-transfection by determining the number of Huh7 cells that had been successfully transfected with eGFP (Green Fluorescent Protein). Since green fluorescent protein has the ability to fluoresce a bright green when observed under a fluorescence microscope GFP (due to the proteins excitation at 395 nm and emission at 509 nm), this enabled the determination of cells that were successfully transfected. In order to determine the transfection efficiency, the Huh7 cells were viewed under the EVOS™ FLoid™

Cell Imaging Station fluorescence microscope (Life Technologies, Thermo Fisher Scientific) with images captured using the FLoid Software v1.4.

2.6 Preparation of Whole Cell Lysates

The pellets of transfected Huh7 cells (stored at -70 °C), were thawed on ice for 30 minutes. Thereafter, to detach/separate the cells, the tubes were briskly flicked. An aliquot of 100 µl SDS Total Cell Lysis Buffer Working Solution (Appendix B: Reagent B3.10) was then supplemented to each sample, followed by gentle mixing to lyse the cells, and the samples were then incubated at 99 °C for 5 minutes. After incubation, the condensation was collected by briefly centrifuging each tube, after which the samples were sonicated three times for 5 minutes each at using a Bandelin Sonorex with Built-In Heating Ultrasonic Bath (Bandelin, Berlin, Germany). Once the whole cell lysate proteins were extracted, 25 µl of each fraction was set aside for protein quantification. The remaining samples were then supplemented with 25 µl 4X Laemmili buffer (Appendix B: Reagent B5.5), heated at 99°C for 5 minutes and then stored at -20°C until further use.

2.7 Subcellular fractionation

2.7.1 Commercial kit

The harvested pellets of transfected Huh7 cells (stored at -70 °C) were thawed on ice for 30 minutes, and the packed cell volumes were determined for each sample (see *Table 2*). The appropriate volume of Cytoplasmic Extraction Buffer (CEB) (i.e. according to the packed cell volume) were then added to each sample and incubated at 4 °C for 10 minutes with continuous gentle shaking. Thereafter, the samples were centrifuged at 500 x g for 5 minutes and the supernatants generated (i.e. cytoplasmic fractions) were transferred to a sterile pre-chilled 1.5 ml microcentrifuge tube. Subsequently, the appropriate volume of ice-cold Membrane Extraction Buffer (MEB) were supplemented to each pellet sample, and the samples were

vortexed for 5 seconds at the highest setting, followed by incubation at 4 °C for 10 minutes with continuous gentle shaking. The samples were then centrifuged at 3000 x g for 5 minutes and the supernatants produced (i.e. membrane fractions) were transferred to a sterile pre-chilled 1.5 ml microcentrifuge tube. Thereafter, the appropriate volume of ice-cold Nuclear Extraction Buffer (NEB) were supplemented to each pellet sample, the samples were then vortexed for 15 seconds at the highest setting and incubated at 4 °C for 30 minutes with continuous gentle shaking. The samples were then centrifuged at 5000 x g for 5 minutes and the supernatants (i.e. soluble nuclear fractions) were transferred to a sterile pre-chilled 1.5 ml microcentrifuge tube. Subsequently, the appropriate volume of room temperature NEB containing $CaCl_2$ and micrococcal nuclease were added to each pellet and the samples were vortexed at the highest setting for 15 seconds, and incubated at room temperature for 15 minutes. Next, the samples were vortexed at the highest setting for 15 seconds and then centrifuged at 16 000 x g for 5 minutes – the supernatant produced (i.e. chromatin-bound nuclear fractions) were then transferred to a sterile pre-chilled 1.5 ml microcentrifuge tube. Thereafter, the appropriate volume of room temperature Pellet Extraction Buffer (PEB) was supplemented to each pellet sample, and the samples were vortexed at the highest setting for 15 seconds, followed by incubation at room temperature for 10 minutes. Then, the samples were centrifuged at 16,000 x g for 5 minutes and the supernatant produced (i.e. cytoskeletal fractions) were transferred to a sterile pre-chilled 1.5 ml microcentrifuge tube. Once all the fractions were extracted, 25 µl of each fraction was set aside for protein quantification. The remaining sample of each fraction was then supplemented with 50 µl 4X Laemmili buffer (APPENDIX B: Reagent B5.5), heated at 99°C for 5 minutes and then stored at -20°C until further use.

Table 2: Volume of Buffer required per 10µl of Packed Cell Volume

Reagent	Buffer volume (µl) per 10µl packed cell volume
CEB	100.0
MEB	100.0
NEB	50.0
NEB + $CaCl_2$ + Micrococcal Nuclease	50.0
PEB	50.0

2.7.2 Manual protocol

Pellets, which were stored at -80°C were thawed on ice for 30 minutes prior to the subcellular fractionation protocol. Thereafter, 200 µl of ice cold Lysis Buffer A (APPENDIX B, Reagent B3.2) supplemented with 2 µl protease inhibitor cocktail was applied to each pellet and these samples were incubated on an end-over-end rotator for 10 minutes at 4°C. The samples were then centrifuged at 2000 x g for 10 minutes at 4°C. Afterwards, the supernatants of each sample were collected – this fraction set comprised of the cytosolic proteins. Subsequently, the pellets were resuspended in 200 µl of ice cold Lysis Buffer B (APPENDIX B, Reagent B3.3) supplemented with 2 µl of protease inhibitor cocktail, vortexed and then incubated on ice for 30 minutes. The samples were then centrifuged at 7000 x g for 10 minutes at 4°C. Thereafter, the supernatants of each sample were collected – this fraction consisted of the membrane-bound proteins from organelles such as the, endoplasmic reticulum, Golgi, mitochondria, etc. After that, 200 µl of ice cold Lysis Buffer C (APPENDIX B, Reagent B3.4) supplemented with 3.5 µL of Benzonase and 2 µl of protease inhibitor cocktail was applied to each sample pellet. These samples were then incubated on an end-over-end rotator for 30 minutes at 4°C to enable the complete solubilisation of the nuclei and digestion of the genomic DNA. Thereafter, the samples were centrifuged at 7800 x g for 10 minutes at 4°C. The supernatants of each sample were then collected – this fraction set consisted of the nuclear proteins. Once the cytosolic,

membrane-bound and nuclear protein fractions were extracted, 25 µl of each fraction was set aside for protein quantification. The remaining sample of each fraction was then supplemented with 50 µl 4X Laemmili buffer (APPENDIX B: Reagent B5.5), heated at 99°C for 5 minutes and then stored at -20°C until further use (*Figure 11*). For this study, control antibodies were selected to test the purity of each fraction. The cytosolic fractions were stained with Anti-Cytokeratin 18, the membrane-bound fractions stained with Anti-Calreticulin and the nuclear fractions were stained with Anti-Histone H3.

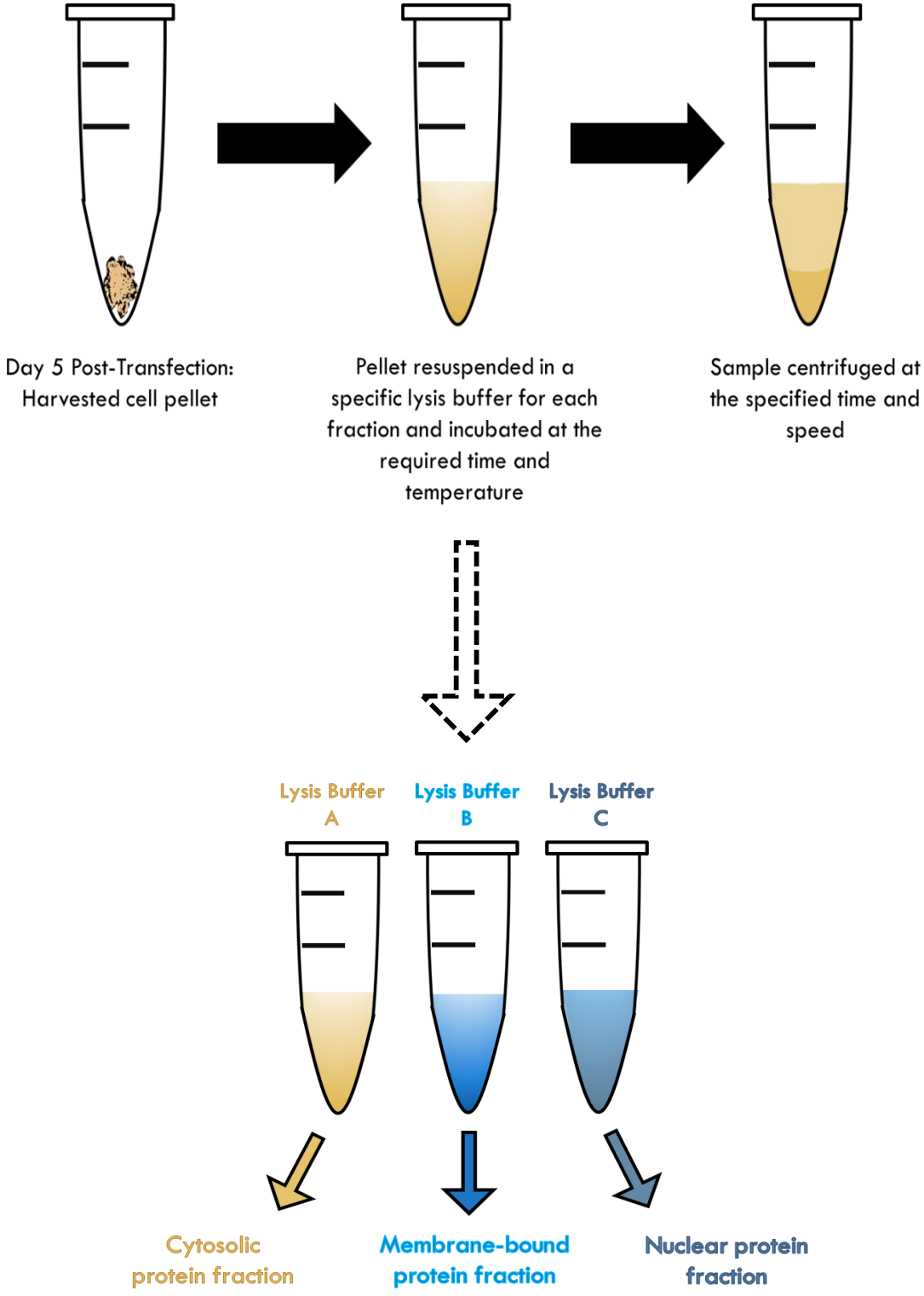


Figure 11: Schematic diagram of the protocol for the manual subcellular fractionation of cultured cells, emphasising the key lysis buffers employed to extract the three fractions of interest namely; cytosolic, membrane-bound and nuclear fractions.

2.8 Protein Concentration Determination Assay

Whole cell lysates (unfractionated) and fractionated sample treatments required protein quantification in order to load the exact amount of protein of each sample in the respective wells. This ensured that the results were consistent throughout the study. Furthermore, by constructing a BCA curve (APPENDIX H, page 118), the precise amount of protein was calculated for each sample prior to loading.

2.8.1 Preparation of Protein Standards

The Pierce® BCA Assay Kit was utilized to quantify the total protein of each sample. This was possible since the assay integrates the renowned biuret reduction of $(Cu)^{+2}$ to Cu^{+1} by protein in an alkaline medium with high precision and the specific colorimetric detection of the cuprous cation (Cu^{+1}) using a distinct reagent containing BCA. The reaction involves the formation of a purple-coloured reaction that develops as a result of the chelation of two BCA molecules with one Cu^{+1} resulting in the formation of a water-soluble complex that has an intense absorbance at 562 nm. *Table 3* displays the preparation of protein standards using 2 mg/ml albumin standard ampules as the stock protein.

Table 3: The Preparation of Protein BSA Standards

Vial	**Volume (µl)**		**BSA Concentration (µg/ml)**
	PBS	**Source of BSA Protein**	
A	0	300 of Stock	2000
B	125	375 of Stock	1500
C	325	325 of Stock	1000
D	175	175 of Vial B	750
E	325	325 of Vial C	500
F	325	325 of Vial E	250

G	325	325 of Vial F	125
H	400	100 of Vial G	25
I	400	0	0

2.8.2 Assay

An aliquot of 25 µl of each standard and duplicate diluted unknown samples (15 µl PBS + 10 µl unknown sample per well) were added to individual wells on a 96-well microplate. Thereafter, 200 µl of BCA working reagent was added to each well and homogenized thoroughly on an IKA-Schüttler MTS4 microplate shaker for 30 seconds. Next, the microplate was covered with a 96-well microplate lid and aluminium foil, then incubated at 37°C for 30 minutes. The microplate was then removed from the incubator and allowed to stand at room temperature for 10 minutes. Lastly, the optical density for each well was determined at 550 nm by using a M640 Microplate Reader (Thermo Fisher Scientific, Waltham, Massachusetts, United States of America).

2.9 Immunoblotting

2.9.1 SDS-PAGE & Protein Transfer

Using the Mini-PROTEAN® Tetra Cell System, the SDS-PAGE analysis was performed. An aliquot of 2 µg of protein sample was loaded onto an SDS-PAGE gel, and electrophoresed at 80V until it reached the separating gel, thereafter it was electrophoresed at 100V until the loading dye reached the bottom of the gel in 1X SDS running buffer. Transfer of proteins from SDS-PAGE gel to nitrocellulose membrane was performed with the Mini-PROTEAN® Trans-Blot Module System. Next, the transfer grid was assembled with sponges and Mini Trans-Blot filter paper being pre-soaked in 1X wet transfer buffer with the air bubbles between the SDS-PAGE gel and the nitrocellulose membrane being removed by rolling a pipette over the filter

paper and sponge prior to sealing the grid. The grid was then placed into the Trans-Blot Module with black side of the grid facing the black side of the module, and the clear side of the grid facing the red side followed by the Trans-Blot Module being placed into the gel tank with the black side of the module being slotted with the black lead, and the red side of the module being slotted with the red lead. Transfer was carried out at 60 V for 75 minutes while continuously stirring 1X wet transfer buffer.

2.9.2 Blocking of the Nitrocellulose Membrane

The success of the transfer was determined by staining the nitrocellulose membrane with 25 ml Ponceau stain for 5 minutes with continuous gentle shaking. The Ponceau stain solution was then removed and the nitrocellulose membrane was washed with Milli-Q water for 10 minutes with continuous gentle shaking. Depending on the success of the transfer, the nitrocellulose membrane was blocked with 25 ml Blocking Solution (APPENDIX B, Reagent B5.3) for 1 hour at room temperature with gentle continuous shaking after which the solution was discarded.

2.9.3 Binding of Antibodies

The nitrocellulose membrane was incubated overnight at 4°C with continuous gentle shaking and 25 ml primary antibody dissolved in 5% (w/v) fat-free milk powder dissolved in TBS-T buffer diluted as follows: 1:25000 rabbit polyclonal antibody against GFP (Abcam Inc., Cambridge, United States of America), 1: 1000 mouse monoclonal antibody against the S region of HBsAg (mAb HB1) (kindly donated by Prof. Dieter Glebe, Institute of Medical Virology, Justus-Liebig University, Giessen, Germany) and 1:1000 mouse monoclonal antibody against HBeAg (kindly donated by Dr Peter Revill, Victorian Infectious Diseases Reference Laboratory, Melbourne, Australia). In addition, the following antibodies were employed as control antibodies: 1:50000 mouse monoclonal to Cytokeratin 18 (CK-18),

1:25000 rabbit monoclonal to Calreticulin and 1:50000 mouse monoclonal to Histone H3 which bind to the cytosolic, membrane-bound and nuclear protein fractions respectively. The following day, the primary antibody was removed, and the nitrocellulose membrane was washed with the addition of 25 ml TBS-T, shaking continuously three times, at 10 minutes per wash, after which the TBS-T buffer was discarded. The nitrocellulose membrane was then incubated for 1 hour with continuous gentle shaking with 25 ml secondary antibody. The secondary antibody was reliant on the species of the primary antibody. Next, the secondary antibody was dissolved in Blocking Solution (APPENDIX B, Reagent B5.3) in combination with 1:50000 Precision Protein™ StrepTactin-HRP conjugate and incubated with either 1:3000 goat anti-mouse IgG (H+L)-HRP conjugate or 1:3000 goat anti-rabbit IgG (H+L)-HRP conjugate (all were purchased from Bio-Rad Laboratories, Hercules, United States of America). Thereafter, the secondary antibody was discarded, and the nitrocellulose membrane was washed with the addition of 25 ml TBS-T, shaking continuously three times, at 10 minutes per wash after which the TBS-T was discarded.

2.9.4 Development of Protein Signal of Interest

Lastly, the nitrocellulose membrane was then placed on a clear overhead projector sheet and the protein signal of interest was developed using the SuperSignal® West Dura Extended Duration Substrate (Pierce Biotechnology). This assay involved the drop wise addition of 600 µl SuperSignal® West Extended Duration Substrate Working Solution over the entire nitrocellulose membrane after which the nitrocellulose membrane was immediately viewed and images captured (*Figure 12*).

2.9.5 Stripping of Nitrocellulose Membrane

The nitrocellulose membrane was then incubated for 1 hour, shaking continuously in Stripping Solution (APPENDIX B, Reagent B5.15) in order to remove the antibody before being reprobed with a new primary antibody.

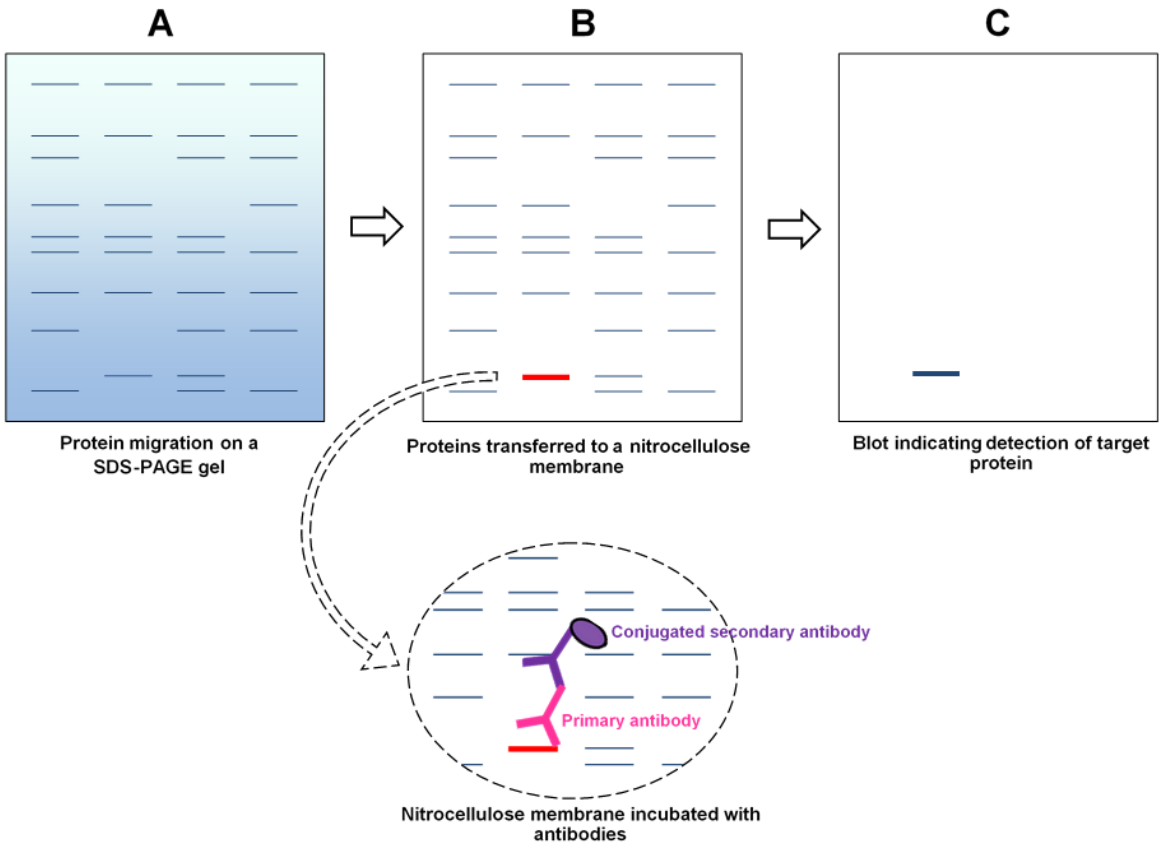


Figure 12: Schematic representation of the Immunoblotting procedure. (A) A hypothetical unstained immunoblot obtained once transferred from an SDS-PAGE gel. (B) The incubation of the immunoblot with primary antibodies directed against a band/protein of interest, followed by the binding of the conjugated secondary antibody to primary antibody which, (C) results in the detection of the target protein.

2.10 Enzyme-linked Immunosorbent Assay (ELISA)

2.10.1 HBeAg ELISA Protocol

The ETI-EBK PLUS (HBeAg) DiaSorin (Sallugia, Italy) commercial kit was utilized in this study. It is exclusively designed for the detection of HBeAg with 96 well ELISA plates (*Figure 13*) coated in mouse monoclonal antibodies that are specific for the HBeAg.

2.10.1.1. Reagent preparation

Microwells were set for the calibrators, controls and test samples as follows; one blank well (well A1) containing only the substrate/chromogen and stop solution, the calibrator tested in triplicate in wells B1, C1 and D1, a negative control (well E1) and a positive control (well F1). For the test samples, a loading datasheet was prepared prior to initiating the protocol in order to minimise human error (APPENDIX G.2, page 114). Prior to the commencement of the assay, all reagents were brought to room temperature (20-25°C) unless specified otherwise. In addition, the working wash buffer and working enzyme tracer solutions were prepared according to the manufacturer guidelines (APPENDIX G.2, page 114). Once all the reagents were primed to room temperature, frozen test samples were thawed and vigorously vortexed before proceeding.

2.10.1.2. Assay procedure

An aliquot of 50 µl incubation buffer was added to all the wells (excluding the blank well). This was then followed by the addition of 100 µl of either the calibrator, controls or sample to its respective microwell. The incubation buffer is light blue and will turn to a green or dark blue on the addition of the calibrators, controls or samples. The microwell plate was then covered with a lid and incubated at 37°C for 2 hours (± 10 minutes). Next, the liquid from the microwells was removed and the plate was placed into the Wellwash™ Microplate Washer (Thermo Fisher Scientific, Waltham, Massachusetts, United States of America). The microwell plate washer

parameters were set at: delivery of 370 µl working wash buffer to each well, soak time at 30 seconds and five wash cycles. Thereafter, residual working wash buffer was removed by inverting the microplate onto a paper towel. Immediately after, 100 µl working enzyme tracer was supplemented into each well (excluding the blank well). The microwell plate was then covered with a lid and the plate was gently tapped on the sides to release any trapped air bubbles in the liquid. The microwell plate was then incubated for 60 minutes (± 5 minutes) at 37°C – the timing of this incubation step is critical. The liquid from the microwells was then aspirated and the plate was placed into the microwell plate washer under the parameters aforementioned. Once more, the residual working wash buffer was removed by inverting the microplate onto a paper towel. Immediately after, 100 µl chromogen/substrate was added to all the microwells including the blank well. The microwell plate was then covered with a lid and aluminium foil, followed by incubation for 30 minutes (± 2 minutes) at room temperature. For this step, it is vital that the microwells are not exposed to direct or intense light and the time limits are not exceeded. Thereafter, 100 µl stop solution was supplemented into each well in the same order that the chromogen/substrate was added. Within 1 hour after the addition of the stop solution, the absorbance values were recorded at 450/630 nm on the M640 Microplate Reader (Thermo Fisher Scientific, Waltham, Massachusetts, United States of America).

2.10.2 HBsAg ELISA Protocol

The Murex® HBsAg Version 3 DiaSorin (Sallugia, Italy) commercial ELISA kit is exclusively designed to determine the presence of HBsAg by utilizing 96 well ELISA plates (*Figure 13*) coated in mouse monoclonal antibodies specific for various epitopes on the ‘a’ determinant of HBsAg, thus inducing a highly sensitive assay for both wild-type and some mutant strains of HBV.

2.10.2.1. Reagent preparation

A sample loading datasheet was prepared prior to commencing the procedure (APPENDIX G.3, page 116) and all reagents were brought to room temperature (unless specified otherwise). The negative control duplicate samples were assigned to wells A1 and B1 and a positive control sample in well C1 as specified in the manufacturer guidelines. In addition, the working wash buffer and substrate solution was prepared according to the kit protocol (APPENDIX G.3, page 116). Once all the reagents were primed to room temperature, frozen test samples were thawed and vigorously vortexed before performing the assay.

2.10.2.2. Assay procedure

An aliquot of 25 µl sample diluent was added to each well with the exception of the blank. Thereafter, 75 µl of sample/control was added to its designated well, with the controls dispensed last. The microwell plate was then covered with a lid and incubated for 60 minutes at 37°C (± 1°C). Next, 50 µl of conjugate was supplemented into each well. The microwell plate was then placed on an IKA-Schüttler MTS4 microplate shaker for 10 seconds. The plate was then covered with a lid and incubated for 30 minutes at 37°C (± 1°C). After incubating, the liquid from the microwells was removed and the plate was placed into Wellwash™ Microplate Washer (Thermo Fisher Scientific, Waltham, Massachusetts, United States of America). The microwell plate washer parameters were set at: delivery of 500 µl working wash buffer to each well, soak time at 30 seconds and five wash cycles. Thereafter, residual working wash buffer was removed by inverting the microplate onto a paper towel. Immediately after washing, 100 µl substrate solution was added to each well. The plate was then covered with a lid and incubated for 30 minutes at 37°C (± 1°C). A purple colour should develop in reactive samples. Next, 50 µl stop solution was supplemented to each well. Within 15 minutes after the addition of the stop solution, the absorbance values were recorded at 450 nm using 620-690 nm as the

reference wavelength on the M640 Microplate Reader (Thermo Fisher Scientific, Waltham, Massachusetts, United States of America).

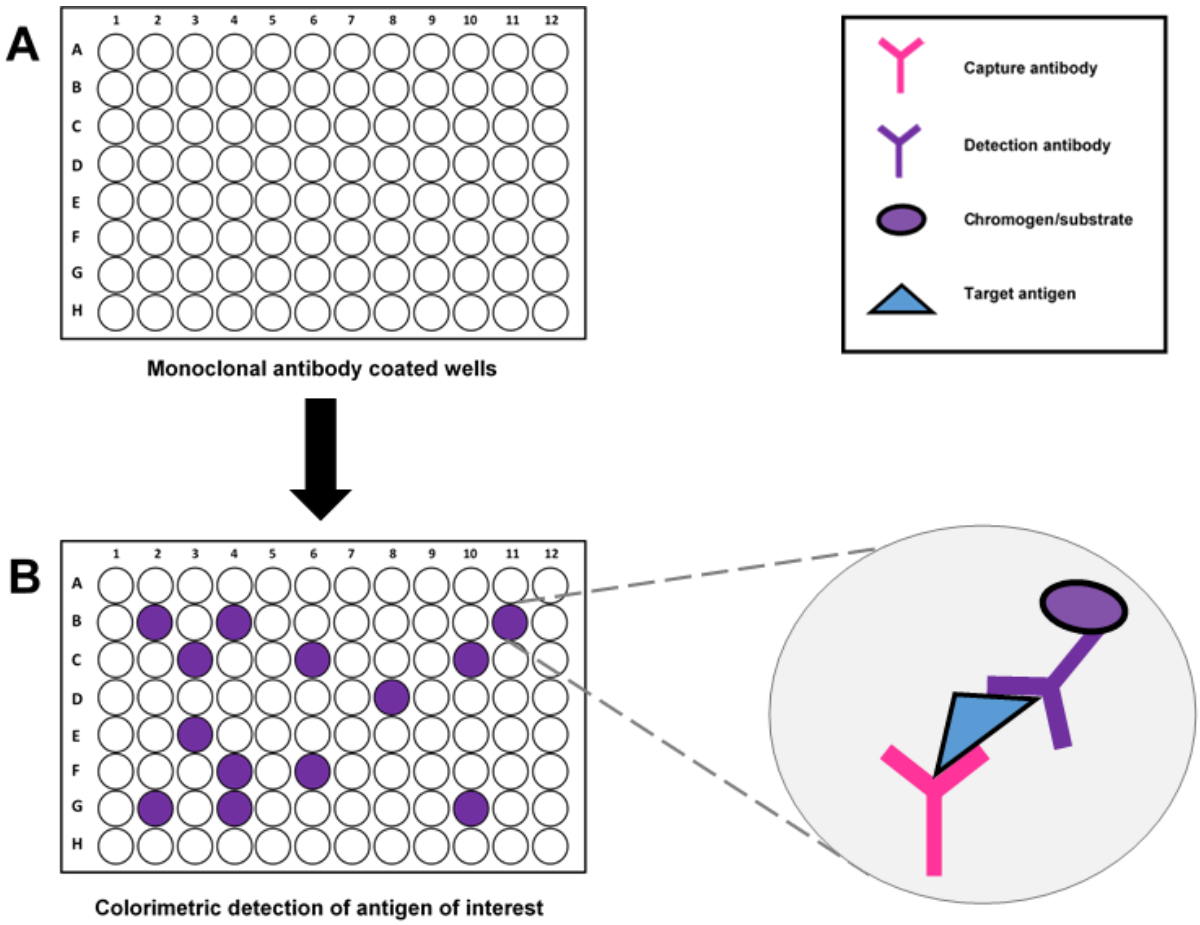


Figure 13: A summary of the ELISA procedure. A) Capture antibodies are pre-coated in the wells of the microplates. B) After the target antigen has been fixed into the well by the capture monoclonal antibodies, a secondary conjugated antibody against a different epitope on the target is added to the well, and the addition of a substrate generates a colorimetric signal in reactive wells.

2.11 Statistics

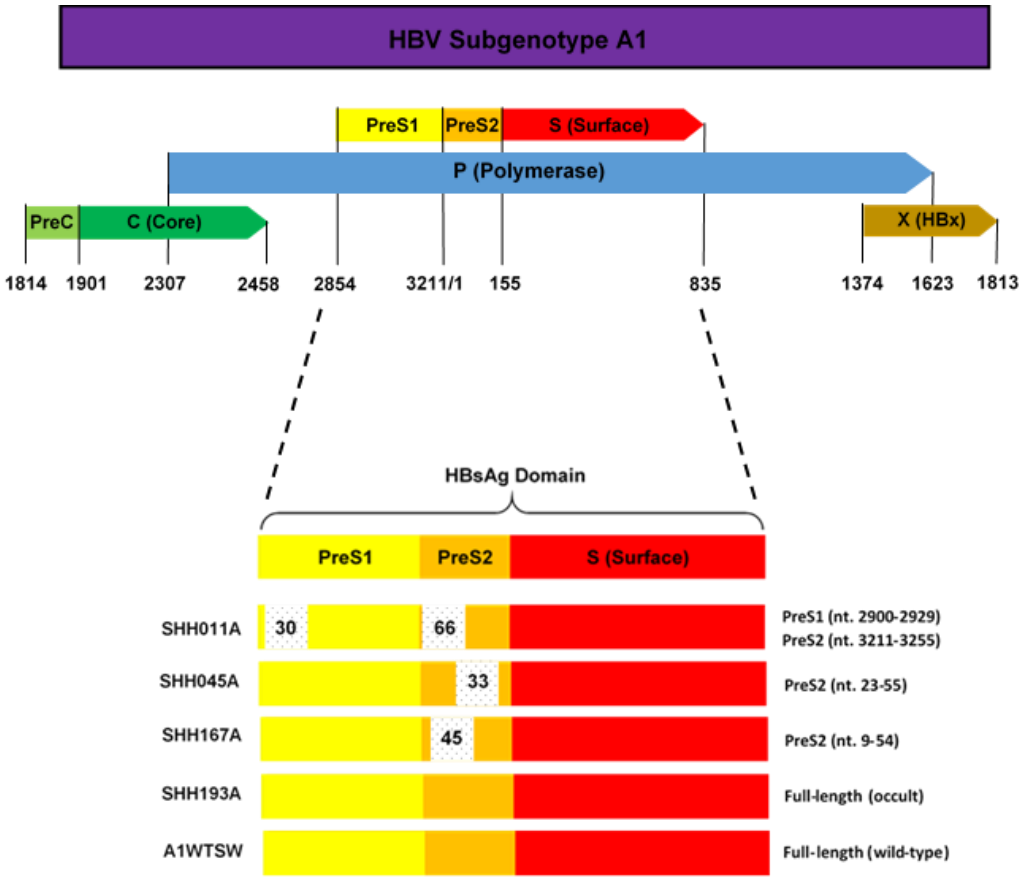
2.11.1 ANOVA Analysis

An ANOVA (Analysis of variance) is a statistical technique that is used to examine if the means of two or more groups are significantly different from one other and assesses the influence/effect of one or more factors by comparing the means of diverse samples. Ultimately, the ANOVA analyses two or more groups simultaneously to determine whether there is any relationship among the groups of dataset or not. In this instance, an ANOVA was carried out to analyze the HBsAg or HBeAg levels of the wild-type, deletion mutant and occult samples at three time points namely; day 1, day 3 and day 5 to determine if there were any significant differences in their expression. The significance of the data was determined by any results with a p-value below 0.05 (i.e. the cut-off value for significance).

2.11.2 F-test Analysis

An f-test was employed to compare the sample variances (which can be any size) to test the null hypothesis that the variances of two samples are equal, this test is the basis of ANOVA. In this study the f-test was used to individually compare the HBsAg expression of the wild-type backbone relative to the occult and deletion mutant constructs. The F critical values (i.e. F statistic) together with the p-values generated from the f-test were used to determine the overall significance of the results and whether or not to reject or accept the null hypothesis. Fundamentally, if the calculated F value was greater than the F critical value and the p-value was above 0.05, then the null hypothesis was rejected.

3.1 Plasmid Preparation: Sequencing & Restriction Digestion



Functional Domain	Region	Amino Acid Position (No. of aa)	Amino Acid Sequence
Myristoylated N-Terminal Glycine	PreS1	ps1G2 (1)	G
NTCP Receptor Binding Site	PreS1	ps1R9-I48 (39)	RKGMGTNLSVPNPLGFFPDHQLDP AFGANSNNPDWDFNPI
T Cell Epitope	PreS1/2	ps1S109-ps2L12 (23)	SPPLRDSHPQAMQWNSTAFHQAL
B Cell Epitope	PreS2	ps1Q132-ps2G25 (13)	QDPRVRGLYFPAG
Neutralising Antibody Target 1	PreS1	ps1V18-ps1D50 (33)	VPNPLGFFPDHQLDPAFGANSNNP DWDFNPIKD
Neutralising Antibody Target 2	PreS2	ps2M1-ps2I45 (45)	MQWNSTAFHQALQDPRVRGLYFP AGGSSSGTLNPVPNTASHISPI

Figure 14: The previously constructed subgenotype A1 1.28 mer replication competent plasmids utilized in this study. The grey dotted area (with numbers) elucidates the size and positions of the deletions. The pink table highlights the functional domains within the PreS1 & PreS2 (image adapted from Wolhuter, 2016).

Previously constructed subgenotype A1 1.28 mer replication competent plasmids, shown to express HBV DNA and proteins *in vitro*, for wild-type (A1 WT SW), occult strain (SHH193A), and with different HBsAg mutations: PreS1 & PreS2 deletion mutant (SHH011A), PreS2 deletion mutants (SHH045A and SHH167A) were utilized in this study (*Figure 14*) (Wolhuter, 2016). Prior to restriction digestion, the sequences of the wild-type, deletion mutant and occult plasmid constructs were viewed *in silico*. These plasmid maps were viewed using the SnapGene software (APPENDIX D, page 104), which can be employed as a powerful prediction tool (see *Table 4*, page 55). For simplicity, the A12C15_OL A1WTSA1.281MER and A12C15 ALT 9.3 plasmid constructs generated by Bhoola et al (2014) and Wolhuter (2016) were renamed A1 WT and A1 WT SW in this study. Similarly, the test samples employed in this study, samples SHH011A, SHH045A, SHH167A and SHH193A are referred to as 011A, 045A, 167A and 193A, respectively (particularly in the figures).

As described by Wolhuter (2016), the A1 WT replication-competent construct was used as the backbone for the generation of the deletion-mutant constructs. Two *Xba*I sites extending over a 784 bp region within the S region were exploited for the insertion of the subgenomic deletion mutant fragments and the occult full-length fragment. However, the original A1 WT construct contained three *Xba*I sites and in order to successfully insert the subgenomic fragments of the deletion and occult strains, the third redundant *Xba*I site had to be removed to avoid unwanted cuts during cloning. The elimination of this additional *Xba*I site restricted from the multiple cloning site of the pcDNA™ 4/TO plasmid vector (functionally insignificant fragment) resulted in the generation of the A12C15 ALT 9.3 (A1 WT SW) backbone, which only harboured two *Xba*I sites. *Figure 15* illustrates the A1 WT SW altered plasmid used as the backbone for the generation of all the deletion-mutants strains namely SHH011A, SHH045A and SHH167A as well as the occult strain (SHH193A).

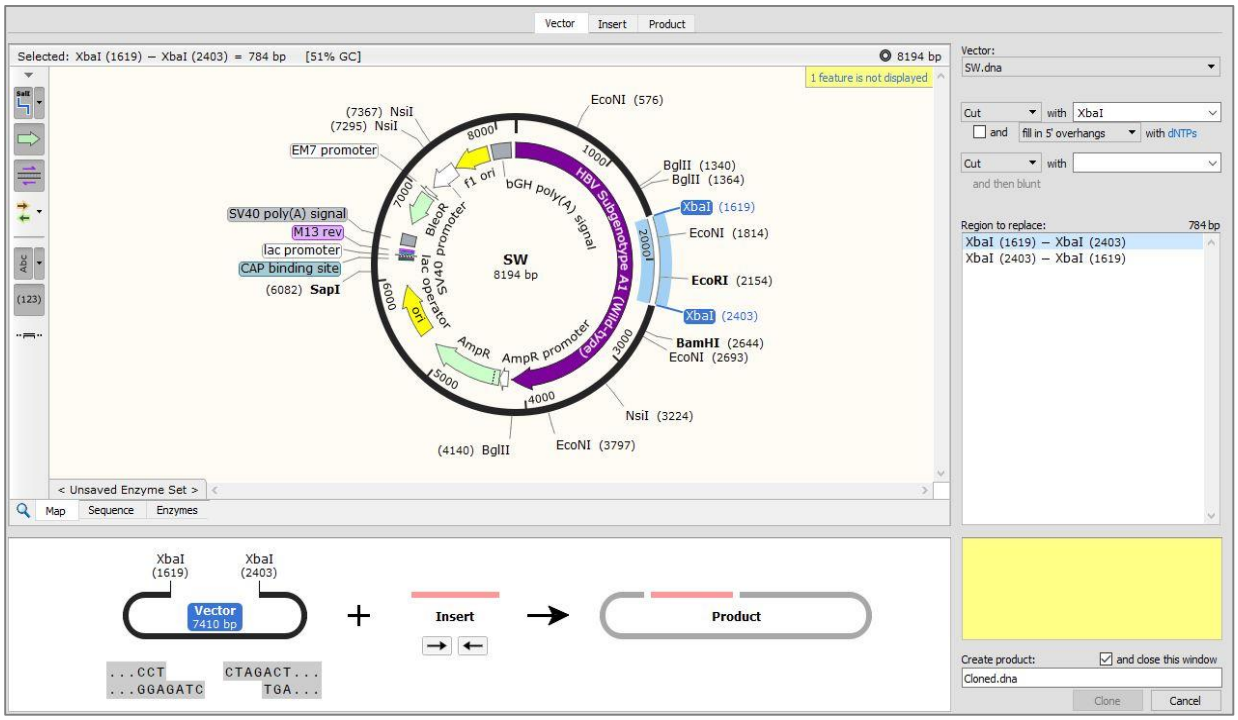
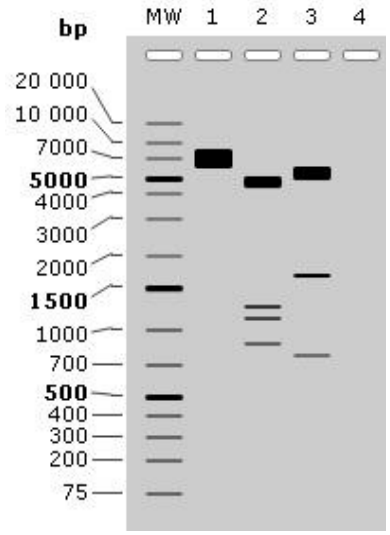
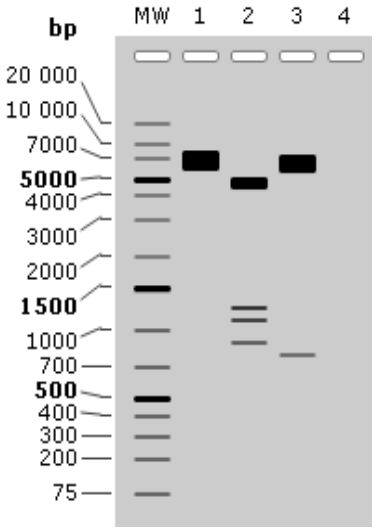
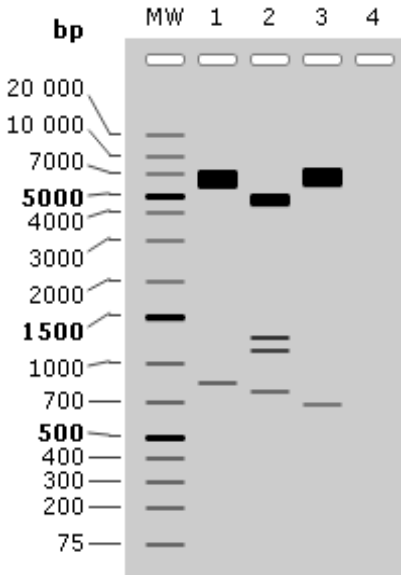


Figure 15: An illustration of the A1 WT SW plasmid construct highlighting the 784 bp region that was replaced with either SHH011A, SHH045A or SHH167A subgenomic deletion fragments or the SHH193A occult full-length fragment.

The plasmid DNA was extracted for the wild-type, occult and deletion mutants transformed into *E. coli*, and sequencing and restriction digestion analysis performed to authenticate that each plasmid was in fact the plasmid of interest. The predicted restriction digestion gels shown in *Table 4* highlight the expected number of fragments and their estimated sizes when individually digested with *Bam*HI, *Eco*NI and *Xba*I restriction enzymes.

Table 4: The predicted restriction digestions of the various plasmids used in the study

SAMPLE	PREDICTED AGAROSE GEL	RESTRICTION ENZYMES AND FRAGMENT SIZES (BP)
A1 WT		MW: GeneRuler™ 1 kb Plus DNA Ladder L1: *Bam*HI 1. 8212 bp L2: *Eco*NI 1. 4991 bp 2. 1238 bp 3. 1104 bp 4. 879 bp L3: *Xba*I 1. 5769 bp 2. 1659 bp 3. 784 bp
A1 WT SW		MW: GeneRuler™ 1 kb Plus DNA Ladder L1: *Bam*HI 1. 8194 bp L2: *Eco*NI 1. 4973 bp 2. 1238 bp 3. 1104 bp 4. 879 bp L3: *Xba*I 1. 7410 bp 2. 784 bp
011A		MW: GeneRuler™ 1 kb Plus DNA Ladder L1: *Bam*HI 1. 7261 bp 2. 837 bp L2: *Eco*NI 1. 4973 bp 2. 1238 bp 3. 1104 bp 4. 783 bp L3: *Xba*I 1. 7410 bp 2. 688 bp

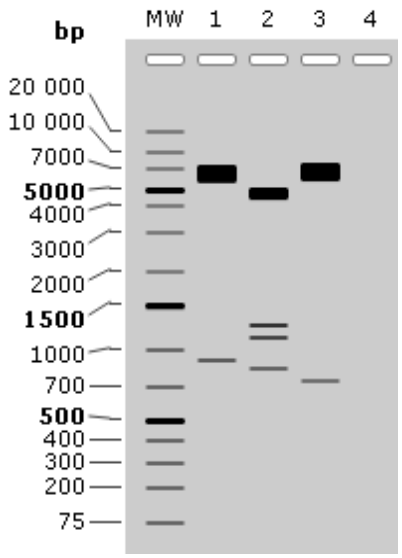
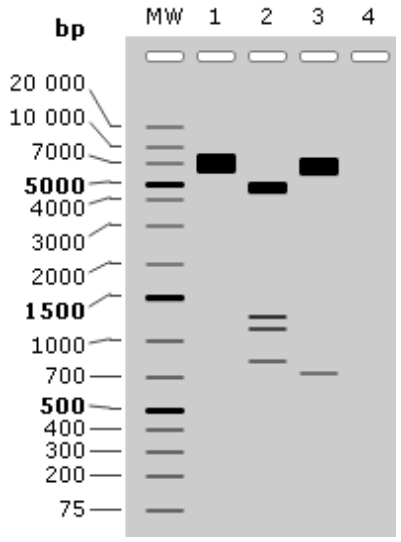
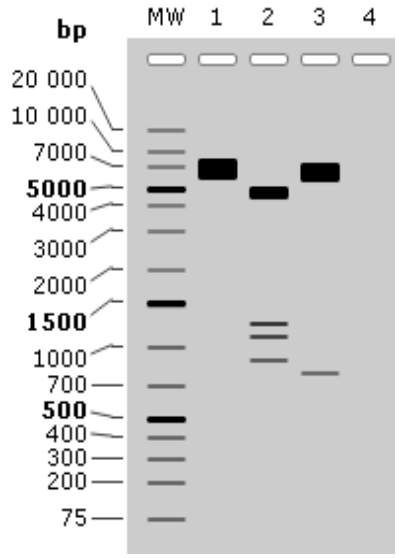
045A		MW: GeneRuler™ 1 kb Plus DNA Ladder L1: *Bam*HI 1. 7261 bp 2. 900 bp L2: *Eco*NI 1. 4973 bp 2. 1238 bp 3. 1104 bp 4. 846 bp L3: *Xba*I 1. 7410 bp 2. 751 bp
167A		MW: GeneRuler™ 1 kb Plus DNA Ladder L1: *Bam*HI 1. 8139 bp L2: *Eco*NI 1. 4973 bp 2. 1238 bp 3. 1104 bp 4. 824 bp L3: *Xba*I 1. 7410 bp 2. 729 bp
193A		MW: GeneRuler™ 1 kb Plus DNA Ladder L1: *Bam*HI 1. 8194 bp L2: *Eco*NI 1. 4973 bp 2. 1238 bp 3. 1104 bp 4. 879 bp L3: *Xba*I 1. 7410 bp 2. 784 bp

Figure 16 illustrates that the respective plasmids were restricted as predicted (*Table 4*) and this was confirmed by sequencing and the alignment to the A1 WT reference sequence (APPENDIX E, page 109), thus demonstrating the integrity of the plasmid constructs.



Figure 16: Agarose gel (0.8%) electrophoresis of the plasmid restriction digestions of the wild-type, occult and deletion mutant strains. The lanes labelled "U" indicates the undigested plasmids and the lanes labelled "B", "E" and "X" denotes the lanes digested with the restriction enzymes BamHI, EcoNI and XbaI, respectively. The "MW" label represents the GeneRuler 1 kb DNA Ladder (molecular weight marker).

3.2 Cell Culture & Transfection

Huh7 cells were employed in this study. These cells are a well-differentiated hepatocyte derived carcinoma cells that adhere to the surface of plates/flasks and are known to grow as monolayers. The cell line was established by Nakabayashi et al (1982), who isolated cells from the hepatoma tissue of a 57-year-old Japanese man (Nakabayashi et al., 1982). These cells are suitable for the transfection assays performed in this study.

3.2.1 Mycoplasma detection assay

Once Huh7 cells were revived and fully recovered from frozen stocks, they were passaged every two to three days and split according to the confluency of the cells. After every tenth passage the cell culture supernatants were tested for *Mycoplasma* and *Acholeplasma* contamination as a precaution. According to the protocol guidelines, a 481 bp band should be seen in every reaction tube (internal control), as well as the negative control to determine the success of the PCR reaction. The presence of a band at ~260 bp indicates the presence of mycoplasma in the supernatant/test sample, this band should only be present in the positive control (*lane 3, Figure 17*). There was no mycoplasma contamination as shown in *Figure 17*.

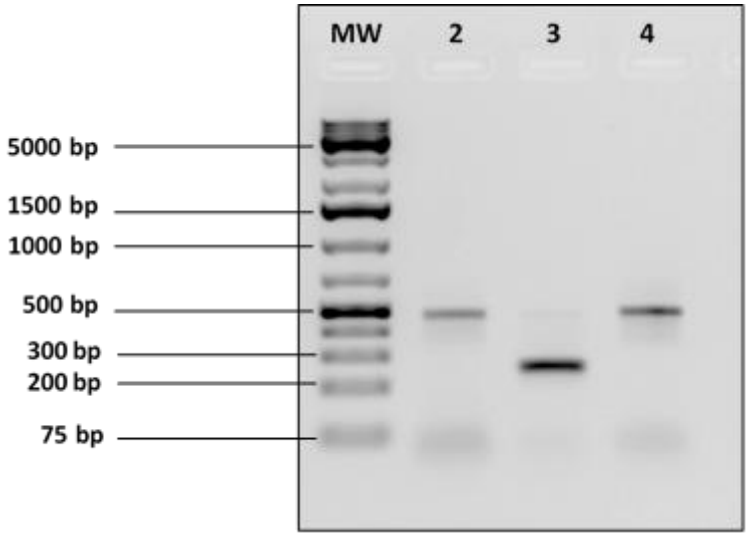


Figure 17: Agarose gel (1.2%) electrophoresis of the PCR amplicons generated from the mycoplasma detection assay. Lane 1: 7µl GeneRuler DNA ladder, lane 2: 8µl test sample, lane 3: 8µl positive control and lane 4: 8µl negative control.

3.2.2 Transfection efficiency

A GFP fluorescent tag (under the regulation of the CMV promoter) was used to measure transfection efficiency. The transfection efficiency was measured on day 1 post transfection by determining the proportion of cells that had successfully been transfected with eGFP. Since green fluorescent protein has the ability to fluoresce a bright green when observed under a fluorescence microscope, this enabled the determination of cells that were successfully

transfected. Based on the results displayed in *Figure 18*, the Huh7 cells were estimated to be transfected at an 80-85% transfection efficiency rate. The cells were then harvested and prepared for the subcellular fractionation protocol.

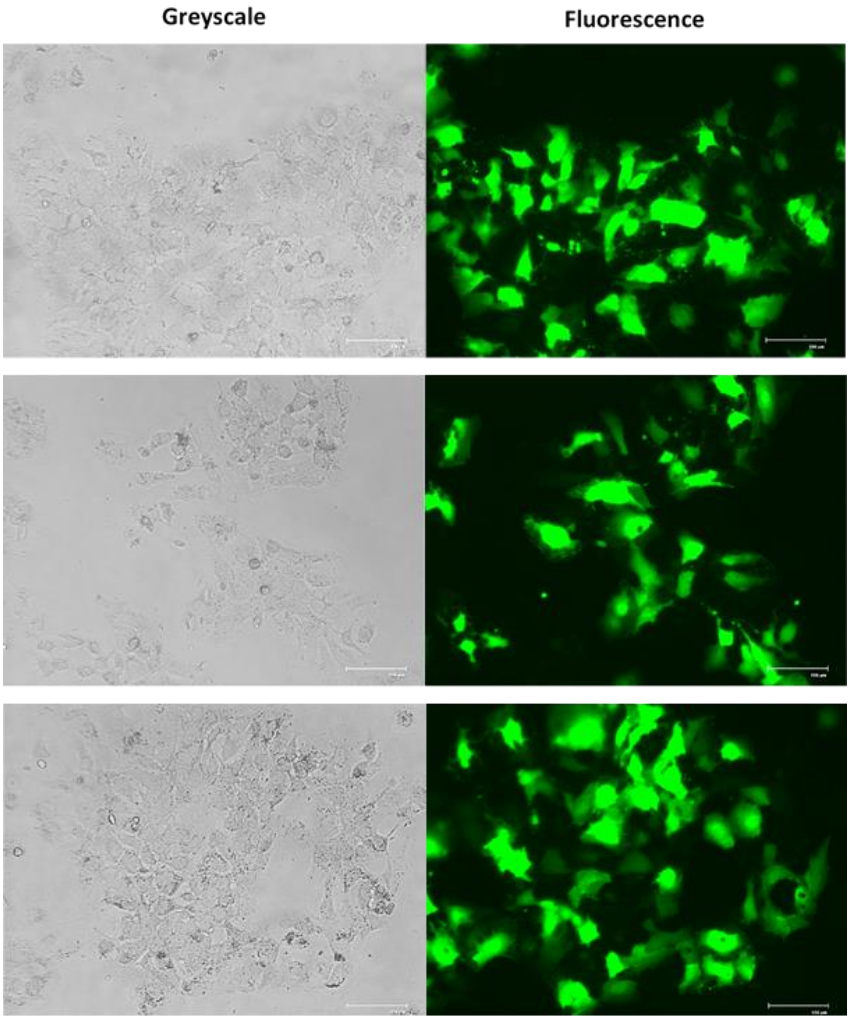


Figure 18: A measurement of the transfection efficiency using GFP expression. Images were viewed the EVOS™ FLoid™ Cell Imaging Station fluorescence microscope (Life Technologies, Thermo Fisher Scientific) with fluorescence and greyscale images captured on the FLoid Software v1.4.

3.3 Subcellular fractionation

3.3.1 Commercial kit optimization

A commercial kit was initially utilized to perform the subcellular fractionation. To determine the effectiveness of the subcellular fractionation generated by this kit, the isolated fractions were analyzed with an immunoblotting assay. The idea is that specific housekeeping proteins

should only be present in the corresponding specific subcellular fractions. Thus, a designated housekeeping protein antibody was assigned to a particular fraction as a marker for the fraction of interest and used to support the purity of the extracted fractions. Additionally, the subcellular fractions were compared to whole cell lysate (i.e. sample that has not been fractionated) to compare the separation of the proteins.

When comparing the whole cell lysate (*lane 2, Figure 19*) to the isolated fractions namely; the cytoplasmic (CPE), membrane (ME), soluble nuclear (SNE), chromatin-bound nuclear (CBNE) and cytoskeletal (CSE) extracts (*lanes 4-7 & lane 9 respectively, Figure 19*), it appeared that the subcellular fractionation was successful since each fraction produced a distinctive banding pattern. The distinguishing banding patterns formed demonstrated that the proteins extracted were specific to each fraction, especially when compared to whole cell lysate, which did not generate any clear protein separation but rather a smear. However, as explained at a later stage, the subcellular fractionation results were not optimal (*see Figure 20*).

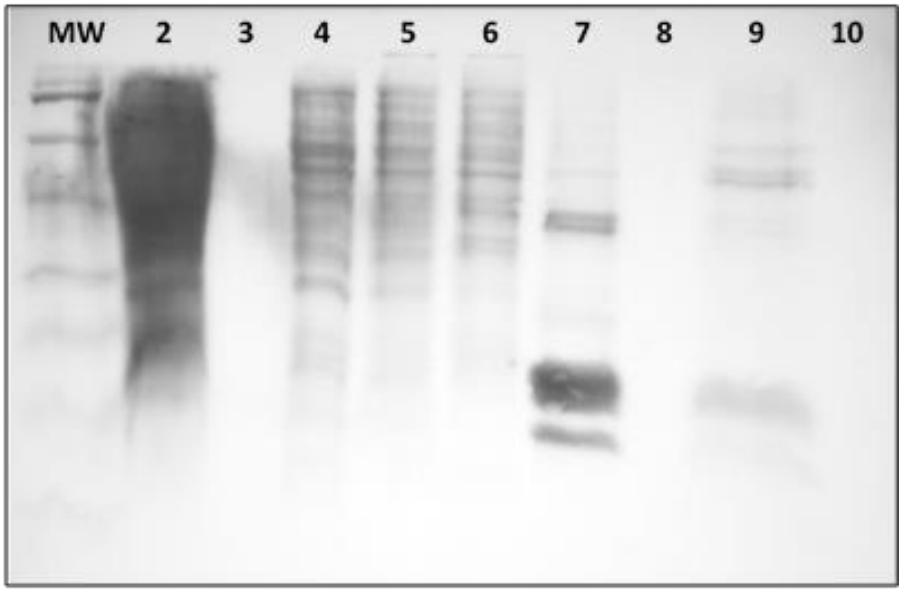


Figure 19: A Ponceau stained blot comprising of whole cell lysate and the five fraction extracts of interest. Lane 1: Precision Plus Protein™ WesternC Standards™, lane 2: whole cell lysate (control), lane 4: CPE, lane 5: ME, lane 6: SNE, lane 7: CBNE and lane 9: CSE. The abbreviations denote the cytoplasmic (CPE), membrane (ME), soluble nuclear (SNE), chromatin-bound nuclear (CBNE) and cytoskeletal (CSE) extracts.

When an unstained blot was further examined against Anti-Cytokeratin 18, it was expected that a single band approximately 45 kDa would solely appear in the cytoskeletal fraction (*Figure 20*). Though there was a strong band intensity in the cytoskeletal extract where the antibody was expected to bind, there were additional bands in the other fractions, which theoretically should have been absent. This indicated that the fractions were cross-contaminated with proteins from other subcellular fractions.

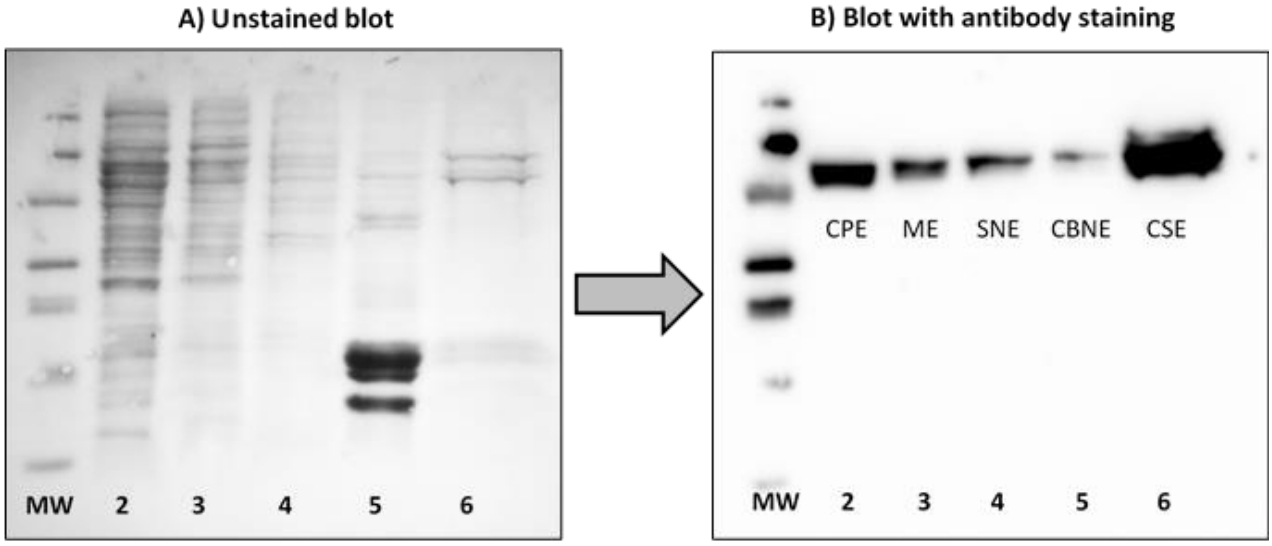


Figure 20: Panel A represents the original Ponceau stained blot comprising of the five fraction extracts of interest. Lane 1: GeneRuler DNA ladder, lane 2: Cytoplasmic extract (CPE), lane 3: Membrane extract (ME), lane 4: Soluble nuclear extract (SNE), lane 5: Chromatin-bound nuclear extract (CBNE) and lane 6: Cytoskeletal extract (CSE). Panel B illustrates the corresponding immunoblot with Anti-Cytokeratin 18 staining.

When comparing the different conditions of subcellular fractionation, the chromatin-bound nuclear extract (CBNE) was used as point of reference in each blot because it has a clear distinctive banding pattern (*Figure 21)*. Ultimately, in order for an optimization protocol to be deemed successful, each fraction should only generate a single band targeted by a specific antibody demonstrating the purity of a fraction.

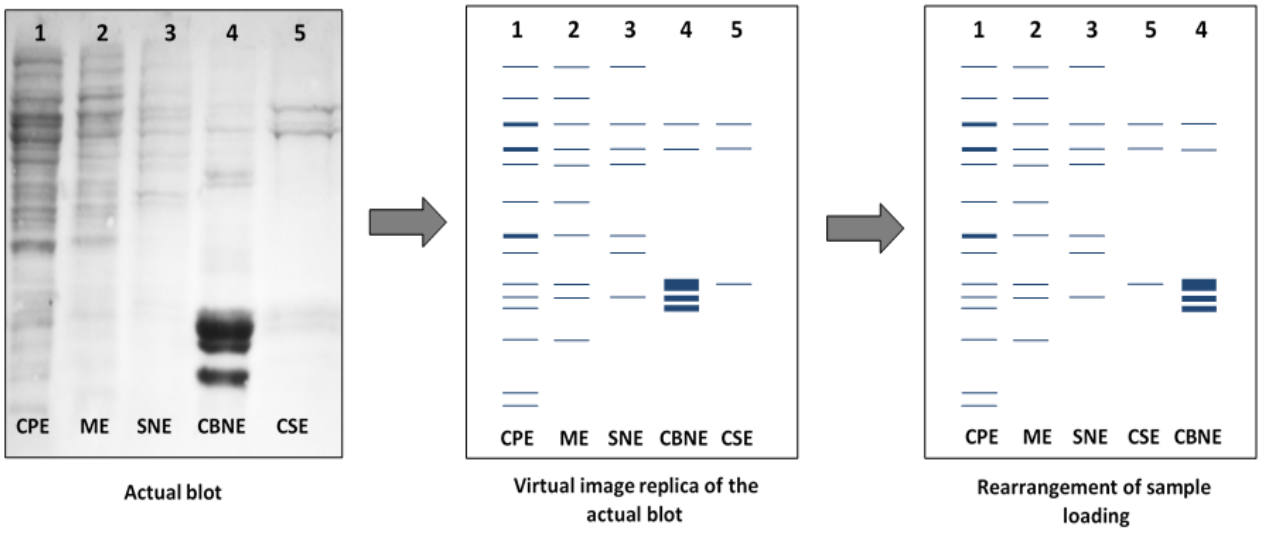


Figure 21: An example of the possible rearrangement of the sample loading to demonstrate how blots can be easily distinguished based on the distinctive banding pattern of the protein migration for the various fractions - especially when using the chromatin-bound nuclear extract (CBNE) as point of reference.

It is important to note that some of the blots were only prepared for the optimization of the subcellular fractionation protocol and thus did not require a molecular weight marker since the focus was purely centered on the presence of the bands in each fraction and not necessarily the size. This was specifically necessary for the optimization trials (*see Figure 22*). Since a molecular marker was not used in the two optimization trial immunoblots, the fractions were loaded in specific rearrangements/combinations to make it distinguishable once stained with antibodies.

Various attempts were made to optimize the commercial kit in order to improve the isolation of the subcellular fractions. This was done by using freshly transfected cells, increasing incubation and centrifugation times as well as including wash steps with PBS after the isolation of each fraction. *Figure 22* illustrates the results of two of the trials run (*i.e. Trial 1* & *Trial 2*) with the aforementioned optimization and troubleshooting. Each of the two trials tested a lower amount of protein in a range between 2 µg - 4 µg, this was done in order to accommodate the relatively lower protein yields found in the cytoskeletal extract.

Based on the findings in *Figure 22*, it is clear that bands are still detected in the other fractions after staining with the primary antibody Anti-Cytokeratin 18, which should only stain the cytoskeletal extract (CSE). Additionally, though the results demonstrated that the kit was not successfully optimized, it also showed that a reduced amount of protein can be applied for the immunoblotting assay, eliminating concern for protein detection at lower yields.

Ultimately, the modifications introduced to improve the overall subcellular fractionation were unsuccessful, as only two out of the five fractions appeared to be improving sufficiently (*Figure 22*). In the end, it was decided to move forward with a different approach and to use a manual subcellular fractionation.

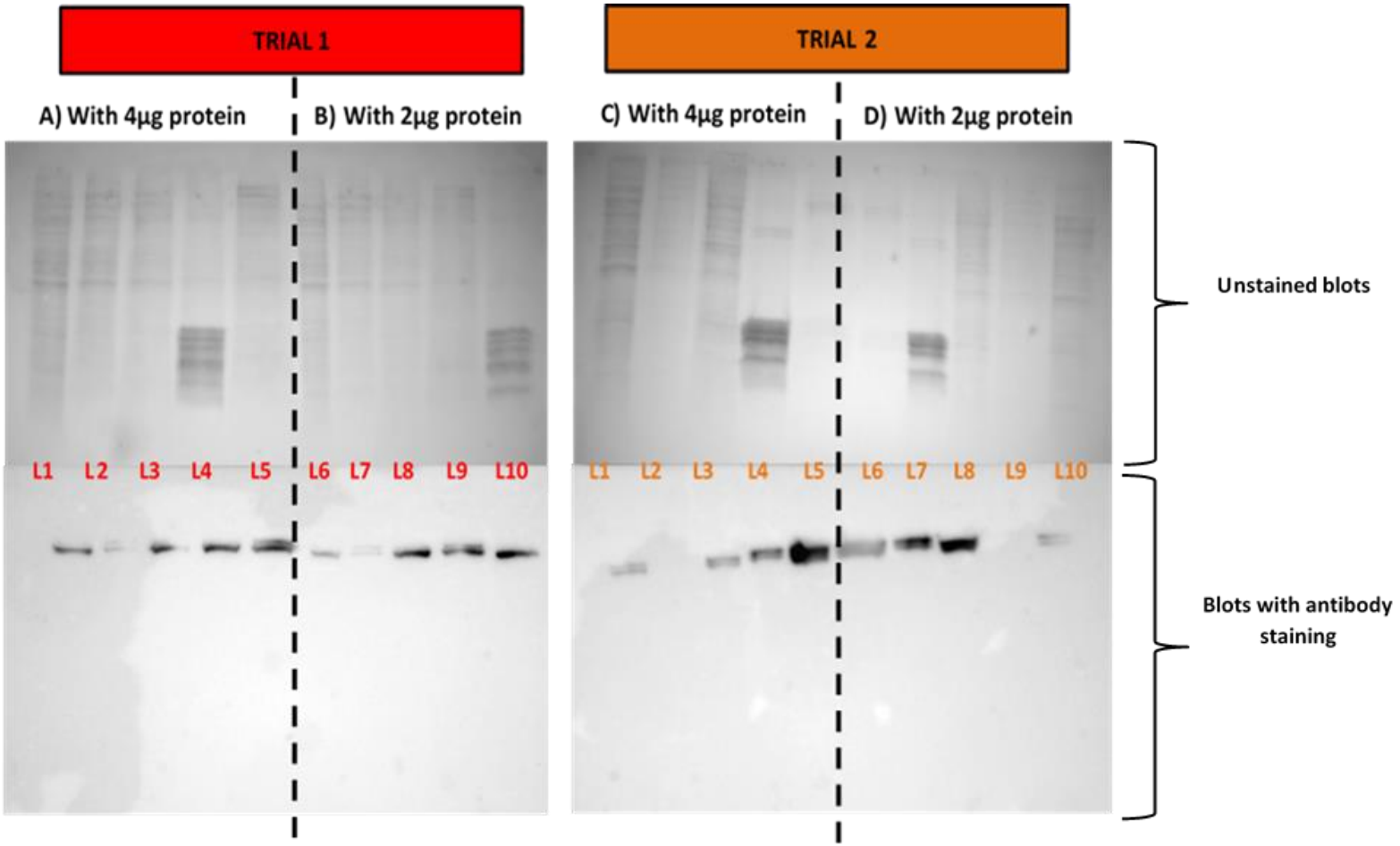


Figure 22: An illustration of two trials both conducted with 2µg and 4µg protein for each fraction as indicated by panels A to D. *For Trial 1: L1:CPE, L2:ME, L3:SNE, L4:CBNE, L5:CSE, L6:CPE, L7:ME, L8:SNE, L9:CSE, L10: CBNE.* *For Trial 2: L1:CPE, L2:ME, L3:SNE, L4:CBNE, L5:CSE, L6:CSE, L7:CBNE, L8:SNE, L9:ME, L10: CPE.* *The abbreviations denote the cytoplasmic (CPE), membrane (ME), soluble nuclear (SNE), chromatin-bound nuclear (CBNE) and cytoskeletal (CSE) extracts.*

3.3.2 Manual Subcellular Fractionation

Interestingly enough, Baghirova et al (2015) has noted the tendency for commercial kits to yield cross-contaminated fractions and as a result they designed a protocol for a manual subcellular fractionation. This protocol enables the extraction of purified proteins from three cellular fractions: the cytosolic, membrane-bound and nuclear fractions. The protocol described utilizes gentle buffers with increasing detergent strength that sequentially lyse the cell membrane, organelle membranes and finally the nuclear membrane. This approach also appeared to be more cost effective in comparison to purchasing a commercial kit, which could only accommodate a limited number of fractionations. Since a large amount of fractionations were required for this study, the manual approach was a suitable alternative method. For these reasons, it was decided to test the efficiency of this manual subcellular fractionation approach, which could then be implemented in the study, if proved to be effective.

Three harvested cell pellets were tested, under three distinct treatments, to obtain the most optimal conditions for the manual subcellular fractionation protocol. Additionally, some of the pellets were divided in half for some treatments (i.e. denoted as "half" pellets) while other treatments tested the complete pellets harvested (i.e. denoted as "whole" pellets). Whole and divided pellets were tested since it was speculated that the pellets harvested at day 5 post-transfection may have been too concentrated in some instances and thus result in cross-contaminated fractions as the lysis buffers may not have been able to efficiently fractionate larger pellets.

Figure 23 demonstrates the effectiveness of the new fractionation approach developed by Baghirova et al (2015). Although increasing the incubation and centrifugation duration produced pure fractions, the best treatment could be seen in pellet 3, which was the standard/set protocol without any alterations. Moreover, this treatment was selected since it was the most successful in extracted proteins from the nuclear fraction, which is the most challenging fraction

to isolate. Anti-Histone H3 (~17 kDa) and Anti-Cytokeratin 18 (~45 kDa) were utilized to analyze the purity of the nuclear and cytosolic fractions, respectively.

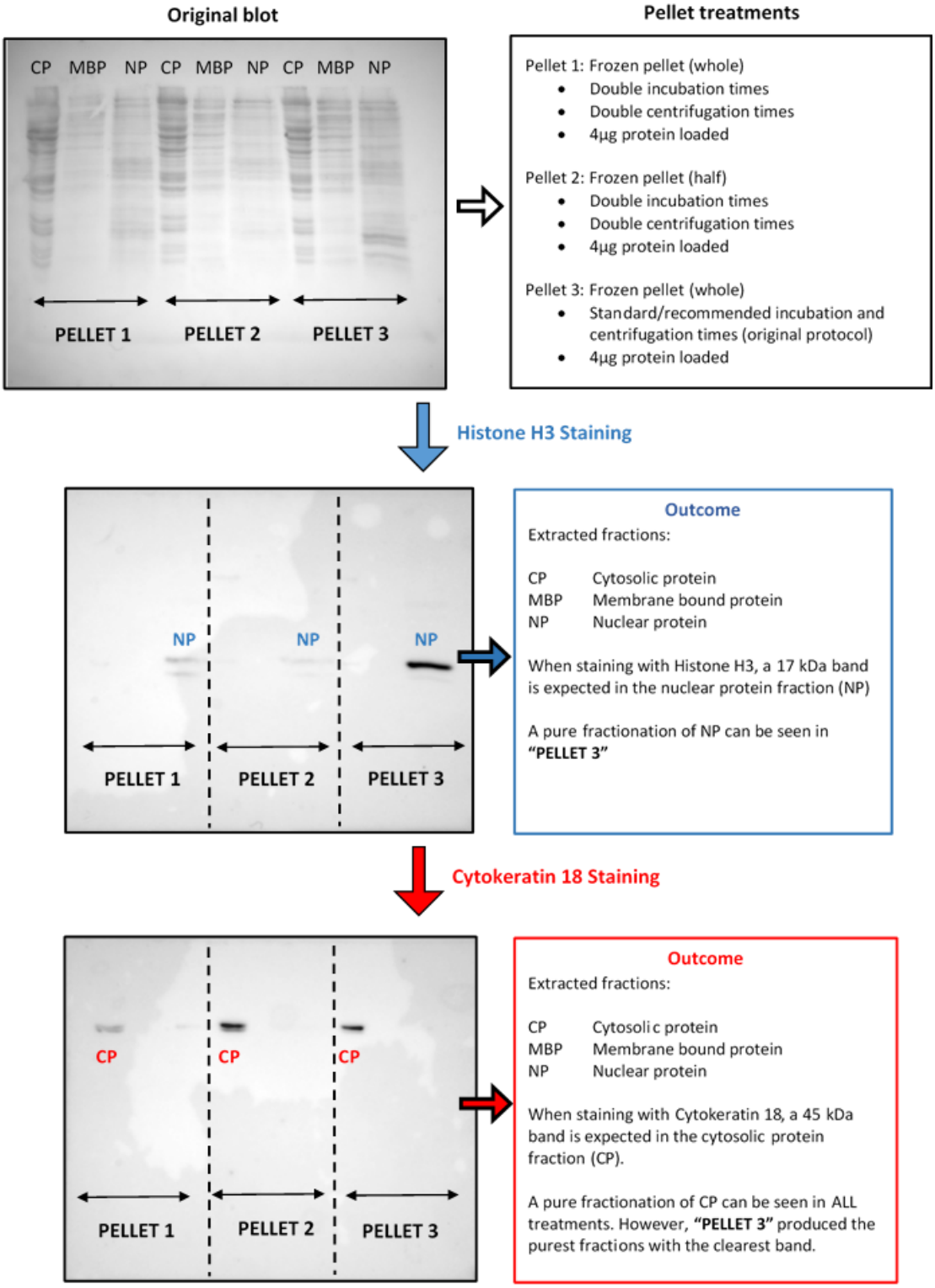


Figure 23: Summary of the optimization for the manual subcellular fractionation. The best treatment could be seen in "Pellet 3" which employed the original protocol without any modifications.

To test the purity of the membrane-bound fraction, blots were reprobed with Anti-Calreticulin. It is expected that staining with Anti-Calreticulin produces two bands of approximately 50 kDa and 63 kDa in size (*see in upcoming figures*). These bands did not appear in the cytosolic or nuclear fractions, which supports the purity of the membrane-bound fractions (*data not shown*).

3.4 Immunoblotting results

Once a successful protocol was established for the subcellular fractionation, it was possible to continue with the immunoblotting assay. To support the identity of each fraction, the control housekeeping antibodies Anti-Cytokeratin 18, Anti-Calreticulin and Anti-Histone H3 were selected to identify the cytosolic, membrane-bound and nuclear fractions, respectively (*Figures 24-26*). In addition, several controls were utilized to demonstrate that no external/alternative influences were a factor on the results, this included: pcDNA™4/TO expression vector, eGFP control, mock negative control (Huh7 cells transfected with transfection reagent and without plasmid DNA), negative control (Huh7 cells transfected without plasmid DNA and without transfection reagent) as well as the HBV positive controls subgenotype A1 wild-type (A1 WT) and the modified version of this A1 wild-type (A1 WT SW).

In order to test the impact of the subcellular fractionation an additional control of unfractionated whole cell lysate samples were included in the study. Both the unfractionated and fractionated control samples (*Figure 24*) and test samples (*Figures 25-26*) were tested with the aforementioned housekeeping protein antibodies. In addition, the eGFP control samples were tested with Anti-eGFP, a single band of ~31 kDa should only be present in each of the eGFP fractions (*Figure 24*). This observation supports that no contamination occurred across the samples during harvesting and extraction of each fraction.

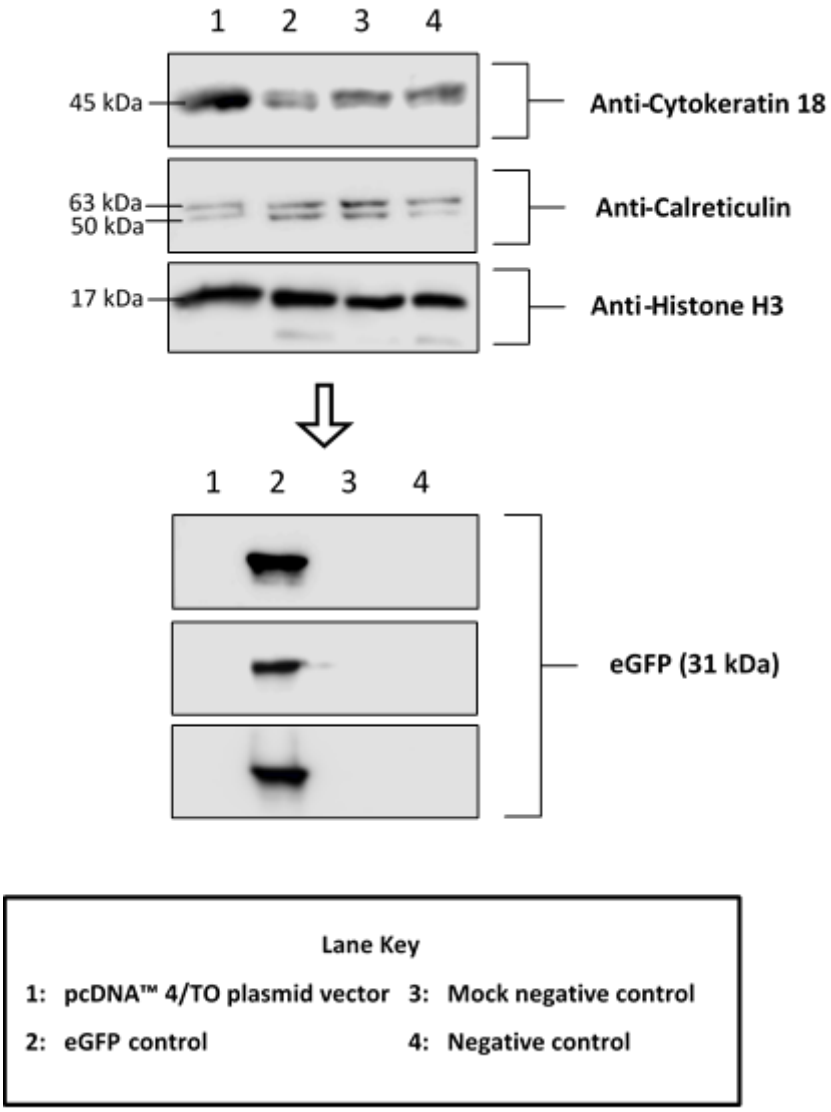


Figure 24: The control antibodies Anti-Cytokeratin 18, Anti-Calreticulin and Anti-Histone H3 selected to identify each fraction of interest as well as the Anti-eGFP utilized to detect the eGFP control plasmid.

Unfractionated samples were stained using the mouse monoclonal antibody against the S region of HBsAg (Anti-HB1). The detection in the unfractionated samples is only present in the wild-type and the shortest deletion mutant (SHH045A) with no or trace amounts of HBsAg proteins in the occult and other deletion mutants (SHH011A and SHH167A) strains (*replicate 2, Figure 25*).

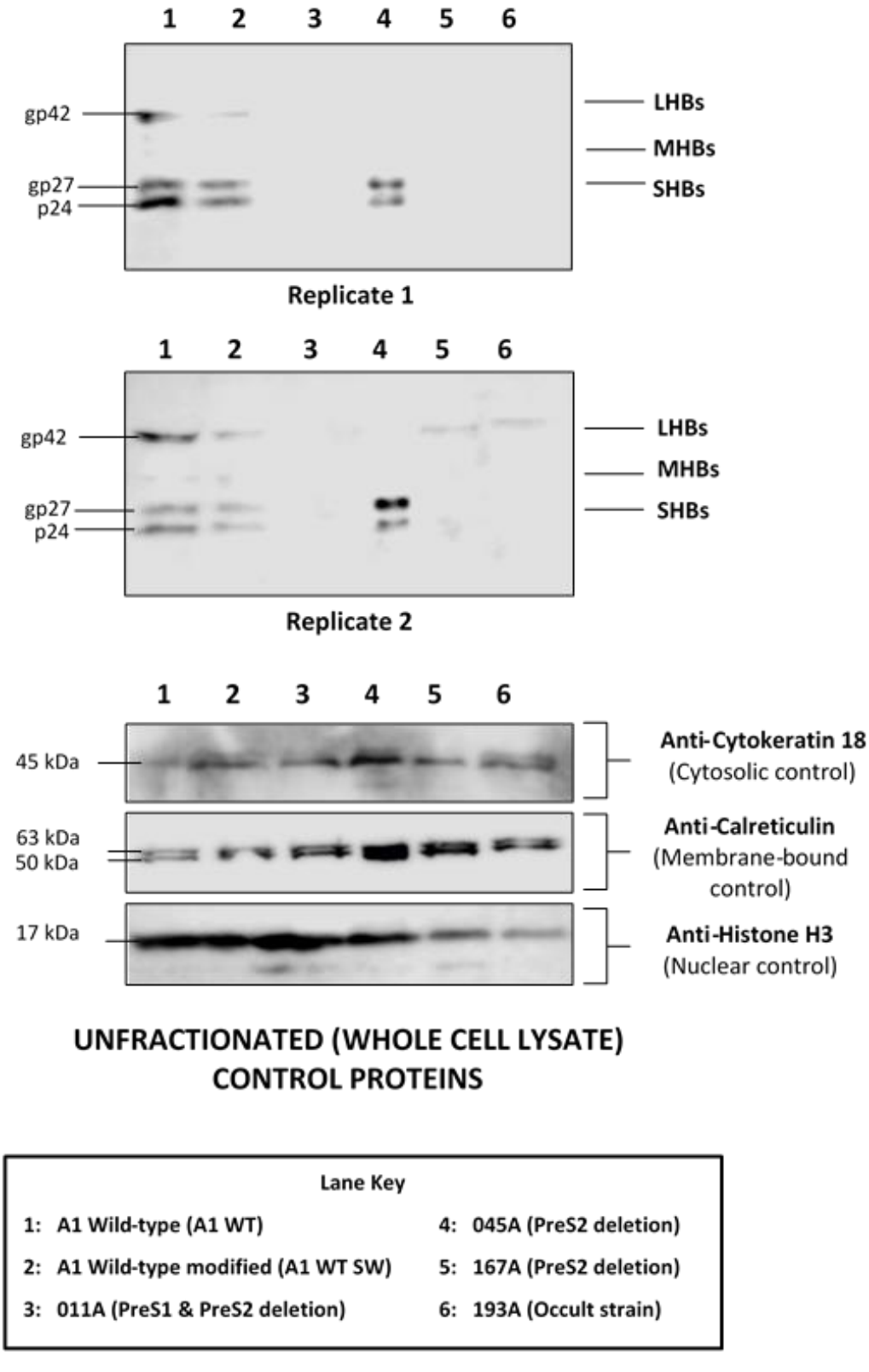


Figure 25: Mouse monoclonal antibody against the S region of HBsAg stained in the unfractionated samples of the wild-type, deletion mutant and occult strains.

The replicates of the whole cell lysate were not completely identical with the LHBs protein band not being visible in the replicate 1 blot (*Figure 25)*. This may be due to the fact the proteins are not as well enriched from whole cell lysates as opposed to using a subcellular fractionation approach, which can enrich proteins at each subcellular level efficiently (*Figure 26*). Even with increased exposure times, the blots were unaltered and longer exposure times only increased the band intensities. Thus, where there were no bands detected, this was found even when increasing the exposure times when imaging the immunoblots.

Interestingly, the results in *Figure 25* demonstrated that the detection of HBsAg proteins in unfractionated whole cell lysate samples is not as efficient in comparison to that of the subcellular isolated fractions. Subcellular fractionation obviously enriches for the various proteins (*Figure 26*).

A summary of the findings in *Figure 26*:

- No HBsAg proteins were detected in the nuclear fraction, which further confirmed the purity of the subcellular fractionation.
- SHBs was detected in the cytosolic and membrane bound fractions and was expressed by all constructs, which would be expected since there are no deletions present in the S region
- The LHBs and MHBs proteins were not expressed by the SHH011A and SHH045A deletion mutants.
- The occult strain (SHH193A) appeared to be aggregating HBsAg proteins mainly in the membrane-bound fraction, as there were no traces of SHBs and MHBs in the cytosolic fraction and only slight traces of LHBs in the cytosolic fraction.

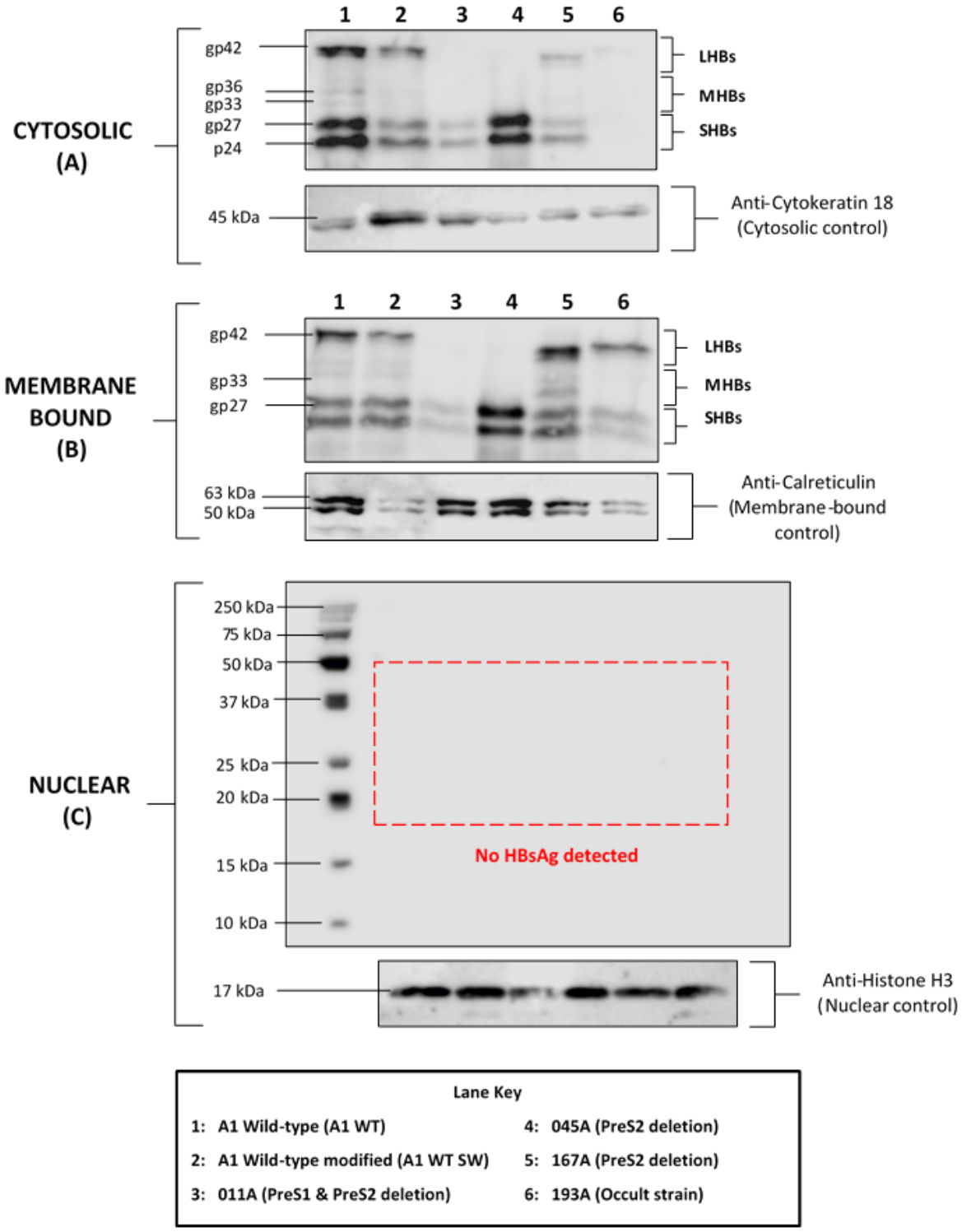


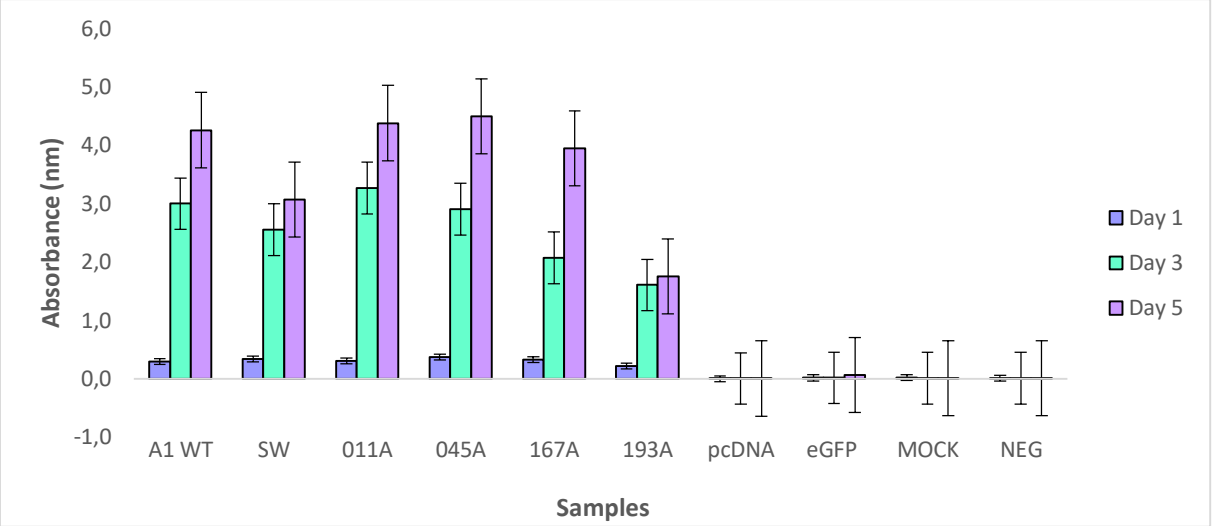
Figure 26: Mouse monoclonal antibody against the S region of HBsAg stained in each fraction of interest, namely; the cytosolic, membrane-bound and nuclear fractions.

3.5 ELISA results

Using ELISA, the extracellular expression of both HBeAg and HBsAg was followed in transfected Huh7 cells on days 1, 3 and 5 post-transfection. Absorbance readings above the calculated cut-off values were considered to be positive for protein expression, while values below the cut-off value represented samples that were negative for protein expression. Accordingly, all the controls utilized in the HBeAg and HBsAg were below the cut-off value and were considered to be negative for protein expression.

3.5.1 HBeAg ELISA results

A two-way ANOVA analysis was performed in order to determine if there were any significant differences amongst the HBeAg expression in the samples at the different time points. *Figure 27* further demonstrates that there was no background noise in the ELISA assay since levels of HBeAg were not detected in the control samples as all the samples absorbance readings were below the cut-off value of 0.068.

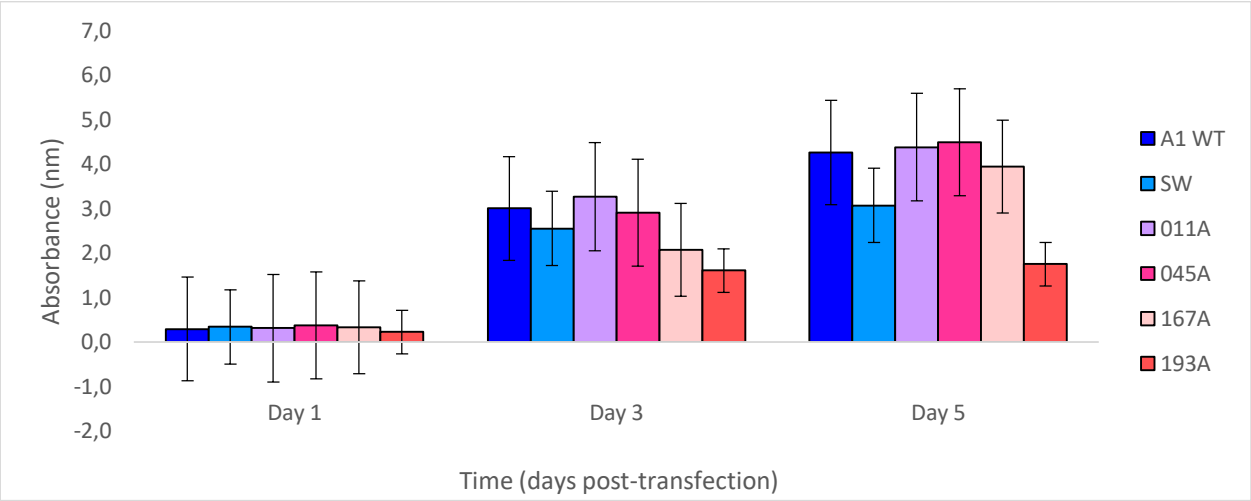


Control Groups	*Count*	*Sum*	*Average*	*Variance*
pcDNA	3	0,0067500	0,0022500	0,0000015
eGFP	3	0,0926000	0,0308667	0,0008970
MOCK	3	0,0355000	0,0118333	0,0000788
NEG	3	0,0189500	0,0063167	0,0000006

Source of Variation	*SS*	*df*	*MS*	*F*	*P-value*	*F crit*
Control Groups	0,001442	3	0,000481	1,966072	0,197732	4,066181

Figure 27: The extracellular HBeAg expression in cultured Huh7 cellular supernatants. The two-way ANOVA statistical analysis of the negative controls.

Based on the ANOVA descriptive statistics summary (generated on the Excel Data Analysis ToolPak) in *Figure 28*, there were no significant difference in the secretion of HBeAg between the deletion mutant and occult constructs relative to constructs A1 and SW. However, there was a significant difference between the the different time points with p-values lower than 0.05.



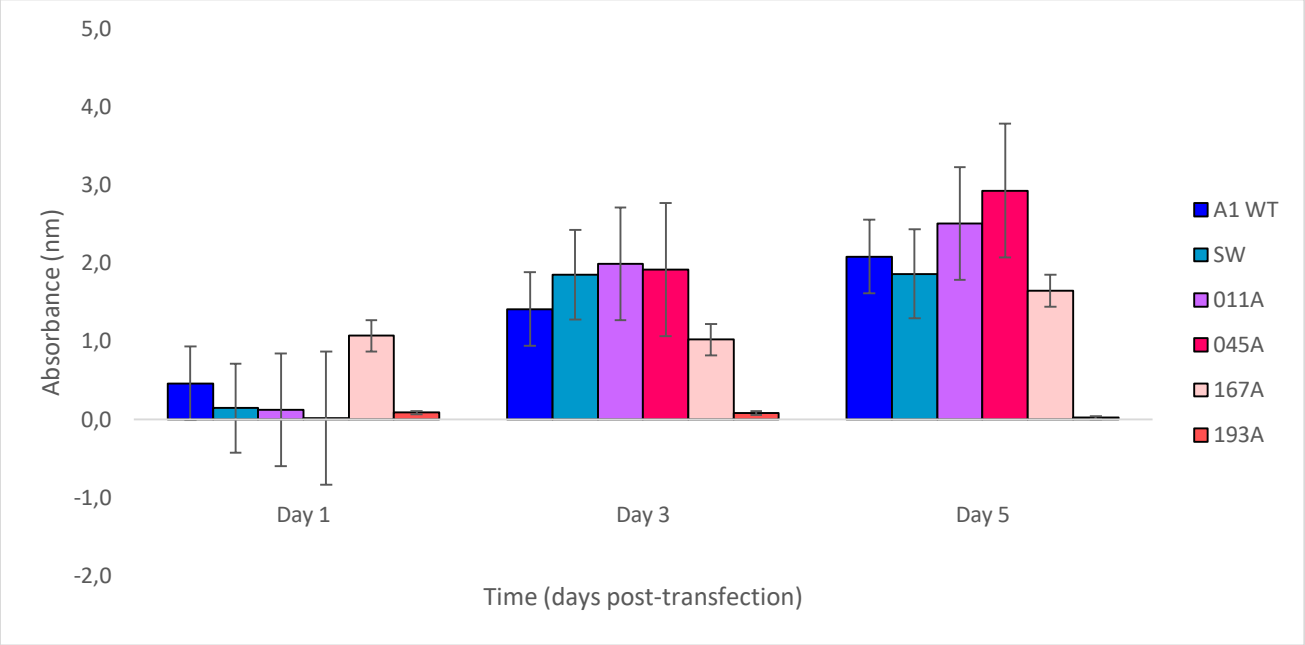
SUMMARY	*Count*	*Sum*	*Average*	*Variance*
A1 WT	3	7,546200	2,515400	4,116166
SW	3	5,958050	1,986017	2,106776
011A	3	7,948600	2,649533	4,433269
045A	3	7,768750	2,589583	4,338036
167A	3	6,343250	2,114417	3,271704
193A	3	3,574250	1,191417	0,713777
Day 1	6	1,845800	0,307633	0,002572
Day 3	6	15,393400	2,565567	0,392869
Day 5	6	21,899900	3,649983	1,130092

Source of Variation	*SS*	*df*	*MS*	*F*	*P-value*	*F crit*
Samples	4,559257196	5	0,911851	2,971745	0,067157	3,325835
Days post-transfection	34,89105193	2	17,445526	56,855381	0,000003	4,102821
Error	3,068403649	10	0,306840			
Total	42,51871278	17				

Figure 28: The extracellular HBeAg expression in cultured Huh7 cellular supernatants of the test sample constructs and positive controls at day 1, 3 & 5 time points analyzed by the two-way ANOVA statistical analysis.

3.5.2 HBsAg ELISA results

Similarly to the HBeAg ELISA results, a two-way ANOVA analysis was used to determine if there were any significant variances in the HBsAg expression amongst the constructs at the different time points (*Figure 29*).



SUMMARY	*Count*	*Sum*	*Average*	*Variance*
A1 WT	3	3.9533000	1.3177667	0.6653124
SW	3	3.8558500	1.2852833	0.9750457
011A	3	4.6180500	1.5393500	1.5714502
045A	3	4.8551500	1.6183833	2.1869071
167A	3	3.7343500	1.2447833	0.1210461
193A	3	0.1881000	0.0627000	0.0013579
Day 1	6	1.8973500	0.3162250	0.1594576
Day 3	6	8.2657000	1.3776167	0.5397536
Day 5	6	11.0417500	1.8402917	1.0062226

Source of Variation	*SS*	*df*	*MS*	*F*	*P-value*	*F crit*
Samples	4.811729	5	0.962346	2.590127	0.093958	3.325835
Days post-transfection	7.326799	2	3.663400	9.859936	0.004313	4.102821
Error	3.715439	10	0.371544			
Total	15.85397	17				

Figure 29: The extracellular HBsAg expression in cultured Huh7 cellular supernatants of the test sample constructs (011A, 045A, 167A, 193A) and positive controls (A1 WT and SW) at day 1, 3 & 5 time points analyzed by the two-way ANOVA statistical analysis.

The ELISA results for HBsAg (*Figure 28)* were similar to that found for HBeAg expression (*Figure 29*), in that the lowest expression levels of HBsAg were found in the occult strain (SHH193A) and the HBsAg expression for the controls were below the cut-off value of 0.1653, rendering the expression in the controls negligible/insignificant.

	A1 WT SW	*A1 WT*
Mean	1.285283	1.317767
Variance	0.975046	0.665312
Observations	3	3
df	2	2
F	1.465546	
P(F<=f) one-tail	**0.405590**	
F Critical one-tail	19	

	A1 WT SW	*045A*
Mean	1.285283	1.618383
Variance	0.975046	2.186907
Observations	3	3
df	2	2
F	2.242876	
P(F<=f) one-tail	**0.308368**	
F Critical one-tail	19	

	A1 WT SW	*011A*
Mean	1.285283	1.539350
Variance	0.975046	1.571450
Observations	3	3
df	2	2
F	1.611668	
P(F<=f) one-tail	**0.382897**	
F Critical one-tail	19	

	A1 WT SW	*167A*
Mean	1.285283	1.244783
Variance	0.975046	0.121046
Observations	3	3
df	2	2
F	8.055162	
P(F<=f) one-tail	**0.110434**	
F Critical one-tail	19	

	A1 WT SW	*193A*
Mean	1.285283	0.062700
Variance	0.975046	0.001358
Observations	3	3
df	2	2
F	718.042253	
P(F<=f) one-tail	**0.001391**	
F Critical one-tail	19	

	A1 WT SW	*A1 WT SW*
Mean	1.285283	1.285283
Variance	0.975046	0.975046
Observations	3	3
df	2	2
F	1	
P(F<=f) one-tail	**0.500000**	
F Critical one-tail	0.052632	

Figure 30: The F-test statistical analysis employed to measure the statistical relationship/association of HBsAg expression between each respective sample in relation to the SW wild-type backbone. The p-values derived from the F-test are highlighted in blue.

When analysing the statistical relationship/association of HBsAg expression amongst each sample in relation to the wild-type backbone SW (*Figure 30*), the results support that there is a significant difference between the occult construct and the deletion mutant constructs relative to the wild-type SW. This is supported by the F-test results, which demonstrated a p-value well below the 0.05 cut-off with the F value substantially greater than the F critical value further demonstrating a significant difference between the SW wild-type backbone and the occult strain. Contrastingly, the F-test p-value results amongst the deletion mutant constructs and the A1 wild-type shows no significant difference when comparing both the F values and p-values (*blue text in Figure 30*).

CHAPTER 4: DISCUSSION

Chronic hepatitis B is a global health burden, which can result in HCC and cirrhosis. The HBV genome evolves rapidly due to the antiviral pressure of host immunity as well as the frequent mutations introduced as a result of the error rate of the viral reverse transcriptase, which lacks proof reading ability (Günther et al., 1999, Chen, 2018). Deletions and mutations found within the viral protein coding regions have been shown to have various clinical repercussions (Bruss et al., 1996). More specific to this study, mutations occurring in the HBsAg have been reported to cause modifications in viral antigenicity (Chen and Oon, 1999, Fan et al., 2001, Kato et al., 1996). The preS region encodes for numerous essential domains such as T cell or B cell epitopes (Chisari and Ferrari, 1995), NTCP receptor binding site (Howard and Allison, 1995) and the HBsAg promoter region (Melegari et al., 1997). Thus, preS deletions can modify HBsAg synthesis and result in intensified virulence with amplified viral replication as well as escape mutants resulting in host immune recognition deficiency (Chen et al., 2006), which can cause prolonged and persistent infection as a result of mutants successful in evading immune surveillance (Chen and Oon, 2002). The implication of preS/S variants has become progressively documented in patients with chronic HBV infection and may be important in the clinical manifestation of the infection.

PreS/S deletion mutants are often recognised in HBV carriers with hepatocellular carcinoma and cirrhosis, suggesting that these inherently occurring variants may advance the progression of hepatocarcinogenesis and overall liver damage (Chen, 2018, Günther et al., 1999, Pollicino et al., 1997). Occult HBV infections are not detected by serological assays conventionally used to detect HBV infection and thus are often missed. Occult HBV infection has been shown to reactivate, to be a risk factor for the development of HCC (Mak et al., 2018) and can be

transmitted iatrogenically by blood transfusion and transplantation (Allain and Cox, 2011, Schmeltzer and Sherman, 2010, Squadrito et al., 2014).

Our previous studies have demonstrated that 23.8% of HIV positive patients were co-infected with HBV prior to the use of anti-retroviral therapy, with approximately 9% of these patients demonstrating the HBsAg-positive phenotype and 15% the HBsAg-negative phenotype or occult infection (Bell et al., 2012). Further molecular work on HBV isolated from these co-infected patients revealed that they were infected with subgenotype A1 and three of these patients were infected with preS deletion mutants and one patient with an occult HBV strain (Makondo et al., 2012). HIV co-infection has been found to be positively associated with the prevalence of preS deletions, being found in 23% of HBV/HIV co-infected individuals compared to 4.9% of HBV mono-infected individuals, computing to a relative risk of 5.759 (1.562 – 21.235) (Li et al., 2017). Moreover, these deletion mutants have been strongly associated with the development of HCC, with an approximately four-fold increased risk in the presence of the mutants (Liu et al., 2009) and these mutants can be used as predictive biomarkers for the development of HCC (Chen et al., 2007). Thus it was important to functionally characterize these mutants *in vitro*. The objective of this study was to examine the intracellular and extracellular expression of the HBsAg and HBeAg proteins by the deletion mutant and occult strains in comparison to subgenotype A1 wild-type following subcellular fractionation.

4.1 Integrity of plasmid constructs

In order to functionally characterise the deletion mutants detected in the HIV-infected patients wild-type replication-competent overlength clone constructs (Bhoola et al., 2014) were previously modified by replacing 784 bp in the preS1/S2/S region with fragments containing the deletions (*Figure 15*) (Wolhuter, 2016). The integrity of these previously constructed

plasmids was confirmed by restriction digestion and sequencing analyses prior to being used in the transfection assay (*Figure 16*).

4.2 Subcellular fractionation

Subcellular fractionation was carried out using both a commercial kit and a manual approach. Although the commercial kit allowed for the subcellular fractionation of the cells there was some cross-contamination across subcellular fractions, with proteins, which are specific for one fraction being present in other fractions (*Figure 20*). This is in agreement with Baghirova et al (2015), who highlight the tendency for commercial kits to yield cross-contaminated fractions even though their manufacturers claim that they can yield pure cellular fractions. The authors also noted that commercial kits do not always work efficiently and can be costly if several fractionations are necessary for the study (Baghirova et al., 2015).

Using the manual approach subcellular fractions with no contamination were extracted giving superior result to the commercial kit (*Figure 23*). This may be because the manual subcellular fractionation protocol utilizes specialised lysis buffers to isolate and concentrate proteins at each particular cellular level. The three buffers employed in the manual approach were namely; Lysis Buffer A, B & C (APPENDIX B, Table B3), which isolated the cytosolic, membrane-bound and the nuclear protein fractions, respectively (Baghirova et al., 2015). The combination of these lysis buffers produced efficient subcellular fractionation, which enriched proteins isolated in each cellular compartment (*Figures 23 and 26*).

Digitonin, the main component of Lysis Buffer A, is a steroidal saponin that permeabilizes the plasma membrane by binding with cholesterol and other b-hydroxysterols, leading to the formation of pores in the cell membrane and its subsequent disruption (Schulz, 1990). Digitonin is an invaluable reagent for the release cytosolic protein because it has the ability to lyse cells without disrupting the membranes of cellular organelles since the cholesterol composition of

these membranes is lower (Baghirova et al., 2015, Schulz, 1990). The cytosolic fraction is mainly composed of the cytoskeleton, which is positively stained by anti-cytokeratin 18, one of the major classes of cytoskeletal intermediate filament proteins (Chu and Weiss, 2002).

Nonidet P-40 a non-ionic, non-denaturing detergent is the main component of Lysis Buffer B, which was used for isolation of the membrane bound fraction. Nonidet P-40 is applied at a low concentration to permeabilize the membranes of the endoplasmic reticulum, Golgi and mitochondria, while preserving the integral structure of the nuclear membrane. This enables the release of proteins from all membrane bound organelles besides the nucleus (Baghirova et al., 2015, Le et al., 2015). Furthermore, because calreticulin, as an ER luminal resident protein is exclusive to the ER, it is used as the control protein for the membrane-bound fractions (Michalak et al., 1999).

Lysis Buffer C, which is used to extract the nuclear fraction is comprised of SDS and sodium deoxycholate. Sodium deoxycholate is a non-denaturing and non-ionic biological detergent while SDS is an anionic detergent that a powerful reagent for membrane solubilisation (Baghirova et al., 2015, Osteikoetxea et al., 2015). Furthermore, benzonase was included in this lysis buffer prior to the extraction of nuclear fractions in order to digest/degrade the DNA and RNA, which enables the unmitigated release of all nuclear proteins (Baghirova et al., 2015, Holden and Horton, 2009). Since histones localize in the nuclei of eukaryotic cells and are a key protein constituent of chromatin involved in the packaging of DNA into structural units (i.e. nucleosomes), it is selected as the control protein for the nuclear fractions (Bustin, 1976, Redon et al., 2002).

4.3 Intracellular expression of HBsAg

HBsAg proteins were better detected in the fractionated samples as opposed to the unfractionated whole cell lysate on day 5 post-transfection. This was clearly shown by the fact

that proteins were more evident on the immunoblots following subcellular fractionation (*Figures 26 and 27)*. An efficient subcellular fractionation method results in the clear separation of the individual components of the cell, such that the exact localization of various cellular and non-cellular (e.g. viral) proteins can be elucidated. Moreover, subcellular fractionation can enrich the various proteins that are found in low concentrations within the whole cell as was evidenced by the detection of HBsAg in the cytosolic and membrane-bound fractions but not in the nuclear fraction nor whole lysate (*Figure 26*).

The purity of the subcellular fractionation method was confirmed by the absence of HBsAg in the nuclear fraction (*Figure 26*). All protein translation of the mRNA viral transcripts occurs in the cytoplasm (Brinkley, 1981). SHBs was detected in the cytosolic and membrane bound fractions and was expressed by all constructs, which would be expected because there were no deletions present in the S region of all constructs tested.

In the immunoblotting assay, the SHH011A and SHH045A deletion mutants did not express any LHBs or MHBs whereas SHBs was detected in both the cytosolic and membrane-bound fractions (*Figure 26*). This result supports that SHBs can be released into the cytosol without the LHBs and MHBs proteins. SHH011A contains a deletion (i.e. pS2del1-22) in the preS2 domain, which completely removes the preS2 start codon (*Figure 14*) (Wolhuter, 2016) which would explain the lack of MHBs protein expression. The additional deletion in the preS1 domain (i.e. pS1del15-25) of SHH011A accounts for the absence of LHBs protein expression. The lack of MHBs expression in the SHH045A construct can be explained by the fact that this construct has a missense mutation (i.e. pS2L1I) in the preS2 domain that removes the start codon for MHBs expression (Wolhuter, 2016). The deletions in the preS1 domain in the case of SHH011A and in the preS2 domain in SHH011A and SHH045A result in the translation of misfolded/mutated LHBs, which would be degraded by the proteasomal regulatory systems in the ER (*discussed later*).

Even though SHH167A, has a deletion within the preS2 domain, it still expressed all three HBsAg proteins, including LHBs in both the cytosolic and membrane-bound fractions as seen in the immunoblotting assay (*Figure 26*). This deletion, even though longer than that found in SHH045A was found more on the amino end of the protein and resulted in a shorter LHBs than that expressed by the wild-type (*Figure 26*). Interestingly enough, following quasispecies analysis, the deletion clones of strain SHH167A,were found in combination with the wild-type clones in the patient serum (Wolhuter, 2016). Previous studies have found similar results. Melegari et al (1997) demonstrated that the predominant population of preS deletion mutants were found in conjunction with low quantities of a wild-type population. It has been suggested that the presence of these wild-type populations may result in genetic trans-complementation (i.e. the genetic capability of two mutant strains of a species combining to regenerate the normal species phenotype) of the deletion mutant constructs (Yook, 2005). This may enable the restoration of the core population in instances where viral replication and protein expression are inhibited/hindered by the presence of deletion mutants (Garcia et al., 2009, Kalinina et al., 2003, Melegari et al., 1997, Pollicino et al., 2012, Wolhuter, 2016). The deletions present in the SHH011A, SHH045A and SHH167A all fall within the B cell epitope domain as well as the neutralising antibody 1 and 2 domains (*Figure 14*) (Wolhuter, 2016), and this may explain the viral persistence of these deletion mutants in the patients.

The occult strain (SHH193A) appeared to be aggregating HBsAg proteins mainly in the membrane-bound fraction, with no traces of SHBs and MHBs and only slight traces of LHBs in the cytosolic fraction (*Figure 26*). This result is consistent with our previous findings using confocal immunofluorescent microscopy, where HBsAg proteins were found to aggregate in the perinuclear region (i.e. the region between the inner and outer membranes surrounding the nucleus) of cells transfected with the occult strain (Simelane, 2018). These results further supported that HBsAg in the occult strain is retained in the cellular compartments, preventing

the secretion of the surface proteins, which results in the HBsAg-negative phenotype characteristic of an OBI patient.

In addition, when performing Western blotting and ELISA analyses, Lin et al (2012) established that intracellular accumulation of HBsAg proteins were present in all preS deletion mutant transfected cells, particularly with regards to S promoter deletion mutant transfected cells. Moreover, immunofluorescence analysis indicated that contrastingly to the wild-type LHBs proteins, mutant LHBs proteins presented a perinuclear staining pattern in non-S-promoter deletion mutants and contrastingly a granular staining in S promoter deletion mutants (Lin et al., 2012); similarly, this result was demonstrated in various other studies (Bock et al., 1997, Fan et al., 2001, Pollicino et al., 2014, Su et al., 2008, Xu and Yen, 1996).

Additionally, Hassemer et al (2017) found that not only do HBV genotypes vary in relation to the expression of intracellular and extracellular HBsAg expression but also found variations in the ratio of LHBs, MHBs and SHBs proteins in the cellular lysates from cells infected with different HBV genotypes (Hassemer et al., 2017). The ratio of LHBs, MHBs and SHBs found in the cellular lysates of this study was similar to that found by Hassemer et al (2017) for genotype A, with SHBs proteins being more expressed than LHBs proteins, and MHBs proteins only slightly expressed in the A1 wild-type. In addition, relative to the wild-type strains, the preS deletions and occult strains ratio of HBsAg proteins vary considerably (*Figure 26*). For instance, both the SHH011A and SHH045A constructs did not express the A1 wild-type ratio of HBsAg, as there was no LHBs and MHBs protein expression. Furthermore, SHH167A expressed smaller LHBs proteins and more MHBs proteins relative to the A1 wild-type, occult and deletion mutant constructs (*Figure 26*). In fact, when comparing the Western blot analysis of the different HBV genotypes in Hassemer et al (2017), the SHH167A construct appears to demonstrate a similar HBsAg expression to the genotype C wild-type HBsAg expression, which expresses the more MHBs in comparison to the other HBV genotypes.

These disparities in HBsAg secretion observed in the deletion mutants and occult strain may intensify the accumulation and retention of HBsAg in the ER, which may ultimately lead to a decline in virion secretion (Bock et al., 1999, Melegari et al., 1997, Pollicino et al., 2012, Xu et al., 1997). Additionally, in eukaryotic cells, the ER supports sterol/lipid manufacturing, calcium storage, the biosynthesis and assemblage of secretory and membrane proteins and acts as a site for protein folding and post-translational modification (Ron and Walter, 2007). To ensure that only correctly folded proteins exit the ER, several stringent regulatory systems in the ER function to retain and degrade unfolded and/or mutant proteins. The accumulation of these mutant/unfolded proteins in the ER lumen can disturb ER homeostasis, thus inflicting stress to the organelle (Fribley et al., 2009, Schröder and Kaufman, 2005). In order to contend with this stress, the cell has developed highly specific signalling pathways commonly known as the unfolded protein response (UPR) to restore the ER functioning and overall performance. Although, if an excess of these misfolded proteins in the ER is not properly managed and resolved, the persistent UPR will prompt stress-associated apoptosis, which will eliminate the impaired cells and thus safeguarding the organism (Kaufman, 2002, Mori, 2000, Ron and Walter, 2007, Schröder and Kaufman, 2005).

Studies have shown that preS deletion mutants, which prompt the ER stress response, also result in the activation and stimulation of vascular growth factor A and Akt/mammalian target of rapamycin (mTOR), which signals ground glass hepatocytes (GGHs) (Yang et al., 2009). These GGHs are a histological indicator of chronic HBV infection and comprises of HBsAg proteins in the ER (Hadziyannis et al., 1973, Wang et al., 2003). Additionally, research has previously demonstrated that on account of ER stress, reactive oxygen species amass and induce oxidative DNA damage which can lead to hepatocarcinogenesis (Huang et al., 2005, Hung et al., 2004, Wang et al., 2003). Thus, these studies and findings indicate that preS deletion mutants may lead to the intracellular retention of HBsAg proteins which may be detrimental to cell survival and may result in the progression of HCC and cirrhosis (Huang et al., 2005).

4.4 Extracellular expression of HBeAg and HBsAg

In the HBsAg and HBeAg ELISA assays, protein expression of the wild-type, deletion mutant and occult strains were examined at days 1, 3 and 5 post-transfection. HBeAg protein expression was not affected by the introduction of deletions in the preS region with no significant variance in the HBeAg expression levels in all the samples, though there was a significant difference between the various time points, increasing with time (*Figure 28*). The precore ORF was not affected by the cloning strategy employed for the construction of the plasmids, thus it would not be expected that the HBeAg expression would be affected. The ELISA results also demonstrated that the HBeAg and HBsAg are expressed at higher levels in the SHH011A and SHH045A deletion mutant strains in comparison to the wild-type strains except at day 1 post transfection where the protein expression was low and gradually increased in expression by day 3 and day 5 post-transfection. Contrastingly, a divergent trend was found in the SHH167A deletion mutant strain, which generated smaller sized LHBs compared to the wild-type and occult constructs. Initially, the SHH167A construct expressed the highest HBsAg levels at day 1 post-transfection, however, by day 3 post-transfection, it reached a plateau and ultimately expressed lower HBsAg levels at day 3 and day 5 post-transfection in comparison to the other deletion mutants and wild-type strains. It is noteworthy to mention that although the HBsAg ELISA is a quantitative assay, the assay alone cannot make a distinction between subviral particles and virion associated HBsAg.

Contrastingly, the occult SHH193A construct demonstrated extremely low levels of HBeAg and particularly low HBsAg expression in comparison to both the wild-type and deletion strains at all three time points, which is a consistent finding with previous results (Wolhuter, 2016). The transfection results of the occult construct imitates the HBsAg-negative phenotype of occult patients *in vivo* (Bell et al., 2012, Raimondo et al., 2008).

4.5 Limitations

The immunoblotting analysis of the intracellular expression of HBeAg was initially proposed for this study. However, HBeAg could not be detected - even in the positive controls. Various attempts were made to optimize this part of the study, including; the testing of various dilutions of the anti-HBeAg antibodies, alternatively testing another batch of anti-HBeAg antibodies as well as increasing the protein concentration of the samples loaded in the gels. The lack of HBeAg detection may have been due to inadequate specific binding by the anti-HBeAg antibodies employed. Another explanation/factor for the lack of HBeAg detection in the immunoblotting assays, could be that the sample extracts generated low yields of HBeAg in this study.

4.6 Conclusion

The high worldwide prevalence of chronic HBV infection is correspondingly associated with the progression of HCC (Bouchard and Navas-Martin, 2011, Neuveut et al., 2010). Though the relationship between chronic HBV infections and HCC has been reported and is well-known, inconsistencies in our understanding of how chronic HBV infection can result in the advancement of HCC is still a challenge. Subgenotype A1, which is the strain prevalent in eastern-southern Africa has been shown to be more hepatocarcinogenic than subgenotypes A2 and D3, the other strains found in South Africa (Kew et al., 2005). The association of subgenotype A1 with HCC has also been shown in Indian patients (Gopalakrishnan et al., 2013). HBV isolates from HCC patients have been shown to have deletions in the preS region, which have been shown to be a risk factor for the development of HCC (Chen et al., 2008, Yin et al., 2010). Moreover, the frequency of these deletion mutants is higher in HBV/HIV co-infected compared to HBV mono-infected individuals (Li et al., 2017). This study describes the functional characterization of these deletion mutants and an occult strain isolated from HIV-infected adults following transfection of Huh7 cells and subcellular fractionation.

The findings of this study demonstrate that the ratio, localization in each cellular compartment and expression of HBsAg proteins of the occult and preS deletion mutant strains were affected relative to the wild-type. The retention of HBsAg in the ER, can result in ER stress and lead to reactive oxygen species accumulation, which can trigger oxidative DNA damage, and ultimately to hepatocarcinogenesis (Huang et al., 2005, Hung et al., 2004, Wang et al., 2003).

APPENDIX A: ETHICS CLEARANCE & PERMISSIONS



Human Research Ethics Committee (Medical) 50 years 1966 – 2016

Research Office Secretariat: Faculty of Health Sciences, Phillip Tobias Building, 3rd Floor, Office 301,
29 Princess of Wales Terrace, Parktown, 2193 Tel +27 (0)11-717-1252 /1234/2656/2700
Private Bag 3, Wits 2050, email: zanele.ndlovu@wits.ac.za
Office email: hrec-medical.researchoffice@wits.ac.za
Website: www.wits.ac.za/research/about-our-research/ethics-and-research-integrity/

Ref: W-CJ-170308-1 08/03/2017

TO WHOM IT MAY CONCERN:

Waiver: This certifies that the following research does not require clearance from the Human Research Ethics Committee (Medical).

Investigator: Ms Hillary Vos (student no. 1498949).

Project title: Study of the expression of HBsAg and HBeAg by deletion mutants and occult strains of subgenotype A1 of HBV using cellular fractionation.

Reason: This is a laboratory study using tissue culture and previously constructed plasmids. There are no human participants.

UNIVERSITY OF THE WITWATERSRAND
PROF PE CLEATON-JONES
HREC (MEDICAL)
2017 -03- 08
JOHANNESBURG

Professor Peter Cleaton-Jones

Chair: Human Research Ethics Committee (Medical)

Copy – HREC (Medical) Secretariat: Zanele Ndlovu, Rhulani Mkansi, Lebo Moeng.

Figure A1 Ethics clearance certificate

PERMISSIONS

Please note that all figures in this dissertation were created by the author except for the following four figures:

Figure 1 by Debarry et al (2017) was used under John Wiley & Sons, Inc. License number: 4537251307696, license date: 27 February 2019.

Figures 2 & 3 by Velkov et al (2018), has been published under the MDPI. All articles published by MDPI are made immediately available worldwide under an open access license which allows all users to reuse published material without permission provided that the original publication is properly cited.

Figure 4 by Kramvis (2016) did not require any special permission:



Figure A2: Creative Commons Attributions Non-Commercial License agreement.

APPENDIX B: COMPOSITION OF REAGENTS & SOLUTIONS

Table B1: Reagents composition for plasmid preparation

Reagent/Solution	Composition
B1.1) Agarose (0.8% (w/v))	0.8 g agarose was dissolved in 100 ml 1X TBE Buffer by heating in a microwave. The agarose gel solution was then supplemented with 3 µl/100 ml ethidium bromide, after which it was poured onto the gel tray apparatus and allowed to solidify for 30 minutes prior to use.
B1.2) Ampicillin (100 mg/ml)	1.0 g Ampicillin was resuspended in 10 ml SABAX water and dissolved by vortexing. The solution was then filter sterilized using a 0.2 µm Minisart® NML single-use syringe filter (Sartorius AG, Goettingen, Germany). Thereafter, 1 ml aliquots of the solution were prepared and placed into sterile 1.5 ml microcentrifuge tubes (wrapped in foil) and stored at -20 °C until further use.
B1.3) Buffer RES-EF	100 µg/ml RNase A was dissolved once off into 1 ml Resuspension Buffer S1-EF by vortexing. Subsequently, all of the resulting solution were supplemented to the remainder of the Resuspension Buffer S1-EF and thoroughly mixed. Aliquots of the solution was then stored at 4 °C until further use.

B1.4) Kanamycin (50 mg/ml)	0.5 g Kanamycin Sulfate was resuspended in 10 ml SABAX water and dissolved by vortexing. The solution was then filter sterilized using a 0.2 µm Minisart® NML single-use syringe filter. Thereafter, 1 ml aliquots were prepared in sterile 1.5 ml microcentrifuge tubes (wrapped in foil) and stored at -20 °C until further use.
B1.5) LB Medium	10 g Bacto-Tryptone 5 g Bacto-Yeast Extract 10 g NaCl Made up to 1 L of sterile distilled water. The solution was then autoclaved at 121°C for 30 minutes and stored at 4 °C until further use.
B1.6) TBE Buffer (1X)	100 ml 20X TBE Buffer was dissolved in 1.9 L sterile distilled water and stored at room temperature until further use.
B1.7) TBE Buffer (20X)	212 g Tris Base 110 g Boric Acid 18.6 g EDTA Disodium Salt Made up to 1 L of sterile distilled water. The solution was then autoclaved at 121°C for 30 minutes and stored at 4 °C until further use.
B1.8) Tris (10 mM, pH 7.5)	0.12 g Tris A volume of 80 ml UltraPure™ water was added to the solution and was adjusted to pH 7.5 with Hydrochloric Acid, 32% (v/v). The solution was then

	made up to a final volume of 100 ml with the UltraPure™ water and autoclaved at 121°C for 30 minutes. The solution was then stored at 4 °C until further use.
B1.9) YT Agar Plates (2X) Supplemented with 100 µg/ml Ampicillin	16 g Bacto-Tryptone 10 g Bacto-Yeast Extract 5 g NaCl 15 g Agar Bacteriological Made up to 1 L of sterile distilled water and autoclaved at 121 °C for 30 minutes. Thereafter, it was allowed to cool for 1 hour at room temperature and then an aliquot of 1 ml 100 mg/ml ampicillin was supplemented to the solution. Subsequently, 50 ml of the solution was poured into 10 cm petri dishes and allowed to dry overnight. The following day the petri dishes were stored at 4 °C until further use.
B1.10) YT Agar Plates (2X) Supplemented with 50 µg/ml Kanamycin	16 g Bacto-Tryptone 10 g Bacto-Yeast Extract 5 g NaCl 15 g Agar Bacteriological Made up to 1 L of sterile distilled water and autoclaved at 121 °C for 30 minutes. Thereafter, it was allowed to cool for 1 hour at room temperature and then an aliquot of 1 ml 50 mg/ml kanamycin was supplemented to the solution. Subsequently, 50 ml of the solution was poured into 10 cm petri dishes and

	allowed to dry overnight. The following day the petri dishes were stored at 4 ℃ until further use.
B1.11) YT Medium (2X)	16 g Bacto-Tryptone 10 g Bacto-Yeast Extract 5 g NaCl Made up to 1 L of sterile distilled water, autoclaved at 121 ℃ for 30 minutes then stored at 4 ℃

Table B2: Reagents composition for Cell culture & Mycoplasma detection Assay

Reagent/Solution	Composition
B2.1) Complete Growth DMEM Medium	435 ml DMEM, GlutaMax™ Supplement, Pyruvate 50 ml Foetal Bovine Serum 5 ml 100X MEM Non-Essential Amino Acids Solution 10 ml 10 000 U/ml Penicillin-Streptomycin
B2.2) PBS	1 PBS tablet was dissolved in 500 ml UltraPure™ distilled water, autoclaved at 121 ℃ for 30 minutes, then stored at 4 ℃ until further use.
B2.3) Polymerase Rehydration Buffer Mixture	An aliquot of 0.5 µl 2.5 U/µl JumpStart™ *Taq* DNA polymerase was supplemented per 23 µl Rehydration Buffer

Table B3: Reagents composition for the Subcellular Fractionation & Whole Cell Lysis Protocols

Reagent/Solution	Composition
B3.1) Cytoplasmic Extraction Buffer (CEB)	Freshly prepared when required: 1 µl 100X Halt Protease Inhibitor Cocktail was supplemented per 100 µl CEB stock solution
B3.2) Lysis Buffer A	150 mM NaCl 50 mM HEPES (pH 7.4) 25 mg/ml Digitonin 1 M Hexylene glycol 1% (v/v) Protease inhibitor cocktail
B3.3) Lysis Buffer B	150 mM NaCl 50 mM HEPES (pH 7.4) 1% (v/v) Nonidet P-40 1 M Hexylene glycol 1% (v/v) Protease inhibitor cocktail
B3.4) Lysis Buffer C	150 mM NaCl 50 mM HEPES (pH 7.4) 0.5% (w/v) Sodium deoxycholate 0.1% (w/v) Sodium dodecyl sulfate 1 M Hexylene glycol 1% (v/v) Protease inhibitor cocktail
B3.5) Membrane Extraction Buffer (MEB)	Freshly prepared when required: 1 µl 100X Halt Protease Inhibitor Cocktail was supplemented per 100 µl MEB stock solution

B3.6)	**NEB (containing $CaCl_2$ & Micrococcal Nuclease)**	Freshly prepared when required: 5 µl 100 mM $CaCl_2$, 3 µl micrococcal nuclease and 1 µl 100X Halt Protease Inhibitor Cocktail was added per 100 µl NEB solution
B3.7)	**Nuclear Extraction Buffer (NEB)**	Freshly prepared when required: 1 µl 100X Halt Protease Inhibitor Cocktail was supplemented per 100 µl NEB stock solution
B3.8)	**Pellet Extraction Buffer (PEB)**	Freshly prepared when required: 1 µl 100X Halt Protease Inhibitor Cocktail was supplemented per 100 µl PEB stock solution
B3.9)	**SDS Total Cell Lysis Buffer Stock Solution**	50 mM Tris-HCl, pH 6.8 2% (w/v) SDS (2 g) 10% (v/v) Glycerol The solution was made up to 100 ml with Milli-Q water and stored at room temperature until further use.
B3.10)	**SDS Total Cell Lysis Buffer Working Solution**	40 µl 25X complete, EDTA-Free protease inhibitor cocktail stock solution was supplemented per ml of SDS Total Cell Lysis Buffer Stock Solution. This solution was always freshly prepared when required

Table B4: Reagents composition for the Protein Concentration Determination Assay

Reagent/Solution	Composition
B4.1) BCA Working Reagent	BCA Working Reagent was prepared by supplementing 50 parts of BCA Reagent A with 1 part of BCA Reagent B.

Table B5: Reagents composition for the Immunoblotting Assay

Reagent/Solution	Composition
B5.1) Acrylamide-Bis-Acrylamide Solution (40% (w/v))	95 g Acrylamide 5 g Bis-Acrylamide Made up to 250 ml with sterile distilled water, filter sterilized with 0.4 µm Minisart® NML single-use syringe filter and stored in aliquots of 50 ml in 50 ml polypropylene tubes (wrapped in foil) at 4 °C until further use.
B5.2) APS (10% (w/v))	1 g APS Made up to 10 ml with sterile distilled water, then stored in aliquots of 1 ml at -20 °C for long-term use or at 4 °C for immediate use.
B5.3) Blocking Solution	5% (w/v) Fat-Free Milk (25 g) Made up to 500 ml with TBS-T and was stored at 4 °C until further use.
B5.4) Complete, EDTA-Free Protease Inhibitor	1 tablet of complete, EDTA-Free Protease Inhibitor Cocktail was dissolved in 2 ml Milli-Q water and stored at 4 °C until further use.

	Cocktail Stock Solution (25X)	
B5.5)	***Laemmili Buffer (4X)***	1 M Tris-HCl pH 6.8 (12.5 ml) 8% (w/v) SDS (4g) 40% (v/v) Glycerol (20 ml) 0.02% (w/v) Bromophenol Blue Sodium Salt for Electrophoresis (0.01 g) Made up to a final volume of 40 ml with Milli-Q water and stored at room temperature. For every 8 ml of Laemmili buffer solution, an aliquot of 2 ml 20% (v/v) β-Mercaptoethanol was supplemented to the solution and stored in a 15 ml polypropylene tube and stored at 4 ℃ until further use.
B5.6)	***Mouse Monoclonal Antibody against the S Region (Antigenic Loop) of HBsAg (mAb HB1) [1:1000]***	25 µl of mouse monoclonal antibody against the S region (antigenic loop) of HBsAg (mAg HB1)
B5.7)	***NaCl (5 M)***	146.1 g Sodium Chloride Made up to a final volume of 500 ml with Milli-Q water, then autoclaved at 121 ℃ for 30 minutes and stored at room temperature until further use.
B5.8)	***NaOH (5 M)***	20 g Sodium Hydroxide Pellets

	Made up to a final volume of 100 ml with Milli-Q water, then autoclaved at 121 °C for 30 minutes and stored at room temperature until further use.
B5.9) Ponceau Stain	0.5% (w/v) Ponceau S, practical grade (5 g) 1% (v/v) Acetic Acid, Glacial (10 ml) Made up to a final volume of 1 L with sterile-distilled water, and stored at room temperature until further use.
B5.10) Rabbit Polyclonal Antibody against GFP [1:25000]	0.5 µl of monoclonal anti-GFP antibody produced in rabbit was dissolved in 25 ml blocking solution and was stored at 4 °C until further use.
B5.11) SDS (10% (w/v))	10% (w/v) SDS (1 g) Made up to 100 ml with sterile-distilled water and stored at room temperature until further use.
B5.12) SDS Running Buffer (10X)	30.3 g Tris 144.1 g Glycine Made up to 800 ml with sterile distilled water and autoclaved at 121 °C for 30 minutes. Next, 10 g SDS Was supplemented to the solution and it was made up to 1 L with sterile distilled water and stored at room temperature until further use.
B5.13) SDS Running Buffer (1X)	200 ml 10X SDS Running Buffer Made up to 2 L with sterile distilled water and stored at room temperature until further use.
B5.14) SDS-PAGE Gel	The SDS PAGE gel was prepared using the Mini-PROTEAN® Tetra HandCast System.

12% (v/v) Separating Gel:

4.0 ml Acrylamide/Bis-Acrylamide Solution (40% (w/v))

3.4 ml Sterile-Distilled Water

2.5 ml Tris-HCl (1.5 M, pH 8.8)

100 µl SDS (10% (w/v))

160 µl APS

14 µl TEMED (10% (w/v))

The separating gel was pipetted into the Mini-PROTEAN® Tetra HandCast System until approximately three-quarters full and overlaid with 100% (v/v) isopropanol to prevent oxidation of the gel and it was allowed to solidify.

4.5% (v/v) Stacking Gel:

600 µl Acrylamide/Bis-Acrylamide Solution (40% (w/v))

2.86 ml Sterile-Distilled Water

500 µl Tris-HCl (1 M, pH 6.8)

40 µl SDS (10% (w/v))

24 µl APS

24 µl TEMED (10% (w/v))

The 100% (v/v) isopropanol was removed using filter paper before pipetting the stacking gel into the Mini-PROTEAN® Tetra HandCast System. A comb was then inserted and the solution was allowed to solidify.

B5.15) Stripping Solution	5% (w/v) Fat-Free Milk Powder (25 g) 0.2% (w/v) NaN_3 (1.0%) Made up to 500 ml with TBS-T and was stored at 4 °C until further use.
B5.16) SuperSignal® West Dura Extended Duration Substrate Working Solution	200 µl SuperSignal® West Dura Stable Peroxide 200 µl SuperSignal® West Dura Luminol/Enhancer The solution was thoroughly mixed and prepared fresh prior to use.
B5.17) TBS (10X)	50 ml 1 M Tris-HCl, pH 8.0 150 ml 5 M NaCl Made up to a final volume of 1L with Milli-Q water, autoclaved at 121 °C for 30 minutes, then stored at room temperature until further use.
B5.18) TBS-T (1X)	200 ml 10X TBS 2 ml Tween® 20 Made up to a final volume of 2 L with Milli-Q water, then stored at room temperature until further use.
B5.19) Tris-HCl (1.5 M, pH 8.8)	90.86 g Tris Made up to a volume of 400 ml with sterile distilled water. The solution was then adjusted to pH 8.8 with Hydrochloric Acid, 32% (v/v). Subsequently, the solution was made up to a final volume of 500 ml with sterile-distilled water and autoclaved at 121 °C for 30 minutes. The solution was then stored at room temperature until further use.

B5.20) Tris-HCl, pH 6.8 (1 M)	12.11 g Tris Made up to a final volume of 50 ml with Milli-Q water. The solution was then adjusted to pH 6.8 with Hydrochloric Acid, 32% (v/v). Subsequently, the solution was made up to a final volume of 100 ml with Milli-Q water, autoclaved at 121 °C for 30 minutes and was stored at room temperature until further use.
B5.21) Tris-HCl, pH 6.8 (1 M)	30.29 g Tris Made up to a volume of 150 ml with sterile distilled water and the solution was adjusted to pH 6.8 with Hydrochloric Acid, 32% (v/v). Subsequently, the solution was made up to a final volume of 250 ml with sterile distilled water, autoclaved at 121 °C for 30 minutes and was stored at room temperature until further use.
B5.22) Tris-HCl (1 M, pH 8.0)	60.57 g Tris Made up to a final volume of 400 ml with Milli-Q water and the solution was adjusted to pH 8.0 with Hydrochloric Acid, 32% (v/v). Subsequently, the solution was made up to a final volume of 500 ml with Milli-Q water, autoclaved at 121 °C for 30 minutes and was stored at room temperature until further use.
B5.23) Wet Transfer Buffer (10X)	30.3 g Tris 144.1 g Glycine Made up to a volume of 800 ml with sterile distilled water and the solution was adjusted to pH8.3 with

	Hydrochloric Acid, 32% (v/v). Thereafter, the solution was made up to a final volume of 1 L with sterile distilled water, autoclaved at 121 °C for 30 minutes and was stored at room temperature until further use.
B5.24) Wet Transfer Buffer (1X)	200 ml 10X Wet Transfer Buffer 400 ml 100% (v/v) Ethanol Made up to a final volume of 2 L with sterile distilled water and stored at room temperature until further use.

APPENDIX C: PRIMER SEQUENCES

Table C1: List of sequencing primers utilized to determine the sequences of HBV clones

Primer	*Primer Sequence*	*Primer Binding Site (nt.)*	*Binding Site*	*Region Covered of HBV (nt.)*	*Size of Sequencing Fragment (bp)*
1040F	5'-TGG TTA CCC TGC CTT AAT GCC TT-3'	1038–1060	HBV	1083-1783	700
2497F	5'-TTC CTT GGA CTC ATA AGG TG-3'	2497-2516	HBV	2556-315	700
3188F	5'-AGT CAG GAA GGC AGC CTA C-3'	3188-3206	HBV	3196-275	700
591F	5'-ATT GCA CCT GTA TTC CCA TCC-3'	591-611	HBV	634-1334	700
pCR-BGH3.1R	5'-TAG AAG GCA CAG TCG AGC-3'	1089-1106	pcDNA^{TM}4/TO Expression Vector	1064-1764	700
Post-BglII	5'-CCG ATA CAG AGC TGA GGC-3'	2036-2042	HBV	1298-1998	700
TO-F	5'-GGT TCC GCG CAC ATT TCC-3'	5039-5056	pcDNA^{TM}4/TO Expression Vector	1064-1864	700

APPENDIX D: THE GENERATION OF A COMPUTATIONAL PLASMID MAP FOR THE RECOMBINANT 1.28 MER HBV A1 WT PLASMID

A computational plasmid map was created for the recombinant 1.28 mer overlength HBV Subgenotype A1 wild-type plasmid developed by Bhoola et al (2014). The accurate identification of restriction sites and possible start and stop codons are fundamental when employing any plasmid in a research study.

D.1) Computational Plasmid map features

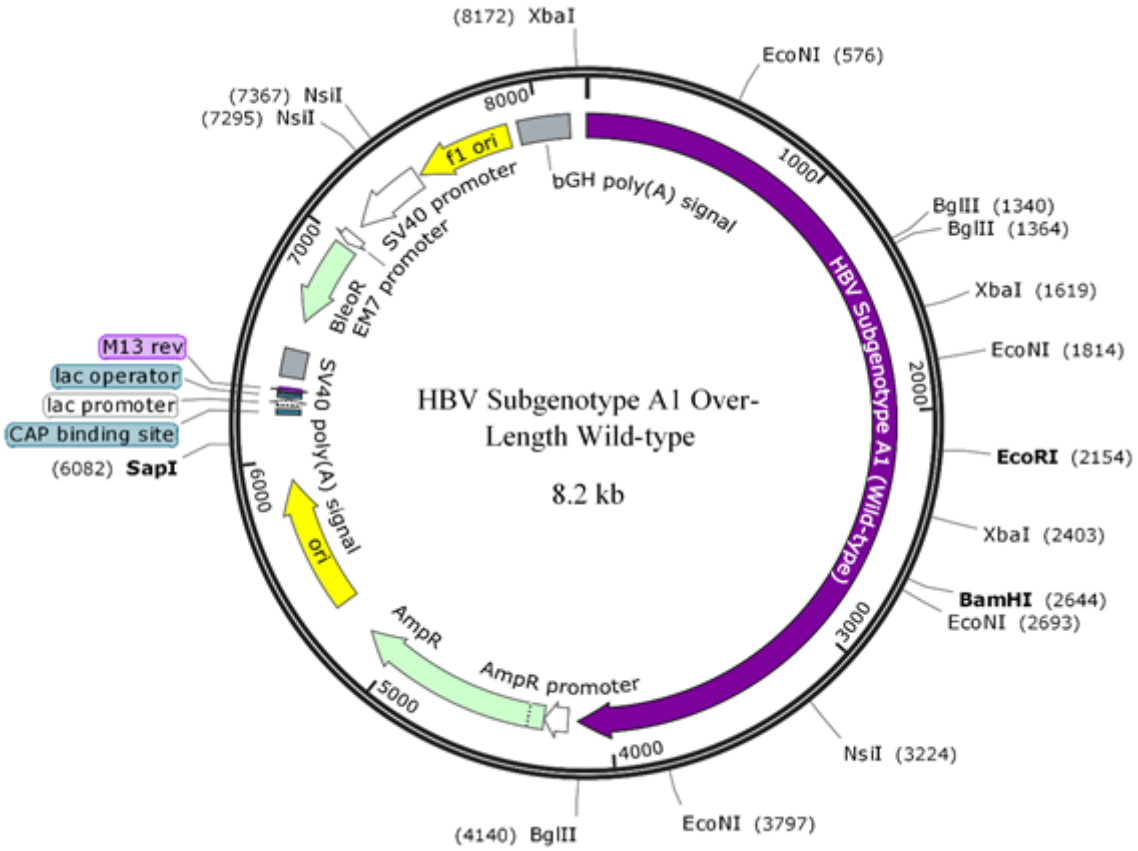


Figure D.1: The HBV Subgenotype A1 Over-length Wild-type constructed according to Bhoola et al (2014) using the SnapGene software.

The SnapGene software (GSL Biotech, available at snapgene.com) was employed to construct the computational plasmid map (*Figure D.1*) according to the protocol performed in Bhoola et al (2014). *Figure D.* 2 illustrates the step-by-step construction of the plasmid.

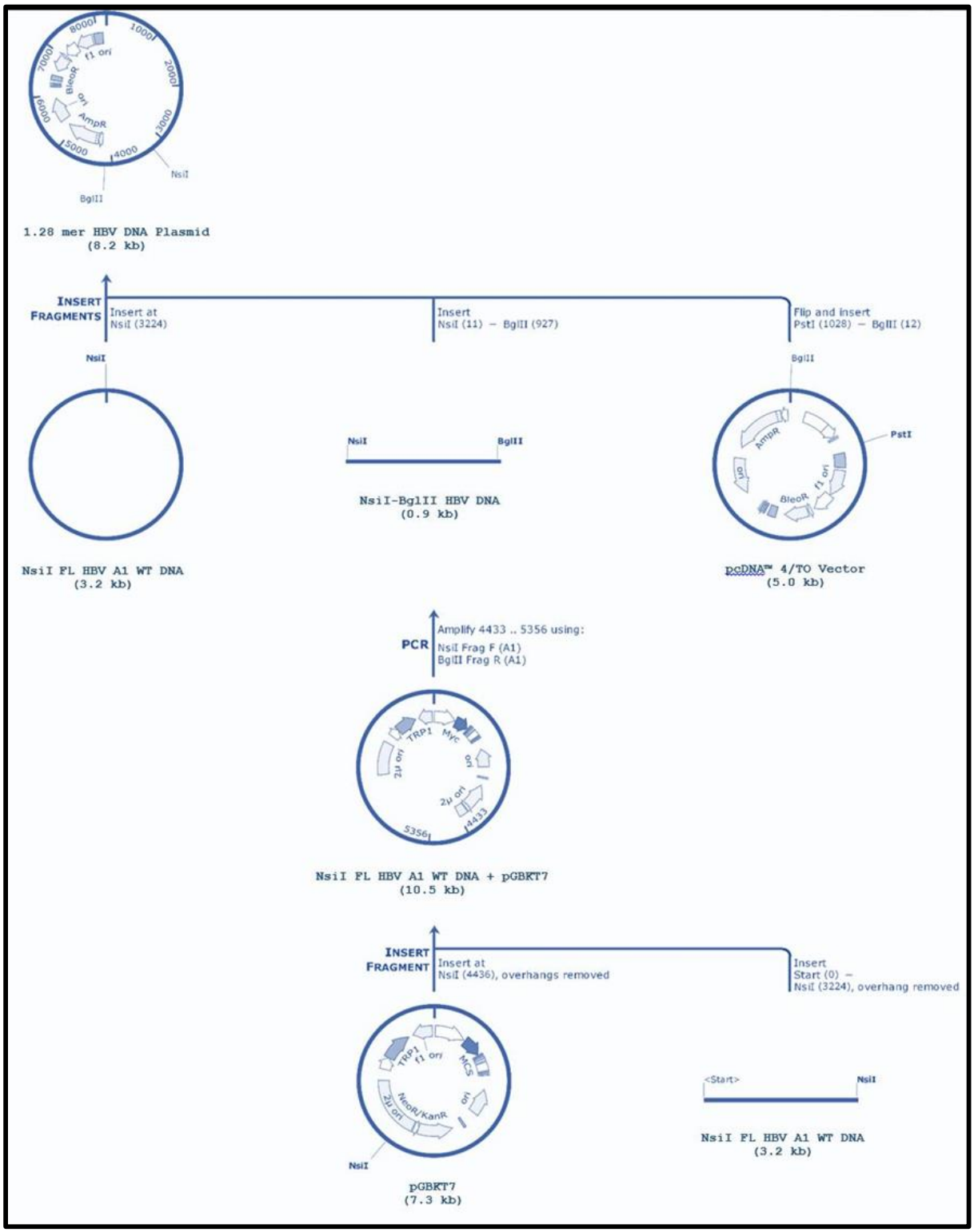


Figure D. 2: Step-by-step protocol of the computational construction of the plasmid map

D.2) Restriction digestion simulation using the computational plasmid construct

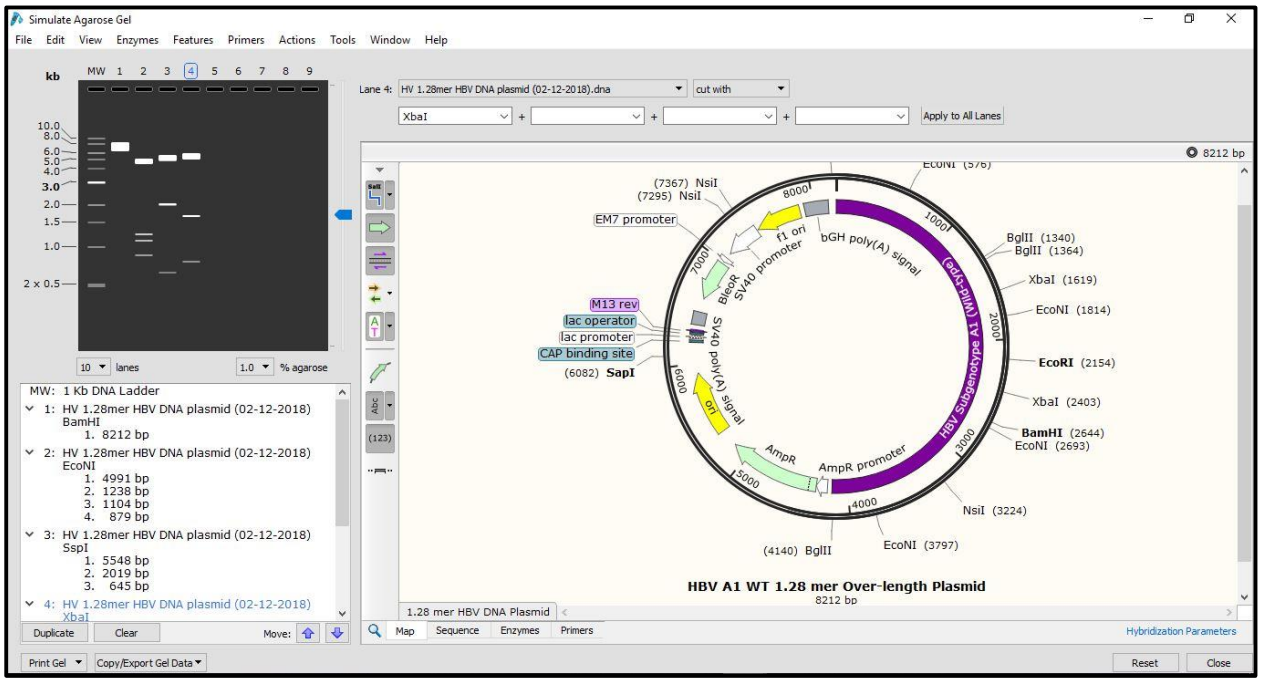


Figure D. 3: An illustration of the SnapGene software employed to simulate the restriction digestions of BamHI, EcoNI, SspI and XbaI. This tool was utilized in order to confirm the integrity of the constructed computational plasmid construct.

Assembling a computational plasmid is pivotal before a user can operate various bioinformatics tools much like the SnapGene software. It allows for a more convenient approach to genetic engineering by predicting the outcome of possible restriction digestions, identifying stop/start codons and its capabilities extend from aligning sequences, simulating agarose gels to primer designing.

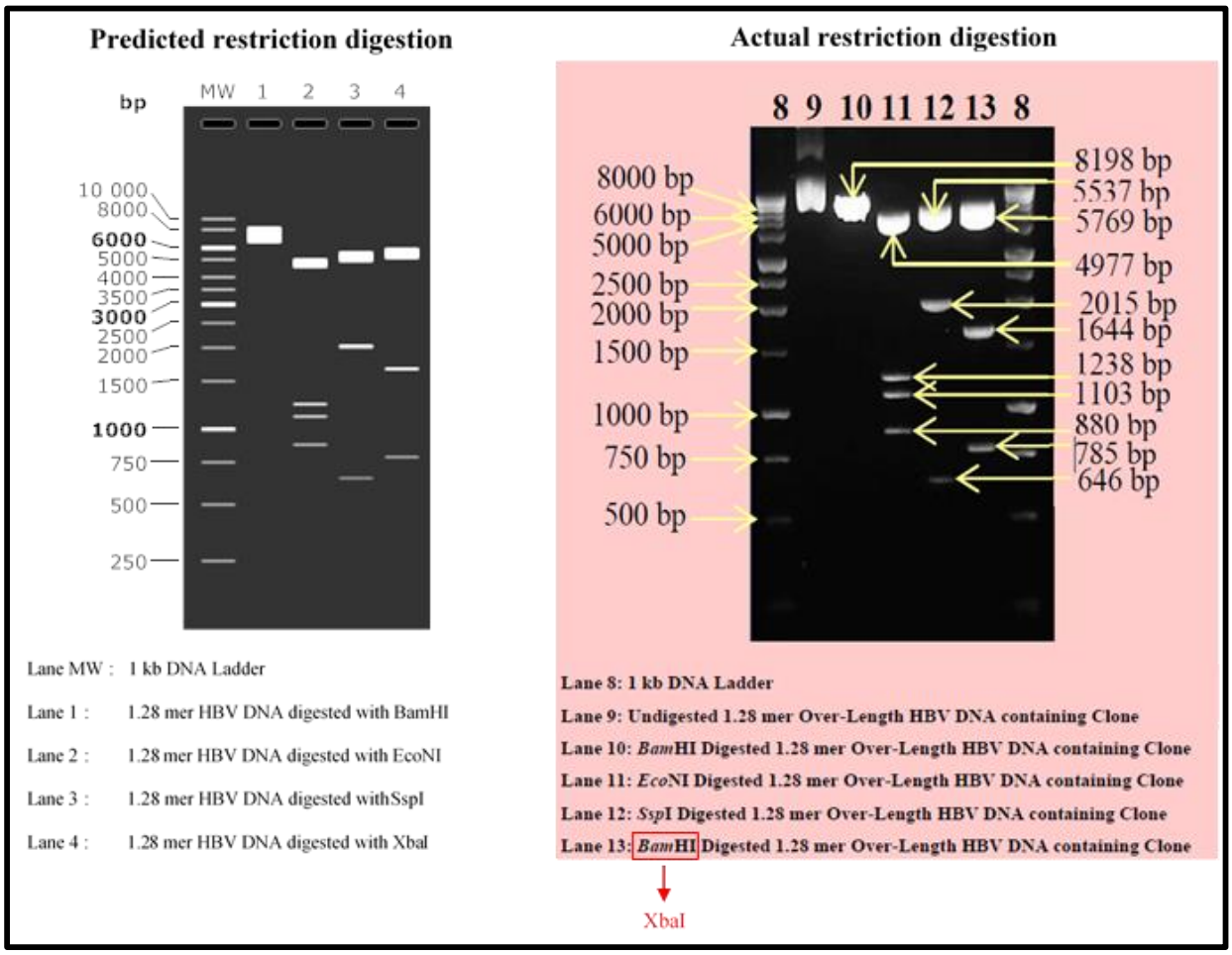


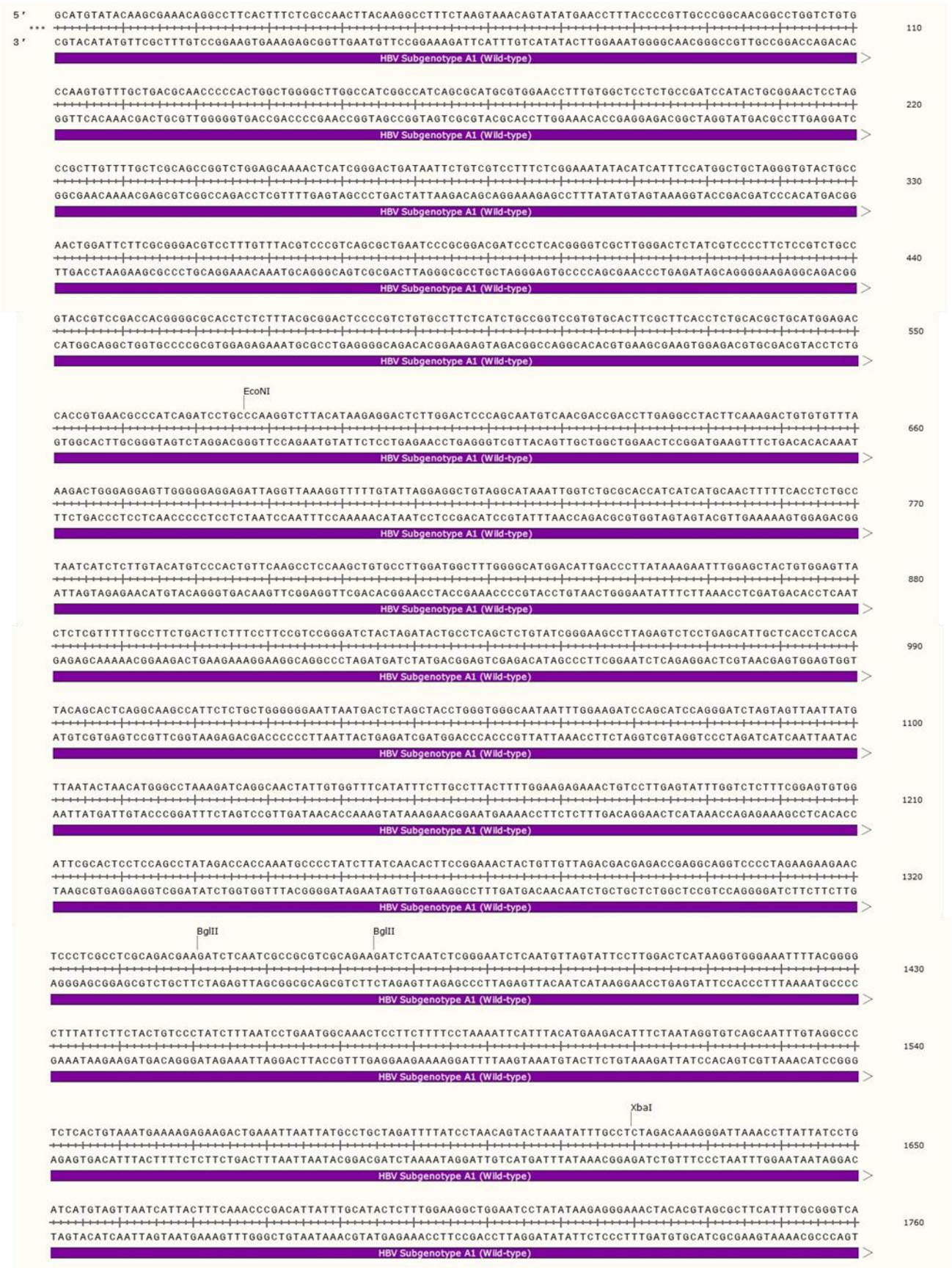
Figure D.4: A comparison of the predicted restriction digestion contrasted with the actual restriction digestions produced by Bhoola et al (2014). The red box highlights an error detected.

Figure D.4 demonstrates the precision of the SnapGene software tool when digesting the 1.28 mer over-length HBV DNA with *Bam*HI, *Eco*NI, *Ssp*I and *Xba*I respectively. A comparison of the fragment sizes generated is shown on *Table D.1*.

Table D.1: Restriction Digestions Comparison Summary

Restriction enzymes	Actual Digestion Estimates	Prediction Digestion based on computational plasmid construct
***Bam*HI**	Fragment 1: 8198 bp	Fragment 1: 8212 bp
***Eco*NI**	Fragment 1: 4977 bp	Fragment 1: 4991 bp
	Fragment 2: 1238 bp	Fragment 2: 1238 bp
	Fragment 3: 1103 bp	Fragment 3: 1104 bp
	Fragment 4: 880 bp	Fragment 4: 879 bp
***Ssp*I**	Fragment 1: 5537 bp	Fragment 1: 5548 bp
	Fragment 2: 2015 bp	Fragment 2: 2019 bp
	Fragment 3: 646 bp	Fragment 3: 645 bp
***Xba*I**	Fragment 1: 5769 bp	Fragment 1: 5769 bp
	Fragment 2: 1644 bp	Fragment 2: 1659 bp
	Fragment 3: 785 bp	Fragment 3: 784 bp

APPENDIX E: COMPLETE SEQUENCE OF HBV SUBGENOTYPE A1 WT



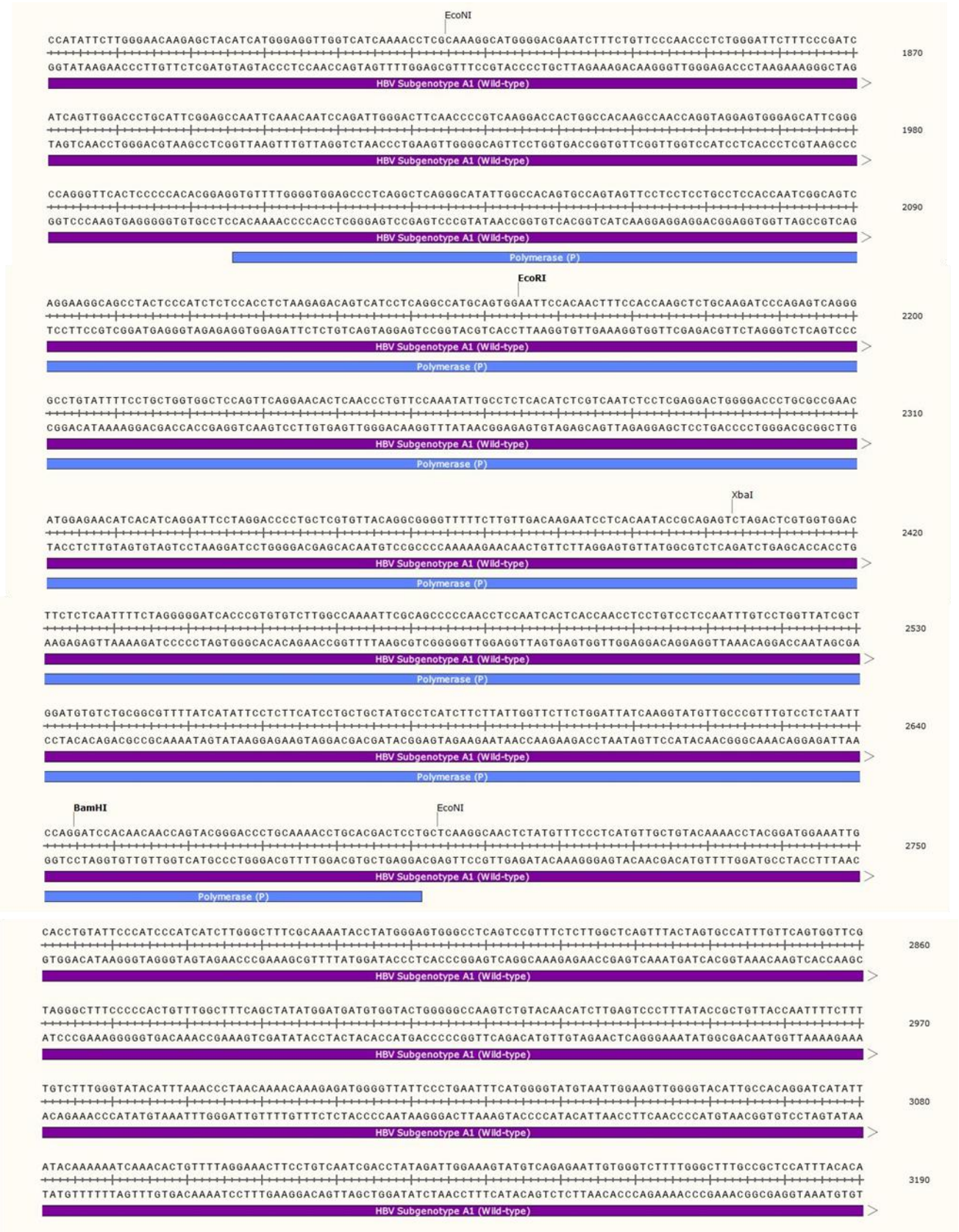

EcoNI
CCATATTCTTGGGAACAAGAGCTACATCATGGGAGGTTGGTCATCAAAACCTCGCAAAGGCATGGGGACGAATCTTTCTGTTCCCAACCCTCTGGGATTCTTTCCCGATC
GGTATAAGAACCCTTGTTCTCGATGTAGTACCCTCCAACCAGTAGTTTTGGAGCGTTTCCGTACCCCTGCTTAGAAAGACAAGGGTTGGGAGACCCTAAGAAAGGGCTAG
1870
HBV Subgenotype A1 (Wild-type)
ATCAGTTGGACCCTGCATTCGGAGCCAATTCAAACAATCCAGATTGGGACTTCAACCCCGTCAAGGACCACTGGCCACAAGCCAACCAGGTAGGAGTGGGAGCATTCGGG
TAGTCAACCTGGGACGTAAGCCTCGGTTAAGTTTGTTAGGTCTAACCCTGAAGTTGGGGCAGTTCCTGGTGACCGGTGTTCGGTTGGTCCATCCTCACCCTCGTAAGCCC
1980
HBV Subgenotype A1 (Wild-type)
CCAGGGTTCACTCCCCCACACGGAGGTGTTTTGGGGTGGAGCCCTCAGGCTCAGGGCATATTGGCCACAGTGCCAGTAGTTCCTCCTCCTGCCTCCACCAATCGGCAGTC
GGTCCCAAGTGAGGGGGTGTGCCTCCACAAAACCCCACCTCGGGAGTCCGAGTCCCGTATAACCGGTGTCACGGTCATCAAGGAGGAGGACGGAGGTGGTTAGCCGTCAG
2090
HBV Subgenotype A1 (Wild-type)
Polymerase (P)
EcoRI
AGGAAGGCAGCCTACTCCCATCTCTCCACCTCTAAGAGACAGTCATCCTCAGGCCATGCAGTGGAATTCCACAACTTTCCACCAAGCTCTGCAAGATCCCAGAGTCAGGG
TCCTTCCGTCGGATGAGGGTAGAGAGGTGGAGATTCTCTGTCAGTAGGAGTCCGGTACGTCACCTTAAGGTGTTGAAAGGTGGTTCGAGACGTTCTAGGGTCTCAGTCCC
2200
HBV Subgenotype A1 (Wild-type)
Polymerase (P)
GCCTGTATTTTCCTGCTGGTGGCTCCAGTTCAGGAACACTCAACCCTGTTCCAAATATTGCCTCTCACATCTCGTCAATCTCCTCGAGGACTGGGGACCCTGCGCCGAAC
CGGACATAAAAGGACGACCACCGAGGTCAAGTCCTTGTGAGTTGGGACAAGGTTTATAACGGAGAGTGTAGAGCAGTTAGAGGAGCTCCTGACCCCTGGGACGCGGCTTG
2310
HBV Subgenotype A1 (Wild-type)
Polymerase (P)
XbaI
ATGGAGAACATCACATCAGGATTCCTAGGACCCCTGCTCGTGTTACAGGCGGGGTTTTTCTTGTTGACAAGAATCCTCACAATACCGCAGAGTCTAGACTCGTGGTGGAC
TACCTCTTGTAGTGTAGTCCTAAGGATCCTGGGGACGAGCACAATGTCCGCCCCAAAAAGAACAACTGTTCTTAGGAGTGTTATGGCGTCTCAGATCTGAGCACCACCTG
2420
HBV Subgenotype A1 (Wild-type)
Polymerase (P)
TTCTCTCAATTTTCTAGGGGGATCACCCGTGTGTCTTGGCCAAAATTCGCAGCCCCCAACCTCCAATCACTCACCAACCTCCTGTCCTCCAATTTGTCCTGGTTATCGCT
AAGAGAGTTAAAAGATCCCCCTAGTGGGCACACAGAACCGGTTTTAAGCGTCGGGGGTTGGAGGTTAGTGAGTGGTTGGAGGACAGGAGGTTAAACAGGACCAATAGCGA
2530
HBV Subgenotype A1 (Wild-type)
Polymerase (P)
GGATGTGTCTGCGGCGTTTTATCATATTCCTCTTCATCCTGCTGCTATGCCTCATCTTCTTATTGGTTCTTCTGGATTATCAAGGTATGTTGCCCGTTTGTCCTCTAATT
CCTACACAGACGCCGCAAAATAGTATAAGGAGAAGTAGGACGACGATACGGAGTAGAAGAATAACCAAGAAGACCTAATAGTTCCATACAACGGGCAAACAGGAGATTAA
2640
HBV Subgenotype A1 (Wild-type)
Polymerase (P)
BamHI
EcoNI
CCAGGATCCACAACAACCAGTACGGGACCCTGCAAAACCTGCACGACTCCTGCTCAAGGCAACTCTATGTTTCCCTCATGTTGCTGTACAAAACCTACGGATGGAAATTG
GGTCCTAGGTGTTGTTGGTCATGCCCTGGGACGTTTTGGACGTGCTGAGGACGAGTTCCGTTGAGATACAAAGGGAGTACAACGACATGTTTTGGATGCCTACCTTTAAC
2750
HBV Subgenotype A1 (Wild-type)
Polymerase (P)
CACCTGTATTCCCATCCCATCATCTTGGGCTTTCGCAAAATACCTATGGGAGTGGGCCTCAGTCCGTTTCTCTTGGCTCAGTTTACTAGTGCCATTTGTTCAGTGGTTCG
GTGGACATAAGGGTAGGGTAGTAGAACCCGAAAGCGTTTTATGGATACCCTCACCCGGAGTCAGGCAAAGAGAACCGAGTCAAATGATCACGGTAAACAAGTCACCAAGC
2860
HBV Subgenotype A1 (Wild-type)
TAGGGCTTTCCCCCACTGTTTGGCTTTCAGCTATATGGATGATGTGGTACTGGGGGCCAAGTCTGTACAACATCTTGAGTCCCTTTATACCGCTGTTACCAATTTTCTTT
ATCCCGAAAGGGGGTGACAAACCGAAAGTCGATATACCTACTACACCATGACCCCCGGTTCAGACATGTTGTAGAACTCAGGGAAATATGGCGACAATGGTTAAAAGAAA
2970
HBV Subgenotype A1 (Wild-type)
TGTCTTTGGGTATACATTTAAACCCTAACAAAACAAAGAGATGGGGTTATTCCCTGAATTTCATGGGGTATGTAATTGGAAGTTGGGGTACATTGCCACAGGATCATATT
ACAGAAACCCATATGTAAATTTGGGATTGTTTTGTTTCTCTACCCCAATAAGGGACTTAAAGTACCCCATACATTAACCTTCAACCCCATGTAACGGTGTCCTAGTATAA
3080
HBV Subgenotype A1 (Wild-type)
ATACAAAAAATCAAACACTGTTTTAGGAAACTTCCTGTCAATCGACCTATAGATTGGAAAGTATGTCAGAGAATTGTGGGTCTTTTGGGCTTTGCCGCTCCATTTACACA
TATGTTTTTTAGTTTGTGACAAAATCCTTTGAAGGACAGTTAGCTGGATATCTAACCTTTCATACAGTCTCTTAACACCCAGAAAACCCGAAACGGCGAGGTAAATGTGT
3190
HBV Subgenotype A1 (Wild-type)



Figure E. 1: The Complete Sequence of the 1.28 mer Over-Length HBV Subgenotype A1 Wild-type Clone employed to generate the computational plasmid construct.

APPENDIX F: PCDNA^{TM} 4/TO EXPRESSION VECTOR

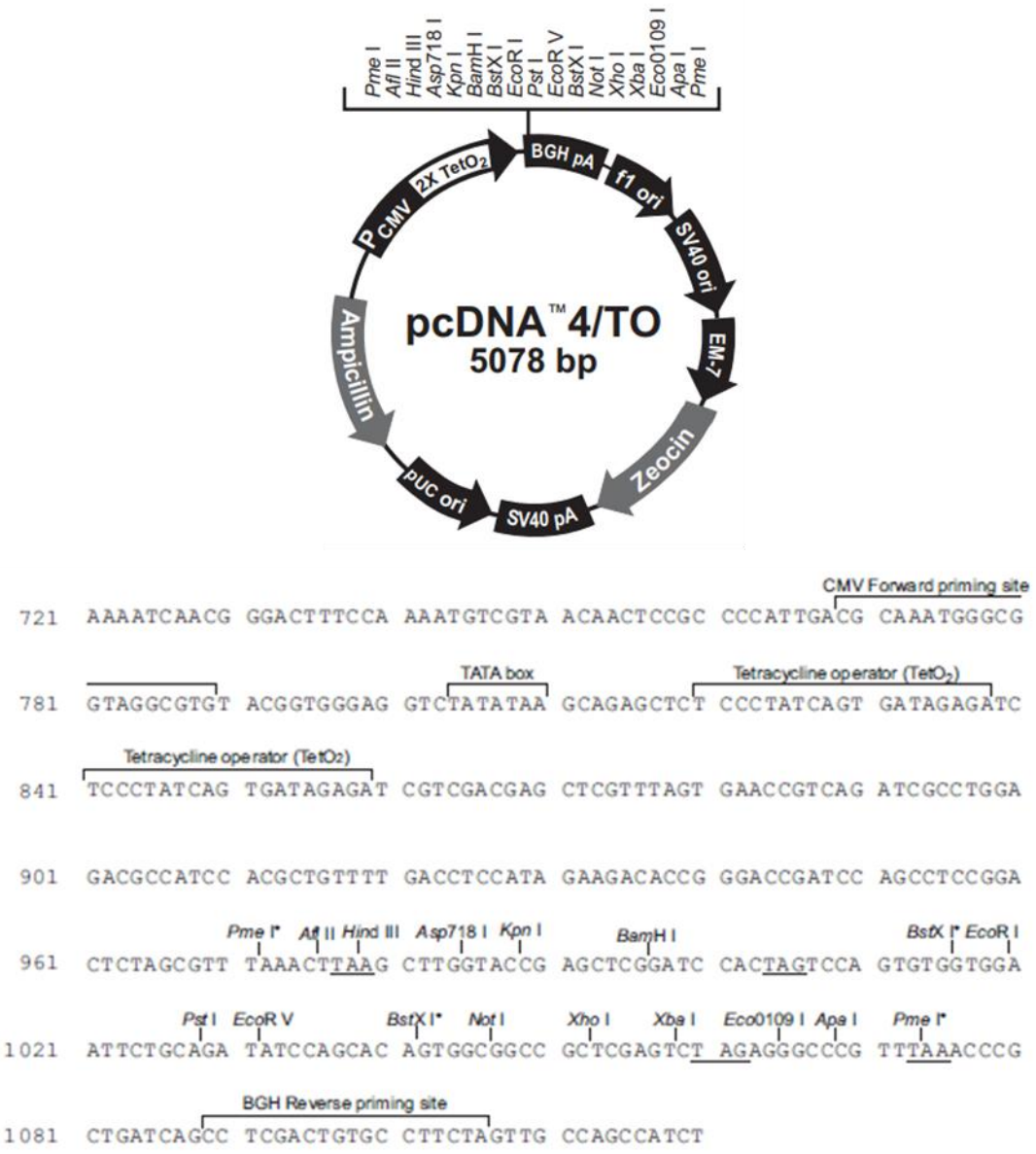


Figure F.1: The Invitrogen Life Technologies pcDNA^{TM} 4/TO expression vector was employed as a negative control in this study. The diagram illustrates both the sequence information and plasmid map to highlight the various features of this commercial plasmid. This includes the multiple cloning site and possible stop codons (underlined) as a guideline when utilizing this expression vector.

APPENDIX G: SUPPLEMENTARY PROTOCOLS

G.1) Mycoplasma Detection Assay

Cell culture supernatant samples were prepared by aliquoting 100 µl of cell culture supernatants to sterile microcentrifuge tubes that were tightly sealed to prevent opening during heating. Next, cell culture supernatant were incubated at 95 °C for 5 minutes, and briefly centrifuged. The provided reaction tubes pre-coated with primers, dNTPs and gel loading buffer/dye were set up as described in the manufacturers guide. Both a negative and positive control was included in the assay. This included: a) performing PCR in the absence of cell culture supernatant and b) performing PCR using an internal control DNA that consists of non-infectious DNA fragments of *Mycoplasma orale* genome, respectively. According to the protocol guidelines, a 481 bp band should be seen in every reaction tube (internal control), including the negative control to determine the success of the PCR reaction. The presence of a band at ~260 bp indicates the presence of mycoplasma in the supernatant/test sample, this band should only be present in the positive control. The PCR reaction set up was prepared as described in *Table G1.1* and the PCR cycling parameters set as illustrated in *Table G1.2* by means of using a thermal cycler.

Table G1.1: PCR Reaction Set Up for the Mycoplasma Detection Assay

Reagent	**Volume (µl)**		
	Test Reaction	**Positive Control**	**Negative Control**
Polymerase/Rehydration Buffer Mixture	23.0	25.0	23.0
Cell Culture Supernatant	2.0	-	-
Nuclease-Free Water	-	-	2.0
Total Volume	25.0	25.0	25.0

Table G1.2: PCR Cycling Parameters for the Mycoplasma Detection Assay

Step	Temperature (°C)	Time (min)	Cycle
Initial Denaturation	94	2:00	1
Denaturation	94	0:30	40
Annealing	55	0:30	
Elongation	72	0:40	
End	4	∞	-

G.2) HBeAg ELISA: Manufacturer Guidelines

- Reagent storage and handling:
    - Do not autoclave solutions containing sodium hypochlorite – rather add bleach to decontaminate waste.
    - Assays that have not been conducted according to the established time and temperature limits must be repeated.
    - If crystallization has occurred in the wash buffer concentrate – warm the buffer to 37°C and mix well before diluting.
    - Do not expose the test components to intense or direct sunlight or temperatures above 25°C.
    - Do not freeze the kit.
    - Working wash buffer containers should be thoroughly cleaned with 70% ethanol and thoroughly rinsed with distilled/deionized water before the preparation of the next batch of working wash buffer.
    - If any reagent contains visible particulate matter, it should be discarded.
    - If the chromogen/substrate turns a dark blue it may be contaminated.

- The volume of the microwell is ~ 400 µl, thus ensure that the volume of working wash buffer dispensed into each well does not exceed this volume causing the wells to overflow.
- All steps must be completed within four hours.
- Avoid handling the bottoms of the microwells since scratches/marks could affect the reading when analyzing the results.

- To prepare the working enzyme tracer solution, dilute the enzyme tracer 1:50 with tracer diluent.
- To prepare the wash solution, dilute the wash buffer concentrate to a 1:25 dilution with distilled/deionized sterile water.
- The loading datasheet was set as follows:

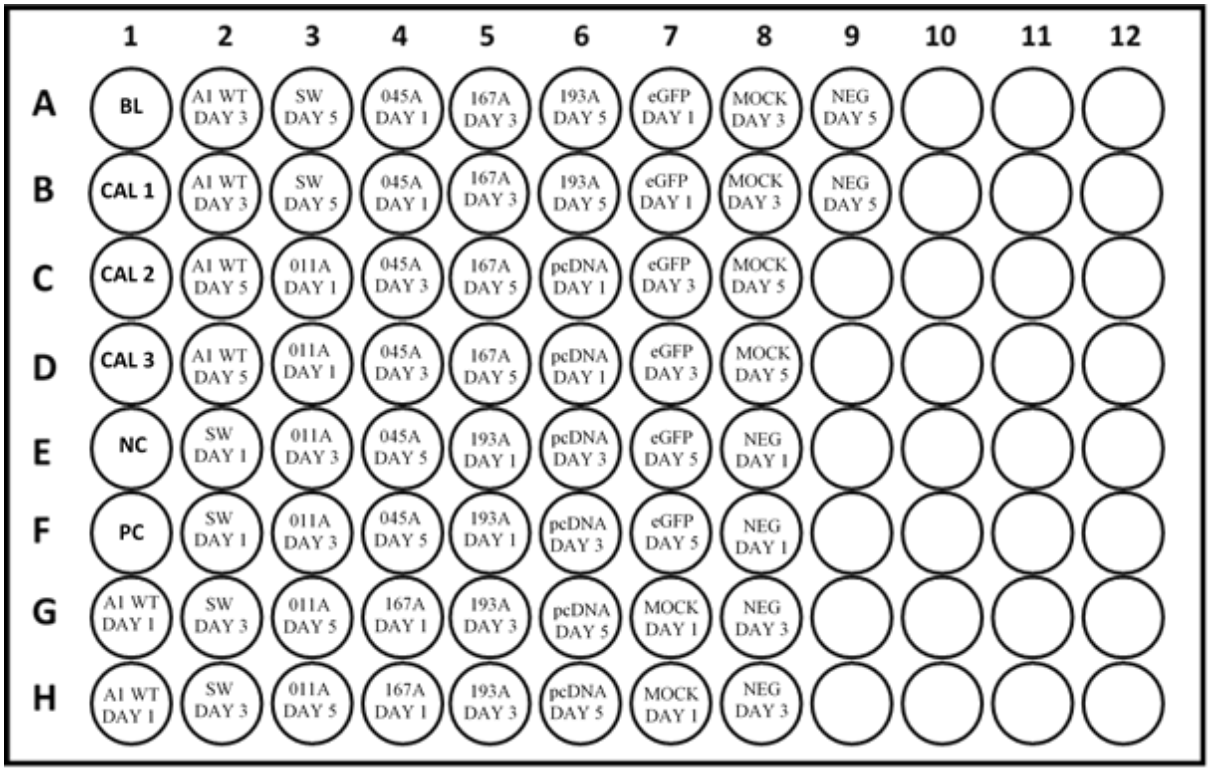


Figure G2.1: The HBeAg ELISA plate set up for the wild-type, deletion mutant and occult strains prepared in duplicate.

G.3) HBsAg ELISA: Manufacturer Guidelines

- Reagent storage and handling
    - The sample diluent provided should be mixed by inversion prior to use.
    - The substrate solution should be pink, if it is purple it should be discarded.
    - Allow all reagents and samples to reach 18-30°C prior to use.
    - The sample diluent should be a green/brown in colour and the conjugate should be red. The substrate solution will initially be pink and become purple when in contact with any reactive wells, then turn orange once the stop solution is added.
- To prepare the working substrate solution, add an equal volume of the pink substrate concentrate to the colourless substrate diluent.
- To prepare the working wash solution, dilute 1 volume of the wash fluid concentrate to 19 volumes of distilled/deionized water (i.e. 1:20 dilution).
- The loading datasheet was set as follows:

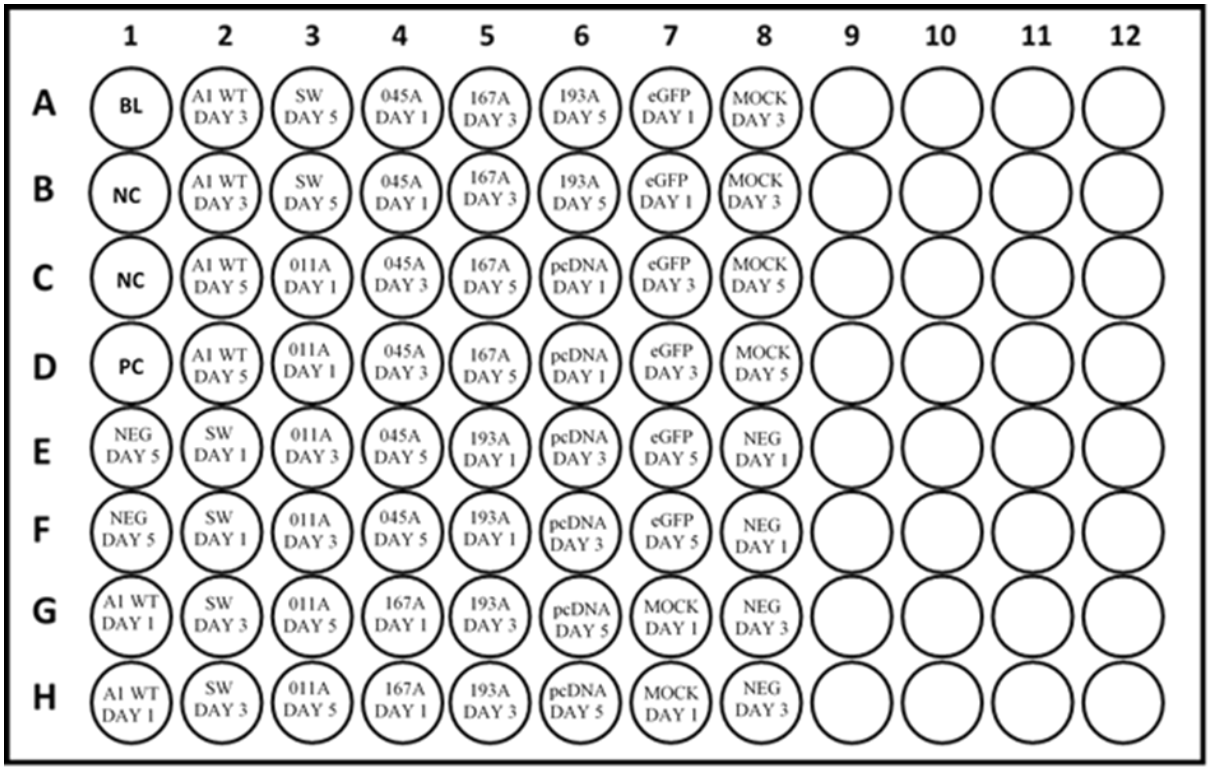


Figure G2.2: The HBsAg ELISA plate set up for the wild-type, deletion mutant and occult strains prepared in duplicate.

APPENDIX H: CALCULATIONS

Transfection Preparation: Cell count & Concentration of cells

H1.1) Cell count

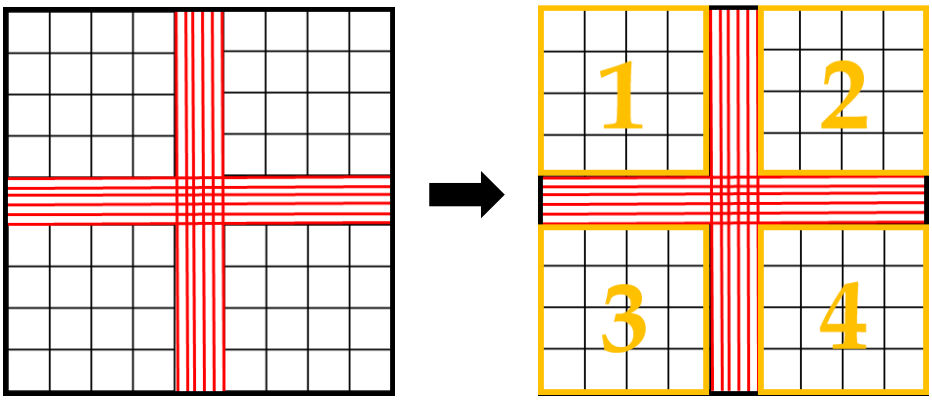


Figure H.1: An illustration of a haemocytometer used to calculate the average number of cells

In order to maintain a consistent concentration of cells (per culture dish) during the transfection assay, a haemocytometer was employed to determine the amount of cells required for each culture dish:

Average number of cells = Total number of cells/Total number of orange squares (i.e. four)

H1.2) Concentration of cells

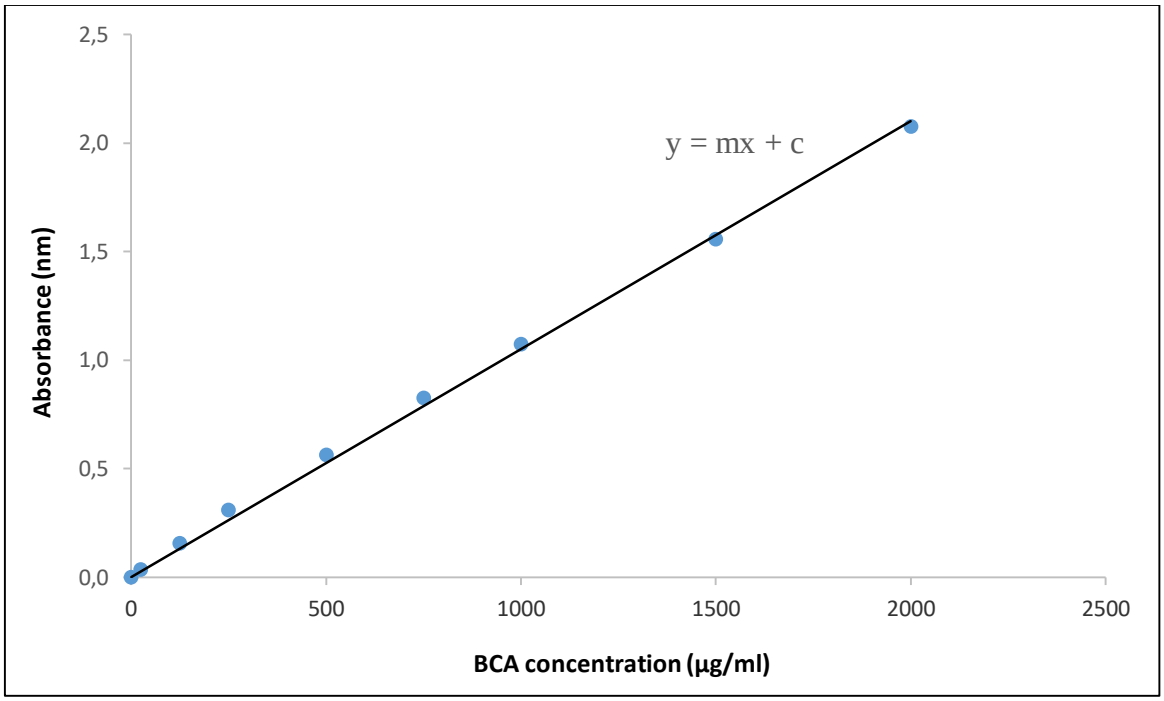
$$[Huh7\ cells](cells/ml) = Average\ number\ of\ cells \times 10^4 \times DF$$

Where, *[Huh7 cells]* denotes the concentration of Huh7 cells per ml and *DF* signifies the Dilution Factor

Protein Quantification: BCA standard curves

A protein quantification assay was performed in order to calculate the exact amount of protein required for each sample, prior to loading, to ensure that the results were consistent throughout the study. A BCA standard curve was constructed to calculate the precise amount of protein required for loading.

i.e.



Where,

y = The absorbance of the sample of interest (nanometer)

m = The gradient (i.e. the slope of the sample of interest)

c = The y-intercept (i.e. the point at which the line crosses the y-axis)

x = The concentration of protein in the sample of interest (µg/ml)

Once solved for x (µg/ml), this value was converted to µg/µl by simply dividing by 1000.

APPENDIX I: PROTEIN & DNA LADDERS

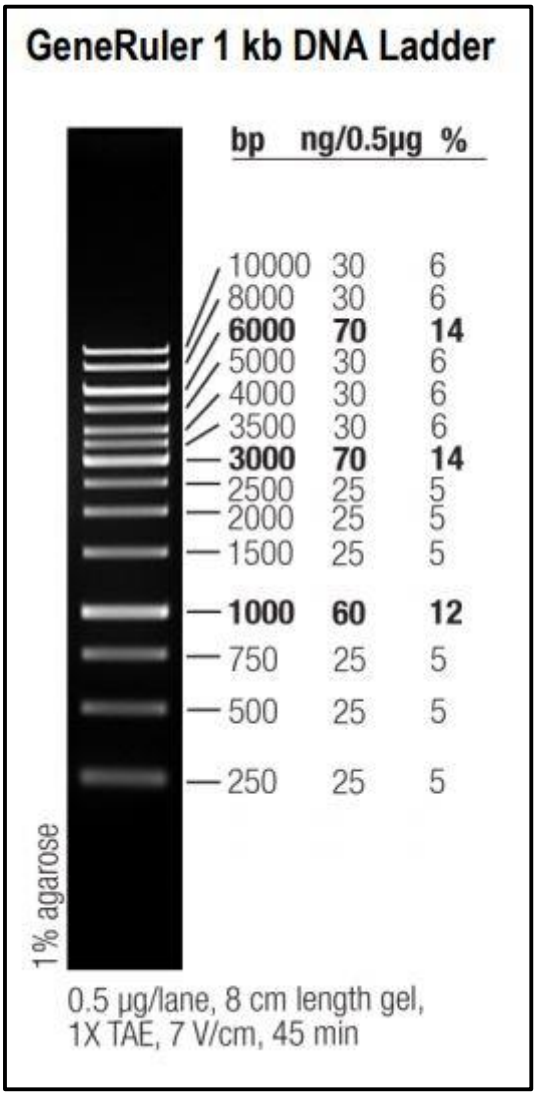


Figure I. 1: The Thermo Scientific GeneRuler 1 kb DNA Ladder was employed for the sizing of the DNA during agarose gel electrophoresis. The ladder is composed of fourteen chromatography-purified individual DNA fragments (in base pair) and contains three reference bands of (6000, 3000 and 1000 bp) for easy alignment and comparison when sizing the varying DNA fragments.

(URL: https://www.thermofisher.com/order/catalog/product/SM0311)

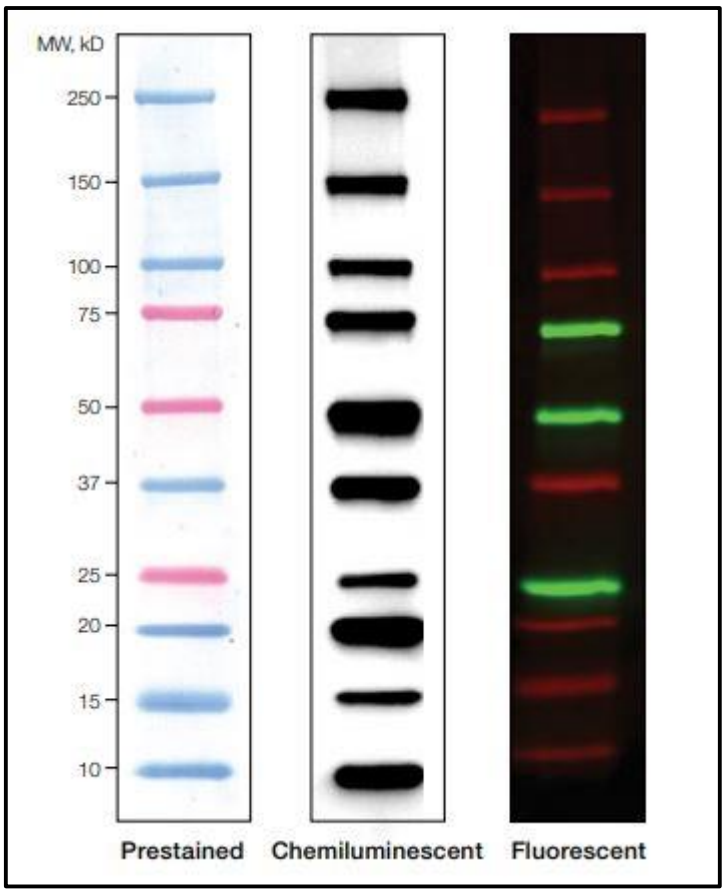


Figure I. 2: The Bio-Rad Laboratories Precision Plus Protein™ WesternC Standards™ were utilized for the sizing of various proteins during SDS-PAGE analyses. It consists of ten unique, prestained protein bands with a molecular weight extending between 10 - 250 kDa. In addition, it consists of an integrated Streptavidin (Strep)-tag sequence to facilitate the detection of proteins of interest when analysing Western blots with Precision Protein StrepTactin-HRP Conjugate.

(URL: http://www.bio-rad.com/webroot/web/pdf/lsr/literature/Bulletin_5561.pdf)

REFERENCES

ALLAIN, J.-P. & COX, L. 2011. Challenges in hepatitis B detection among blood donors. *Current opinion in hematology,* 18**,** 461-466.

ALTER, H. J., HOLLAND, P. V., PURCELL, R. H., LANDER, J. J., FEINSTONE, S. M., MORROW, A. G. & SCHMIDT, P. J. 1972. Posttransfusion hepatitis after exclusion of commercial and hepatitis-B antigen-positive donors. *Annals of Internal Medicine,* 77**,** 691-699.

ARBUTHNOT, P., CAPOVILLA, A. & KEW, M. 2000. Putative role of hepatitis B virus X protein in hepatocarcinogenesis: Effects on apoptosis, DNA repair, mitogen-activated protein kinase and JAK/STAT pathways. *Journal of gastroenterology and hepatology,* 15**,** 357-368.

BAGHIROVA, S., HUGHES, B. G., HENDZEL, M. J. & SCHULZ, R. 2015. Sequential fractionation and isolation of subcellular proteins from tissue or cultured cells. *MethodsX,* 2**,** 440-445.

BARTENSCHLAGER, R. & SCHALLER, H. 1988. The amino-terminal domain of the hepadnaviral P-gene encodes the terminal protein (genome-linked protein) believed to prime reverse transcription. *The EMBO journal,* 7**,** 4185-4192.

BECK, J. & NASSAL, M. 2007a. Hepatitis B virus replication. *World journal of gastroenterology: WJG,* 13**,** 48.

BECK, J. & NASSAL, M. 2007b. Hepatitis B virus replication. *World journal of gastroenterology: WJG,* 13**,** 48-64.

BELL, T. G., MAKONDO, E., MARTINSON, N. A. & KRAMVIS, A. 2012. Hepatitis B virus infection in human immunodeficiency virus infected southern African adults: occult or overt–that is the question. *PLoS One,* 7**,** e45750.

BELLONI, L., POLLICINO, T., DE NICOLA, F., GUERRIERI, F., RAFFA, G., FANCIULLI, M., RAIMONDO, G. & LEVRERO, M. 2009. Nuclear HBx binds the HBV minichromosome and modifies the epigenetic regulation of cccDNA function. *Proceedings of the National Academy of Sciences***,** pnas. 0908365106.

BHOOLA, N. H., REUMANN, K., KEW, M. C., WILL, H. & KRAMVIS, A. 2014. Construction of replication competent plasmids of hepatitis B virus subgenotypes A1, A2 and D3 with authentic endogenous promoters. *Journal of virological methods,* 203**,** 54-64.

BIRNBAUM, F. & NASSAL, M. 1990. Hepatitis B virus nucleocapsid assembly: primary structure requirements in the core protein. *Journal of virology,* 64**,** 3319-3330.

BLÄCKBERG, J. & KIDD-LJUNGGREN, K. 2000. Occult hepatitis B virus after acute self-limited infection persisting for 30 years without sequence variation. *Journal of hepatology,* 33**,** 992-997.

BLUMBERG, B. S. 1977. Australia antigen and the biology of hepatitis B. *Science,* 197**,** 17-25.

BLUMBERG, B. S., ALTER, H. J. & VISNICH, S. 1984. A New Antigen in Leukemia Sera. *Jama,* 252**,** 252-257.

BLUMBERG, B. S., GERSTLEY, B. J. S., HUNGERFORD, D. A., LONDON, W. T. & SUTNICK, A. I. 1967. A serum antigen (Australia antigen) in Down's syndrome, leukemia, and hepatitis. *Annals of internal medicine,* 66**,** 924-931.

BLUMBERG, B. S., LAROUZE, B., LONDON, W. T., WERNER, B., HESSER, J. E., MILLMAN, I., SAIMOT, G. & PAYET, M. 2000. The relation of infection with the hepatitis B agent to primary hepatic carcinoma. *Hepatitis B And The Prevention Of Primary Cancer Of The Liver: Selected Publications of Baruch S Blumberg.* World Scientific.

BOCK, C. T., TILLMANN, H. L., MANNS, M. P. & TRAUTWEIN, C. 1999. The pre-S region determines the intracellular localization and appearance of hepatitis B virus. *Hepatology,* 30**,** 517-525.

BOCK, C. T., TILLMANN, H. L., MASCHEK, H. J., MANNS, M. P. & TRAUTWEIN, C. 1997. A preS mutation isolated from a patient with chronic hepatitis B infection leads to virus retention and misassembly. *Gastroenterology,* 113**,** 1976-1982.

BOUCHARD, M. J. & NAVAS-MARTIN, S. 2011. Hepatitis B and C virus hepatocarcinogenesis: lessons learned and future challenges. *Cancer letters,* 305**,** 123-143.

BOUCHARD, M. J. & SCHNEIDER, R. J. 2004. The enigmatic X gene of hepatitis B virus. *Journal of virology,* 78**,** 12725-12734.

BRINKLEY, B. R. 1981. Organization of the cytoplasm. *Cold Spring Harbor Symposium on Quantitative Biology,* 46**,** 1029-1040.

BRUNS, M., MISKA, S., CHASSOT, S. & WILL, H. 1998. Enhancement of hepatitis B virus infection by noninfectious subviral particles. *Journal of virology,* 72**,** 1462-1468.

BRUSS, V. 2004. Envelopment of the hepatitis B virus nucleocapsid. *Virus research,* 106**,** 199-209.

BRUSS, V., GERHARDT, E., VIELUF, K. & WUNDERLICH, G. 1996. Functions of the large hepatitis B virus surface protein in viral particle morphogenesis. *Intervirology,* 39**,** 23-31.

BUSTIN, M. 1976. Chromatin structure and specificity revealed by immunological techniques. *FEBS letters,* 70**,** 1-10.

BUYNAK, E. B., ROEHM, R. R., TYTELL, A. A., BERTLAND, A. U., LAMPSON, G. P. & HILLEMAN, M. R. 1976. Vaccine against human hepatitis B. *Jama,* 235**,** 2832-2834.

CHANG, M.-L. & LIAW, Y.-F. 2014. Hepatitis B flares in chronic hepatitis B: pathogenesis, natural course, and management. *Journal of hepatology,* 61**,** 1407-1417.

CHAZOUILLERES, O., MAMISH, D., KIM, M., CAREY, K., WRIGHT, T., FERRELL, L., ROBERTS, J. & ASCHER, N. 1994. " Occult" hepatitis B virus as source of infection in liver transplant recipients. *The Lancet,* 343**,** 142-146.

CHEN, B.-F. 2018. Hepatitis B virus pre-S/S variants in liver diseases. *World journal of gastroenterology,* 24**,** 1507.

CHEN, B. F., LIU, C. J., JOW, G. M., CHEN, P. J., KAO, J. H. & CHEN, D. S. 2006. High prevalence and mapping of pre-S deletion in hepatitis B virus carriers with progressive liver diseases. *Gastroenterology,* 130**,** 1153-1168.

CHEN, C.-H., CHANGCHIEN, C.-S., LEE, C.-M., HUNG, C.-H., HU, T.-H., WANG, J.-H., WANG, J.-C. & LU, S.-N. 2008. Combined mutations in pre-s/surface and core promoter/precore regions of hepatitis B virus increase the risk of hepatocellular carcinoma: a case-control study. *The Journal of infectious diseases,* 198**,** 1634-1642.

CHEN, C. H., HUNG, C. H., LEE, C. M., HU, T. H., WANG, J. H., WANG, J. C., LU, S. N. & CHANGCHIEN, C. S. 2007. Pre-S deletion and complex mutations of hepatitis B virus related to advanced liver disease in HBeAg-negative patients. *Gastroenterology,* 133**,** 1466-1474.

CHEN, D.-S. 1993. From hepatitis to hepatoma: lessons from type B viral hepatitis. *Science,* 262**,** 369-371.

CHEN, M., SÄLLBERG, M., HUGHES, J., JONES, J., GUIDOTTI, L. G., CHISARI, F. V., BILLAUD, J.-N. & MILICH, D. R. 2005. Immune tolerance split between hepatitis B virus precore and core proteins. *Journal of virology,* 79**,** 3016-3027.

CHEN, M. T., BILLAUD, J.-N., SÄLLBERG, M., GUIDOTTI, L. G., CHISARI, F. V., JONES, J., HUGHES, J. & MILICH, D. R. 2004. A function of the hepatitis B virus precore protein is to regulate the immune response to the core antigen. *Proceedings of the National Academy of Sciences,* 101**,** 14913-14918.

CHEN, S.-J., ZHAO, Y.-X., FANG, Y., XU, W.-Z., MA, Y.-X., SONG, Z.-W., TENG, X. & GU, H.-X. 2012. Viral deletions among healthy young Chinese adults with occult hepatitis B virus infection. *Virus research,* 163**,** 197-201.

CHEN, W. N. & OON, C. J. 1999. Human hepatitis B virus mutants: significance of molecular changes. *FEBS letters,* 453**,** 237-242.

CHEN, W. N. & OON, C. J. 2002. Pre-S deletion mutants co-exist with wild-type virus at low viral replication stage in Singapore chronic hepatitis B virus carriers. *Current microbiology,* 44**,** 145-147.

CHISARI, F. V. 1992. Hepatitis B virus biology and pathogenesis. *Mol Genet Med,* 2**,** 67-104.

CHISARI, F. V. & FERRARI, C. 1995. Hepatitis B virus immunopathogenesis. *Annual review of immunology,* 13**,** 29-60.

CHU, P. & WEISS, L. 2002. Keratin expression in human tissues and neoplasms. *Histopathology,* 40**,** 403-439.

CLARK, D. N. & HU, J. 2015. Unveiling the roles of HBV polymerase for new antiviral strategies. *Future virology,* 10**,** 283-295.

CLIPPINGER, A. J., GEARHART, T. L. & BOUCHARD, M. J. 2009. Hepatitis B virus X protein modulates apoptosis in primary rat hepatocytes by regulating both NF-κB and the mitochondrial permeability transition pore. *Journal of virology,* 83**,** 4718-4731.

DANE, D., CAMERON, C. & BRIGGS, M. 1970. Virus-like particles in serum of patients with Australia-antigen-associated hepatitis. *The Lancet*, 295**,** 695-698.

DEBARRY, J., CORNBERG, M. & MANNS, M. P. 2017. Challenges in warranting access to prophylaxis and therapy for hepatitis B virus infection. *Liver International,* 37**,** 67-72.

ECHEVARRÍA, J. M. & AVELLÓN, A. 2008. Improved detection of natural hepatitis B virus surface antigen (HBsAg) mutants by a new version of the VITROS® HBsAg assay. *Journal of medical virology,* 80**,** 598-602.

EL–SERAG, H. B. & RUDOLPH, K. L. 2007. Hepatocellular carcinoma: epidemiology and molecular carcinogenesis. *Gastroenterology,* 132**,** 2557-2576.

FAN, Y., LU, C., CHEN, W., YAO, W., WANG, H., CHANG, T., LEI, H., SHIAU, A. & SU, I. 2001. Prevalence and significance of hepatitis B virus (HBV) pre-S mutants in serum and liver at different replicative stages of chronic HBV infection. *Hepatology (Baltimore, Md.),* 33**,** 277.

FLINT, S. J., ENQUIST, L. W., RACANIELLO, V. R., SKALKA, A. M., FLINT, S., ENQUIST, L., RACANIELLO, V. & SKALKA, A. 2008. Principles of Virology.

FRIBLEY, A., ZHANG, K. & KAUFMAN, R. J. 2009. Regulation of apoptosis by the unfolded protein response. *Apoptosis.* Springer.

GANEM, D. & PRINCE, A. M. 2004. Hepatitis B virus infection—natural history and clinical consequences. *New England Journal of Medicine,* 350**,** 1118-1129.

GARCIA, T., LI, J., SUREAU, C., ITO, K., QIN, Y., WANDS, J. & TONG, S. 2009. Drastic reduction in the production of subviral particles does not impair hepatitis B virus virion secretion. *Journal of virology,* 83**,** 11152-11165.

GEARHART, T. L. & BOUCHARD, M. J. 2010a. The hepatitis B virus X protein modulates hepatocyte proliferation pathways to stimulate viral replication. *Journal of virology,* 84**,** 2675-2686.

GEARHART, T. L. & BOUCHARD, M. J. 2010b. Replication of the hepatitis B virus requires a calcium-dependent HBx-induced G1 phase arrest of hepatocytes. *Virology,* 407**,** 14-25.

GISH, R. G., GIVEN, B. D., LAI, C.-L., LOCARNINI, S. A., LAU, J. Y., LEWIS, D. L. & SCHLUEP, T. 2015. Chronic hepatitis B: virology, natural history, current management and a glimpse at future opportunities. *Antiviral research,* 121**,** 47-58.

GOPALAKRISHNAN, D., KEYTER, M., SHENOY, K. T., LEENA, K. B., THAYUMANAVAN, L., THOMAS, V., VINAYAKUMAR, K., PANACKEL, C.,

KORAH, A. T. & NAIR, R. 2013. Hepatitis B virus subgenotype A1 predominates in liver disease patients from Kerala, India. *World Journal of Gastroenterology: WJG,* 19**,** 9294.

GÜNTHER, S., FISCHER, L., PULT, I., STERNECK, M. & WILL, H. 1999. Naturally occurring variants of hepatitis B virus. *Advances in virus research.* Elsevier.

HADZIYANNIS S, TASSOPOULOS N, HEATHCOTE E & AL., E. 2006. Long-term therapy with adefovir dipivoxil for HBeAg-negative chronic hepatitis B for up to 5 years. *Gastroenterology,* 131**,** 1743–1751.

HADZIYANNIS, S., GERBER, M., VISSOULIS, C. & POPPER, H. 1973. Cytoplasmic hepatitis B antigen in" ground-glass" hepatocytes of carriers. *Arch. Pathol.,* 96**,** 327-30.

HASSEMER, M., FINKERNAGEL, M., PEIFFER, K.-H., GLEBE, D., AKHRAS, S., REUTER, A., SCHEIBLAUER, H., SOMMER, L., CHUDY, M. & NÜBLING, C. M. 2017. Comparative characterization of hepatitis B virus surface antigen derived from different hepatitis B virus genotypes. *Virology,* 502**,** 1-12.

HOLDEN, P. & HORTON, W. A. 2009. Crude subcellular fractionation of cultured mammalian cell lines. *BMC research notes,* 2**,** 243.

HOWARD, C. R. & ALLISON, L. M. 1995. Hepatitis B surface antigen variation and protective immunity. *Intervirology,* 38**,** 35-40.

HSU, A., LAI, C.-L. & YUEN, M.-F. 2011. Update on the risk of hepatocellular carcinoma in chronic hepatitis B virus infection. *Current hepatitis reports,* 10**,** 106-111.

HU, J. & LIU, K. 2017. Complete and incomplete hepatitis B virus particles: formation, function, and application. *Viruses,* 9**,** 56.

HUANG, W., HSIEH, Y.-H., SU, I.-J., WANG, H.-C., CHANG, W.-W., LEI, H.-Y., LAI, M.-D. & CHANG, W.-T. 2005. Pre-S mutant surface antigens in chronic hepatitis B virus infection induce oxidative stress and DNA damage. AACR.

HUNG, J.-H., SU, I.-J., LEI, H.-Y., WANG, H.-C., LIN, W.-C., CHANG, W.-T., HUANG, W., CHANG, W.-C., CHANG, Y.-S. & CHEN, C.-C. 2004. Endoplasmic reticulum stress stimulates the expression of cyclooxygenase-2 through activation of NF-κB and pp38 mitogen-activated protein kinase. *Journal of Biological Chemistry,* 279**,** 46384-46392.

KALININA, T., RIU, A., FISCHER, L., SANTANTONIO, T., WILL, H. & STERNECK, M. 2003. Selection of a secretion-incompetent mutant in the serum of a patient with severe hepatitis B. *Gastroenterology,* 125**,** 1077-1084.

KATO, J., HASEGAWA, K., TORII, N., YAMAUCHI, K. & HAYASHI, N. 1996. A molecular analysis of viral persistence in surface antigen-negative chronic hepatitis B. *Hepatology,* 23**,** 389-395.

KAUFMAN, R. J. 2002. Orchestrating the unfolded protein response in health and disease. *The Journal of clinical investigation,* 110**,** 1389-1398.

KEW, M. C. 1994. Hepatitis viruses and hepatocellular carcinoma. *South African Medical Journal,* 84**,** 550–556.

KEW, M. C., KRAMVIS, A., YU, M. C., ARAKAWA, K. & HODKINSON, J. 2005. Increased hepatocarcinogenic potential of hepatitis B virus genotype A in Bantu-speaking sub-Saharan Africans. *Journal of medical virology,* 75**,** 513-521.

KIM, J. H., PARK, Y. K., PARK, E. S. & KIM, K. H. 2014. Molecular diagnosis and treatment of drug-resistant hepatitis B virus. *World journal of gastroenterology: WJG,* 20**,** 5708-5720.

KIMBI, G. C., KRAMVIS, A. & KEW, M. C. 2004. Distinctive sequence characteristics of subgenotype A1 isolates of hepatitis B virus from South Africa. *Journal of general virology,* 85**,** 1211-1220.

KRAMVIS, A. 2016. The clinical implications of hepatitis B virus genotypes and HBeAg in pediatrics. *Reviews in medical virology,* 26**,** 285-303.

KRAMVIS, A., ARBUTHNOT, P., SWABY, L. A. & UKOMADU, C. 2008. Hepatitis B virus prevalence, natural history, and treatment in Africans in Africa and the United States. *Curr Hepatitis B Rep,* 2**,** 143-149.

KRAMVIS, A., BUKOFZER, S., KEW, M. C. & SONG, E. 1997. Nucleic acid sequence analysis of the precore region of hepatitis B virus from sera of southern African black adult carriers of the virus. *Hepatology,* 25**,** 235-240.

KRAMVIS, A., KEW, M. & FRANCOIS, G. 2005. Hepatitis B virus genotypes. *Vaccine,* 23**,** 2409-2423.

KRAMVIS, A. & KEW, M. C. 2007. Epidemiology of hepatitis B virus in Africa, its genotypes and clinical associations of genotypes. *Hepatology Research,* 37**,** S9-S19.

KRAMVIS, A., KEW, M. C. & BUKOFZER, S. 1998. Hepatitis B virus precore mutants in serum and liver of Southern African Blacks with hepatocellular carcinoma. *Journal of hepatology,* 28**,** 132-141.

KRAMVIS, A., KOSTAKI, E.-G., HATZAKIS, A. & PARASKEVIS, D. 2018. Immunomodulatory Function of HBeAg Related to Short-Sighted Evolution, Transmissibility, and Clinical Manifestation of Hepatitis B Virus. *Frontiers in microbiology,* 9.

KRAMVIS, A., WEITZMANN, L., OWIREDU, W. K. & KEW, M. C. 2002. Analysis of the complete genome of subgroup A′ hepatitis B virus isolates from South Africa. *Journal of general virology,* 83**,** 835-839.

KURBANOV, F., TANAKA, Y. & MIZOKAMI, M. 2010. Geographical and genetic diversity of the human hepatitis B virus. *Hepatology Research,* 40**,** 14-30.

KUROKI, K., FLOREANI, M., MIMMS, L. T. & GANEM, D. 1990. Epitope mapping of the PreS1 domain of the hepatitis B virus large surface protein. *Virology,* 176**,** 620-624.

KWON, S. Y. L., C.H 2011. Epidemiology and prevention of hepatitis B virus infection. *The Korean journal of hepatology,* 17**,** 87-95.

LAMONTAGNE, R. J., BAGGA, S. & BOUCHARD, M. J. 2016. Hepatitis B virus molecular biology and pathogenesis. *Hepatoma research,* 2**,** 163.

LANG, T., LO, C., SKINNER, N., LOCARNINI, S., VISVANATHAN, K. & MANSELL, A. 2011. The hepatitis B e antigen (HBeAg) targets and suppresses activation of the toll-like receptor signaling pathway. *Journal of hepatology,* 55**,** 762-769.

LE, A. V.-P., HUANG, D., BLICK, T., THOMPSON, E. W. & DOBROVIC, A. 2015. An optimised direct lysis method for gene expression studies on low cell numbers. *Scientific reports,* 5**,** 12859.

LE POGAM, S., CHUA, P. K., NEWMAN, M. & SHIH, C. 2005. Exposure of RNA templates and encapsidation of spliced viral RNA are influenced by the arginine-rich domain of human hepatitis B virus core antigen (HBcAg 165-173). *Journal of virology,* 79**,** 1871-1887.

LEE, W. M. 1997. Hepatitis B virus infection. *New England journal of medicine,* 337**,** 1733-1745.

LEWELLYN, E. B. & LOEB, D. D. 2011. The arginine clusters of the carboxy-terminal domain of the core protein of hepatitis B virus make pleiotropic contributions to genome replication. *Journal of virology,* 85**,** 1298-1309.

LI, K.-W., KRAMVIS, A., LIANG, S., HE, X., CHEN, Q.-Y., WANG, C., YANG, Q.-L., HU, L.-P., JIA, H.-H. & FANG, Z.-L. 2017. Higher prevalence of cancer related mutations 1762T/1764A and PreS deletions in hepatitis B virus (HBV) isolated from HBV/HIV co-infected compared to HBV-mono-infected Chinese adults. *Virus research,* 227**,** 88-95.

LIANG, T. J. 2009. Hepatitis B: the virus and disease. *Hepatology,* 49.

LIAW, Y.-F. 2009. HBeAg seroconversion as an important end point in the treatment of chronic hepatitis B. *Hepatology international,* 3**,** 425-433.

LIAW, Y. F., TAI, D. I., CHU, C. M. & CHEN, T. J. 1988. The development of cirrhosis in patients with chronic type B hepatitis: a prospective study. *Hepatology,* 8**,** 493-496.

LIN, C.-M., WANG, G.-M., JOW, G.-M. & CHEN, B.-F. 2012. Functional analysis of hepatitis B virus pre-s deletion variants associated with hepatocellular carcinoma. *Journal of biomedical science,* 19**,** 17.

LIU, S., ZHANG, H., GU, C., YIN, J., HE, Y., XIE, J. & CAO, G. 2009. Associations between hepatitis B virus mutations and the risk of hepatocellular carcinoma: a meta-analysis. *Journal of the National Cancer Institute,* 101**,** 1066-1082.

LUCIFORA, J., ARZBERGER, S., DURANTEL, D., BELLONI, L., STRUBIN, M., LEVRERO, M., ZOULIM, F., HANTZ, O. & PROTZER, U. 2011. Hepatitis B virus X protein is essential to initiate and maintain virus replication after infection. *Journal of hepatology,* 55**,** 996-1003.

LUDGATE, L., NING, X., NGUYEN, D. H., ADAMS, C., MENTZER, L. & HU, J. 2012. Cyclin-Dependent Kinase 2 Phosphorylates S/TP Sites in Hepadnavirus Core Protein C-terminal Domain and Is Incorporated into Viral Capsids. *Journal of virology***,** JVI. 01218-12.

LURMAN, A. 1885. Eine icterus epidemic. *Berl Klin Woschenschr* 22**,** 20–23.

MAK, D., DE VILLIERS, C. B., CHASELA, C., URBAN, M. I. & KRAMVIS, A. 2018. Analysis of risk factors associated with hepatocellular carcinoma in black South Africans: 2000–2012. *PloS one,* 13**,** e0196057.

MAKONDO, E., BELL, T. G. & KRAMVIS, A. 2012. Genotyping and molecular characterization of hepatitis B virus from human immunodeficiency virus-infected individuals in southern Africa. *PloS one,* 7**,** e46345.

MARION, P. L. & ROBINSON, W. S. 1983. Hepadna viruses: hepatitis B and related viruses. *Current topics in microbiology and immunology.* Springer.

MCPHERSON, R. A. & PINCUS, M. R. 2017. *Henry's Clinical Diagnosis and Management by Laboratory Methods E-Book*, Elsevier Health Sciences.

MELEGARI, M., SCAGLIONI, P. P. & WANDS, J. R. 1997. The small envelope protein is required for secretion of a naturally occurring hepatitis B virus mutant with pre-S1 deleted. *Journal of virology,* 71**,** 5449-5454.

MELEGARI, M., WOLF, S. K. & SCHNEIDER, R. J. 2005. Hepatitis B virus DNA replication is coordinated by core protein serine phosphorylation and HBx expression. *Journal of virology,* 79**,** 9810-9820.

MICHALAK, M., CORBETT, E. F., MESAELI, N., NAKAMURA, K. & MICHAL, O. 1999. Calreticulin: one protein, one gene, many functions. *Biochemical Journal,* 344**,** 281-292.

MIZOKAMI, M., ORITO, E., OHBA, K.-I., IKEO, K., LAU, J. Y. & GOJOBORI, T. 1997. Constrained evolution with respect to gene overlap of hepatitis B virus. *Journal of molecular evolution,* 44**,** S83-S90.

MORI, K. 2000. Tripartite management of unfolded proteins in the endoplasmic reticulum. *Cell,* 101**,** 451-454.

MPHAHLELE, M. J., LUKHWARENI, A., BURNETT, R. J., MOROPENG, L. M. & NGOBENI, J. M. 2006. High risk of occult hepatitis B virus infection in HIV-positive patients from South Africa. *Journal of clinical virology,* 35**,** 14-20.

NAKABAYASHI, H., TAKETA, K., MIYANO, K., YAMANE, T. & SATO, J. 1982. Growth of human hepatoma cell lines with differentiated functions in chemically defined medium. *Cancer research,* 42**,** 3858-3863.

NASSAL, M. 1992. The arginine-rich domain of the hepatitis B virus core protein is required for pregenome encapsidation and productive viral positive-strand DNA synthesis but not for virus assembly. *Journal of virology,* 66**,** 4107-4116.

NEUVEUT, C., WEI, Y. & BUENDIA, M. A. 2010. Mechanisms of HBV-related hepatocarcinogenesis. *Journal of hepatology,* 52**,** 594-604.

OSTEIKOETXEA, X., SÓDAR, B., NÉMETH, A., SZABÓ-TAYLOR, K., PÁLÓCZI, K., VUKMAN, K. V., TAMÁSI, V., BALOGH, A., KITTEL, Á. & PÁLLINGER, É. 2015. Differential detergent sensitivity of extracellular vesicle subpopulations. *Organic & biomolecular chemistry,* 13**,** 9775-9782.

PERLMAN, D. H., BERG, E. A., O'CONNOR, P. B., COSTELLO, C. E. & HU, J. 2005. Reverse transcription-associated dephosphorylation of hepadnavirus nucleocapsids. *Proceedings of the National Academy of Sciences,* 102**,** 9020-9025.

PETIT, M.-A., MAILLARD, P., CAPEL, F. & PILLOT, J. 1986. Immunochemical structure of the hepatitis B surface antigen vaccine—II. Analysis of antibody responses in human sera against the envelope proteins. *Molecular immunology,* 23**,** 511-523.

POLLICINO, T., AMADDEO, G., RESTUCCIA, A., RAFFA, G., ALIBRANDI, A., CUTRONEO, G., FAVALORO, A., MAIMONE, S., SQUADRITO, G. & RAIMONDO, G. 2012. Impact of hepatitis B virus (HBV) preS/S genomic variability on HBV surface antigen and HBV DNA serum levels. *Hepatology,* 56**,** 434-443.

POLLICINO, T., CACCIOLA, I., SAFFIOTI, F. & RAIMONDO, G. 2014. Hepatitis B virus PreS/S gene variants: pathobiology and clinical implications. *Journal of hepatology,* 61**,** 408-417.

POLLICINO, T., SQUADRITO, G., CERENZIA, G., CACCIOLA, I., RAFFA, G., CRAXì, A., FARINATI, F., MISSALE, G., SMEDILE, A. & TIRIBELLI, C. 2004. Hepatitis B virus maintains its pro-oncogenic properties in the case of occult HBV infection. *Gastroenterology,* 126**,** 102-110.

POLLICINO, T., ZANETTI, A. R., CACCIOLA, I., PETIT, M. A., SMEDILE, A., CAMPO, S., SAGLIOCCA, L., PASQUALI, M., TANZI, E. & LONGO, G. 1997. Pre-S2

defective hepatitis B virus infection in patients with fulminant hepatitis. *Hepatology,* 26**,** 495-499.

PRINCE, A. M. 1968. An antigen detected in the blood during the incubation period of serum hepatitis. *Proceedings of the National Academy of Sciences,* 60**,** 814-821.

PRINCE, A. M., SZMUNESS, W., MICHON, J., DEMAILLE, J., DIEBOLT, G., LINHARD, J., QUENUM, C. & SANKALE, M. 1975. A case/control study of the association between primary liver cancer and hepatitis B infection in Senegal. *International Journal of Cancer,* 16**,** 376-383.

RAIMONDO, G., ALLAIN, J.-P., BRUNETTO, M. R., BUENDIA, M.-A., CHEN, D.-S., COLOMBO, M., CRAXÌ, A., DONATO, F., FERRARI, C. & GAETA, G. B. 2008. Statements from the Taormina expert meeting on occult hepatitis B virus infection. *Journal of hepatology,* 49**,** 652-657.

RAWAT, S. & BOUCHARD, M. J. 2015. The hepatitis B virus (HBV) HBx protein activates AKT to simultaneously regulate HBV replication and hepatocyte survival. *Journal of virology,* 89**,** 999-1012.

RAZAVI-SHEARER, D., GAMKRELIDZE, I., NGUYEN, M. H., CHEN, D.-S., DAMME, P. V. & ABBAS, Z. 2018. Global prevalence, treatment, and prevention of hepatitis B virus infection in 2016: a modelling study. *The lancet Gastroenterology & hepatology*.

REDON, C., PILCH, D., ROGAKOU, E., SEDELNIKOVA, O., NEWROCK, K. & BONNER, W. 2002. Histone H2a variants H2AX and H2AZ. *Current opinion in genetics & development,* 12**,** 162-169.

RON, D. & WALTER, P. 2007. Signal integration in the endoplasmic reticulum unfolded protein response. *Nature reviews Molecular cell biology,* 8**,** 519.

SCAGLIONE, S. J. & LOK, A. S. 2012. Effectiveness of hepatitis B treatment in clinical practice. *Gastroenterology,* 142**,** 1360-1368. e1.

SCHMELTZER, P. & SHERMAN, K. E. 2010. Occult hepatitis B: clinical implications and treatment decisions. *Digestive diseases and sciences,* 55**,** 3328-3335.

SCHÖDEL, F., PETERSON, D., ZHENG, J., JONES, J., HUGHES, J. & MILICH, D. 1993. Structure of hepatitis B virus core and e-antigen. A single precore amino acid prevents nucleocapsid assembly. *Journal of Biological Chemistry,* 268**,** 1332-1337.

SCHRÖDER, M. & KAUFMAN, R. J. 2005. The mammalian unfolded protein response. *Annu. Rev. Biochem.,* 74**,** 739-789.

SCHULZ, I. 1990. [19] Permeabilizing cells: Some methods and applications for the study of intracellular processes. *Methods in enzymology*. Elsevier.

SEEGER, C. & MASON, W. S. 1996. Replication of the hepatitis virus genome. *DNA replication in eukaryotic cells. Cold Spring Harbor Laboratory Press, Cold Spring Harbor, NY,* 815-831.

SEEGER, C. & MASON, W. S. 2000. Hepatitis B virus biology. *Microbiology and molecular biology reviews,* 64**,** 51-68.

SEEGER, C. & MASON, W. S. 2015. Molecular biology of hepatitis B virus infection. *Virology,* 479**,** 672-686.

SEEGER, C. & SOHN, J. A. 2014. Targeting hepatitis B virus with CRISPR/Cas9. *Molecular Therapy-Nucleic Acids,* 3.

SHI, Y.-H. & SHI, C.-H. 2009. Molecular characteristics and stages of chronic hepatitis B virus infection. *World journal of gastroenterology: WJG,* 15**,** 3099.

SIMELANE, D. 2018. *Expression of envelope proteins by pre-S1/pre-S2 deletion mutants of HBV isolated from Southern African HIV-positive patients.* University of the Witwatersrand.

SLAGLE, B. L., ANDRISANI O.M, BOUCHARD M.J, LEE C.G, OU J.H & A., S. 2015. Technical standards for hepatitis B virus X protein (HBx) research. *Hepatology,* 61(4)**,** 1416–1424.

SOBOTTA, D., SOMINSKAYA, I., JANSONS, J., MEISEL, H., SCHMITT, S., HEERMANN, K.-H., KALUZA, G., PUMPENS, P. & GERLICH, W. H. 2000. Mapping of immunodominant B-cell epitopes and the human serum albumin-binding site in natural hepatitis B virus surface antigen of defined genosubtype. *Journal of General Virology,* 81**,** 369-378.

SONG, E., DUSHEIKO, G. M., BOWYER, S. & KEW, M. C. 1984. Hepatitis B Virus Replication in Southern African Blacks with HBsAg-Positive Hepatocellular Carcinoma. *Hepatology,* 4**,** 608-610.

SQUADRITO, G., SPINELLA, R. & RAIMONDO, G. 2014. The clinical significance of occult HBV infection. *Annals of gastroenterology,* 27**,** 15.

STANNARD, L. M. & HODGKISS, M. 1979. Morphological irregularities in Dane particle cores. *Journal of General Virology,* 45**,** 509-514.

SU, I. J., WANG, H. C., WU, H. C. & HUANG, W. Y. 2008. Ground glass hepatocytes contain pre-S mutants and represent preneoplastic lesions in chronic hepatitis B virus infection. *Journal of gastroenterology and hepatology,* 23**,** 1169-1174.

SUGAUCHI, F., KUMADA, H., ACHARYA, S. A., SHRESTHA, S. M., GAMUTAN, M. T. A., KHAN, M., GISH, R. G., TANAKA, Y., KATO, T. & ORITO, E. 2004. Epidemiological and sequence differences between two subtypes (Ae and Aa) of hepatitis B virus genotype A. *Journal of General Virology,* 85**,** 811-820.

SUGAUCHI, F., OHNO, T., ORITO, E., SAKUGAWA, H., ICHIDA, T., KOMATSU, M., KURAMITSU, T., UEDA, R., MIYAKAWA, Y. & MIZOKAMI, M. 2003. Influence of hepatitis B virus genotypes on the development of preS deletions and advanced liver disease. *Journal of medical virology,* 70**,** 537-544.

SUGIYAMA, M., TANAKA, Y., KATO, T., ORITO, E., ITO, K., ACHARYA, S. K., GISH, R. G., KRAMVIS, A., SHIMADA, T. & IZUMI, N. 2006. Influence of hepatitis B virus

genotypes on the intra-and extracellular expression of viral DNA and antigens. *Hepatology,* 44**,** 915-924.

TAKASHIMA, H., ARAKI, K., MIYAZAKI, J., YAMAMURA, K. & KIMOTO, M. 1992. Characterization of T-cell tolerance to hepatitis B virus (HBV) antigen in transgenic mice. *Immunology,* 75**,** 398.

TANAKA, Y., HASEGAWA, I., KATO, T., ORITO, E., HIRASHIMA, N., ACHARYA, S. K., GISH, R. G., KRAMVIS, A., KEW, M. C. & YOSHIHARA, N. 2004. A case-control study for differences among hepatitis B virus infections of genotypes A (subtypes Aa and Ae) and D. *Hepatology,* 40**,** 747-755.

TENNEY, D., LEVINE, S., ROSE, R., WALSH, A., WEINHEIMER, S., DISCOTTO, L., PLYM, M., POKORNOWSKI, K., YU, C. & ANGUS, P. 2004. Clinical emergence of entecavir-resistant hepatitis B virus requires additional substitutions in virus already resistant to Lamivudine. *Antimicrobial agents and chemotherapy,* 48**,** 3498-3507.

THIO, C. L. & LOCARNINI, S. 2007. Treatment of HIV/HBV coinfection: clinical and virologic issues. *AIDS reviews,* 9**,** 40-53.

TIOLLAIS, P., POURCEL, C. & DEJEAN, A 1985. The hepatitis B virus. *Nature,* 317**,** 489-495.

TONG, S. & REVILL, P. 2016. Overview of hepatitis B viral replication and genetic variability. *Journal of hepatology,* 64**,** S4-S16.

VELKOV, S., OTT, J., PROTZER, U. & MICHLER, T. 2018. The Global Hepatitis B Virus Genotype Distribution Approximated from Available Genotyping Data. *Genes,* 9**,** 495.

VISVANATHAN, K., SKINNER, N. A., THOMPSON, A. J., RIORDAN, S. M., SOZZI, V., EDWARDS, R., RODGERS, S., KURTOVIC, J., CHANG, J. & LEWIN, S. 2007. Regulation of Toll-like receptor-2 expression in chronic hepatitis B by the precore protein. *Hepatology,* 45**,** 102-110.

WANG, H.-C., WU, H.-C., CHEN, C.-F., FAUSTO, N., LEI, H.-Y. & SU, I.-J. 2003. Different types of ground glass hepatocytes in chronic hepatitis B virus infection contain specific pre-S mutants that may induce endoplasmic reticulum stress. *The American journal of pathology,* 163**,** 2441-2449.

WEI, Y., NEUVEUT, C., TIOLLAIS, P. & BUENDIA, M.-A. 2010. Molecular biology of the hepatitis B virus and role of the X gene. *Pathologie Biologie,* 58**,** 267-272.

WOLHUTER, S. 2016. *Functional characterisation of pre S1/pre S2 deletion mutants of hepatitis B virus isolated from Southern Africans.*

XU, Z., JENSEN, G. & YEN, T. 1997. Activation of hepatitis B virus S promoter by the viral large surface protein via induction of stress in the endoplasmic reticulum. *Journal of virology,* 71**,** 7387-7392.

XU, Z. & YEN, T. 1996. Intracellular retention of surface protein by a hepatitis B virus mutant that releases virion particles. *Journal of virology,* 70**,** 133-140.

YAN, H., ZHONG, G., XU, G., HE, W., JING, Z., GAO, Z., HUANG, Y., QI, Y., PENG, B. & WANG, H. 2012. Sodium taurocholate cotransporting polypeptide is a functional receptor for human hepatitis B and D virus. *elife,* 1**,** e00049.

YANG, J. C., TENG, C. F., WU, H. C., TSAI, H. W., CHUANG, H. C., TSAI, T. F., HSU, Y. H., HUANG, W., WU, L. W. & SU, I. J. 2009. Enhanced expression of vascular endothelial growth factor-A in ground glass hepatocytes and its implication in hepatitis B virus hepatocarcinogenesis. *Hepatology,* 49**,** 1962-1971.

YIM, H. J. & LOK, A. S. F. 2006. Natural history of chronic hepatitis B virus infection: what we knew in 1981 and what we know in 2005. *Hepatology,* 43**,** S173-S181.

YIN, J., XIE, J., ZHANG, H., SHEN, Q., HAN, L., LU, W., HAN, Y., LI, C., NI, W. & WANG, H. 2010. Significant association of different preS mutations with hepatitis B-related cirrhosis or hepatocellular carcinoma. *Journal of gastroenterology,* 45**,** 1063-1071.

YOOK, K. 2005. Complementation. *WormBook: The Online Review of C. elegans Biology [Internet]*. WormBook.